INVESTIGATION OF THE SURFACES OF DEALKALIZED AND WEATHERED FLOAT GLASS

A Thesis Submitted to
the Graduate School of Engineering and Sciences of
İzmir Institute of Technology
in Partial Fulfillment of the Requirements for the Degree of

MASTER OF SCIENCE

in Materials Science and Engineering

by
Ümmügülsüm SEZİŞ

July 2016
İZMİR

We approve the thesis of **Ümmügülsüm SEZİŞ**

Examining Committee Members:

_____

Asst. Prof. Dr. Ufuk ŞENTÜRK
Department of Materials Science and Engineering, Izmir Institute of Technology

_____

Prof. Dr. Mustafa Muammer DEMİR

Department of Materials Science and Engineering, Izmir Institute of Technology

_____

Prof. Dr. Yüksel ABALI
Department of Chemistry, Celal Bayar University

15 July 2016

_____

Asst. Prof. Dr. Ufuk ŞENTÜRK
Supervisor, Department of Materials Science and Engineering
Izmir Institute of Technology

_____

Asst. Prof. Dr. Hadi M. ZAREIE
Co-Supervisor, Department of Materials Science and Engineering
Izmir Institute of Technology

_____

Prof. Dr. Mustafa M. DEMİR
Head of the Department of Materials Science and Engineering

_____

Prof. Dr. Bilge KARAÇALI
Dean of the Graduated School of Engineering and Sciences

ACKNOWLEDGEMENTS

I express my deep gratitude to my advisor Asst. Prof. Dr. Ufuk ŞENTÜRK from whom I have learned not only the whole theory, material science, glass science and experimental techniques, but also the value of assiduity, and the virtue of being honest. I want to thank for his understanding, constantly invaluable guidance, encouragement, motivation, incredible support, and immense knowledge in every stage of my thesis study. I feel lucky to be able to work with him, learn from him, and I am proud of being one of his students.

I gratefully acknowledge Şişecam for funding this project, and to all the staff of Surface Technology Research Group of Şişecam Science and Technology Center for their kindness and cooperation during my study period. I am indebted to Dr. İlkay SÖKMEN for her help throughout my research and to her working group: Dr. Selen ERKAN, Dr. Tuncay TURUTOĞLU, Lukáš ŠIMURKA and Ezgi BİÇER for their support in several matters. I am thankful to Çiğdem YAMAÇ and Emel MERCAN for their kind help during the preparations of my samples and their friendship.

Besides my advisor, I would like to thank the other members of my thesis committee for their encouragement and insightful comments.

I would like to kindly thank you my co-advisor Asst. Prof. Dr. Hadi M. ZAREIE and his working group, notably Yaman GÖKSEL and Begüm DEMİRKURT for their help on Raman analysis. I thank profusely all the staff Center for Materials Research at IZTECH, especially Mine BAHÇECİ for her help in the AFM studies.

For their warm friendship and technical support, thank you to Dilek GÜL, Hakan GÖKTÜRK and Tuğçe SEMERCİ.

My warmest thanks go to Dilek and Sedat ELTİMUR, İlknur ÇAKMAK ULUKAYA, Bedriye ATİLA, Fatma KOÇAR, Şebnem DAĞLI, Meryem DENİZ, Adile ALPERİ, Serpil ÇELİK, Şeyma KAYA, Osman Giray YÖRÜK, Gazi ÖZDEMİR, and to my precious friend Elona FETAHU, who were like my family in Urla, and who always supported me.

To my wonderful family – Mom and Dad, Ayşe and Cafer SEZİŞ. They have always been with me, every step of the way, and I express my heartfelt gratitude for their unconditional love, support, encouragement, and instilling in me the belief that I could do anything I put my mind to.

ABSTRACT

INVESTIGATION OF THE SURFACES OF DEALKALIZED AND WEATHERED FLOAT GLASS

In this study, the effects of surface dealkalization due to SO_2 or SO_3 gas treatment of commercial soda lime silica float glass on the weathering behavior was investigated. Only the air side of the glass was studied. The changes in the glass surface were analyzed for their topography and structure. The surface topography was studied using atomic force microscopy (AFM). The findings show the formation of micro-cracks on the surfaces of as-produced glass surfaces when treated with sulfur gas. The weathered surfaces show an increased roughness with increased weathering. The surface structure was investigated using attenuated total reflection-Fourier transform infrared (ATR-FTIR) spectroscopy, specular reflectance infrared (SR-IR) spectroscopy, and micro-Raman spectroscopy techniques

The results of the studies, ATR-FTIR and SR-IR techniques provided a reasonable insight on the surface structural changes while micro-Raman spectroscopy failed to detects these differences. ATR-FTIR and SR-IR the overall comparison of the effects of peak position with and without sulfur gas treatment suggests a wide scatter within each group. This scatter implies that sulfur gas treatment does not have any statistically significant effects. Also, the change in peak positions are no clear evidence of a decreasing or increasing peak position as the weathering period is increased by weathering effect. Additionally, the calculated penetration depth is found to be ~0,6-1 μm for these techniques. Namely, the penetration depth greater than the surface modification was observed. The results showed was not significantly affected by the surface dealkalization and weathering reactions. The analysis of the surface topography using AFM technique showed the formation of micro-cracks like features on the surfaces of sulfur treated glasses. These features are thought to occur under the sodium sulfate salt residue that is formed during the high temperature dealkalization reactions on the surface. Results sample preparation, i.e. cleaning, was found to have a significant effect on the surface properties. A method has been developed to minimize the effects of sample preparation on the surface of the glass.

ÖZET

ALKALİSİ GİDERİLMİŞ, HAVA VE NEME MARUZ KALMIŞ DÜZ CAMLARIN YÜZEYLERİNİN İNCELENMESİ

Bu çalışmada, float metodu ile üretilen düz camların nem ortamındaki korozyon davranışları ve SO_2/SO_3 gaz dealkalizasyonunun bu camlar üzerine etkileri incelenmiştir. Bu çalışma için camın sadece hava yüzeyi kullanılmıştır, camın kalay yüzeyinde bir inceleme yapılmamıştır ve genel olarak dealkalizasyon işlemi uygulanmış ve uygulanmamış olmak üzere iki farklı tip numune kullanılmıştır. Nemli ortamda cam yüzey değişimleri üzerine yüzey temizleme işlemlerinin ve dealkalizasyonun etkileri detaylı bir şekilde ele alınmıştır. Ayrıca yaşlandırma öncesi ve sonrası cam yüzey yapı ve topografya değişimleri incelenmiştir. Yüzey topografyası atomik kuvvet mikroskobu (AFM), yüzey yapısı ise attenuated total reflection-fourier transform infrared (ATR-FTIR) spektroskopi, specular reflectance infrared (SR-IR) spektroskopi ve micro-Raman spectroskopi teknikleri kullanılarak araştırılmıştır.

Bu çalışma sonucunda, ATR-FTIR ve SR-IR analiz sonuçları yaşlandırma etkisi hakkında bilgi verirken micro-Raman analizleri bu çalışma için sonuç vermemiştir. ATR-FTIR ve SR-IR analizleri için hesaplanan penetrasyon derinliği yaşlanma sonucu cam yüzeyinde meydana gelen değişimden büyüktür. ATR-FTIR ve SR-IR sonuçları incelenirken buna dikkat edilmelidir. Bu çalışmada AFM analiz sonuçları göstermiştir ki etanol yüzeyde giderilmesi güç bir film oluşturmuştur ve bu sebeple yüzey temizliği için kimyasal sıvı olarak izopropil alkol kullanılmıştır. Ayrıca, AFM analiz sonuçları sülfür gazı uygulaması yapılan cam yüzeylerde yaklaşık 2 nm derinliğinde çatlaklar olduğunu göstermiştir. Bu çatlakların sülfürleme sonucu yüzeyde oluşan sodyum tuzlarının altında olduğu düşünülmektedir.

To my Mom and Dad…

TABLE OF CONTENTS

LIST OF FIGURES

Figure **Page**

LIST OF TABLES

Table **Page**

LIST OF ABBREVIATIONS

SLS ..... Soda-lime-silica
SLSFG ..... Soda-lime-silica float glass
BO ..... Bridging oxygen
NBO ..... Non-bridging oxygen
FTIR ..... Fourier transform infrared
ATR-FTIR ..... Attenuated total reflection-Fourier transform infrared
FT-IRRS ..... Fourier transform infrared reflection spectroscopy
SR-IR ..... Specular reflectance infrared
AFM ..... Atomic force microscopy
PF-QNM-AFM ..... Quantitative nanomechanical peak force atomic force microscopy
XPS ..... X-ray photoelectron spectroscopy
DM H_2O ..... Demineralized water
UB ..... Ultrasonic bath
IPA ..... Isopropyl alcohol

CHAPTER 1

INTRODUCTION

In this chapter, firstly information is given about history of glass. Then the glass system is briefly described, and disclosed the differences between glass and crystalline structure, and information is given about the kinds of glass.

1.1. Glass and General Overview of Glass

The word glass is derived from a Latin term *glaesum* (Varshneya, 1994). According to Doremus "the word glass is derived from an Indo-European root meaning 'shiny' " (Doremus, 1994). It is not known when and where the first glass produced (Cummings, 2002). However, it is thought the manufacturing of glass began around 1500 B.C. in Mesopotamia and Egypt (Kennedy, 1997). Glass science developed with the commercial use of glass. More than 99% of the commercial glass compositions consists of oxides (Varshneya, 1994).

According to the researcher J. Fanderlik, who worked on glass, "A glass is a material, formed by cooling from the normal liquid state, which has shown no discontinuous change and any temperature, but has become more or less rigid through a progressive increase in its viscosity" (Doremus, 1994). Definition of the glass by the American Society for Testing and Materials is given as: "an inorganic product of fusion which has been cooled to a rigid condition without crystallizing". This definition is too limiting. Many organic glass systems are known that is not made with the only fusion method. The appearance of glasses is actually solid-like. Glass can be briefly described in the following way; 'solid with liquid like structure', 'a non-crystalline solid', or simply as 'an amorphous solid' (Varshneya, 1994). In other words glass is 'an amorphous solid completely lacking in long-range, periodic atomic structure and exhibiting a region of glass transformation behavior'. There are four major groups of constituents of glass: glass formers, intermediates, modifiers and fining agents.

The glass formers is providing the basis of network (such as silica (SiO_2), boric oxide (B_2O_3), phosphorus oxide (P_2O_5) and germanium dioxide (GeO_2). The glass modifiers are used to decrease the melt temperature of the glass. Glass modifiers are

alkali oxides. Some properties of the glass deteriorates by addition of modifiers, and to atone for these properties loss, intermediates are added (such as Al_2O_3, MgO). In the final glass, fining agents can add to diminish the amount of bubbles (such as As_2O_3, Sb_2O_3) (Guo, 2006).

The difference between glass and crystal is due to the connection with each unit of the tetrahedral lattice. This difference is shown in Figure 1.1.

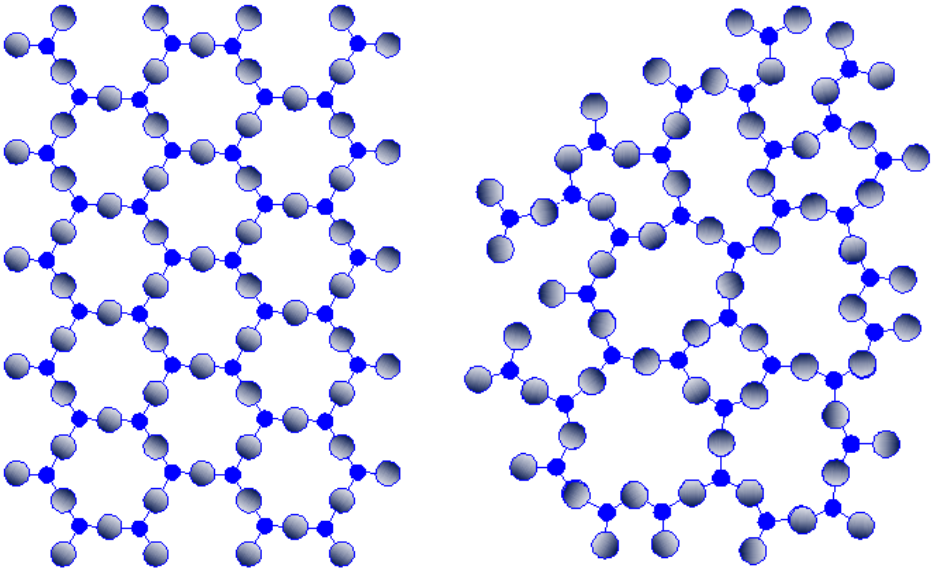

(a) (b)

Figure 1.1. Atomic structure of 2D A_2O_3 (a) crystal form (b) glass form
(Source: Zachariasen's Random Network Theory- Park, 2008)

Glass Types: There are many different types of commercial glass. Glass, desired physical and chemical properties can be produced depending on the application. Some types of commercial glass and their wt% components are given Table 1.1.

Table 1.1. Commercial glass compositions (wt %)
(Source: Varshneya, 1994)

	SiO_2	Al_2O_3	B_2O_3	SO_3	CaO	MgO	BaO	PbO	Na_2O	K_2O	ZnO	As_2O_5
Vitreous Silica	100.0											
Vycor	94.0		5.0						1.0			
Plate	72.7	0.5		0.5	13.0				13.2			Tr.
Window	72.0	0.6		0.7	10.0	2.5			14.2			Tr.
Bottle or container	74.0	1.0		Tr.	5.4	3.7	Tr.		15.3	0.6		Tr.
Bulb	73.6	1.0			5.2	3.6			16.0	0.6		Tr.
Tubing	72.1	1.6			5.6	3.1			16.3	1.0		
Lime tableware	74.0	0.5			7.5				18.0			Tr.
Pyrex type	81.0	2.0	12.0						4.5			
Thermometer	72.9	6.2	10.4		0.4	0.2			9.8	0.1		Tr.
Borosilicate Crown	69.6		9.9				2.5		8.4	8.4		0.3
Lead Tableware	67.0	0.4						17.0	6.0	9.6		Tr.
Glass halogen lamp	60.0	14.3		0.3	6.5		18.3		0.01	Tr.		
E glass	52.9	14.5	9.2		17.4	4.4				1.0		
S glass	65.0	25.0				10.0						
Optical flint	49.8	0.1					13.0	18.7	1.2	8.2	8.0	0.4

1.2. Motivation

The study aims understanding of the mechanisms the surface mechanical properties of soda-lime-silicate float glass, and for that SO_2/SO_3 gases treated and untreated glass is used. In this study, we had three goals:

- One of the goals of this study was to understanding of the surface property changes high temperature gas treated dealkalization. SO_2/SO_3 treated and untreated glasses were provided by Şişecam. Dealkalization were investigated both positive and negative effects to soda-lime-silicate float glass surface, and various effects of the manufacturing process on surface was understand.
- A second goal of the study was to investigate the effect of surface cleaning procedures.
- A third goal in this study was to understand the changes in surface structure and topography as a result of the corrosion, and the dealkalization effect on corrosion has been taken into account.

1.3. Thesis Structure

In this chapter (Chapter 1), general information about glass, the kinds of glass, and physical and chemical properties of glass are given. In chapter 2, information about float glass structure, and the flat glass manufacturing process will be given, and dealkalization and corrosion effects will explained. Chapter 3 will also explain surface analysis methods, and experimental methods for this study. Chapters 4 of this thesis will debate the results from the studies on soda-lime-silica float glass surfaces. The effects of surface cleaning treatments and dealkalization on the corrosion of the only air side float glass surface will be discussed.

CHAPTER 2

BACKGROUND AND LITERATURE REVIEW

2.1. Float Glass Structure, Composition and Properties

Flat soda-lime-silica glasses are usually produced using the float glass process (Goodman & Derby, 2011). Float glass method was developed in 1959 by Pilkington. The molten glass flows out of the furnace on to a bed of molten tin in a controlled atmosphere is maintained at high temperature (controlled atmosphere; nitrogen and oxygen). While passing through the rollers, the glass is being cooled from an initial temperature of near 1100 °C to approximately 600 °C, and so becoming viscous enough not to damage the bottom surface while moving along the rollers (Synowicki, et al., 2011). The speed available along the tin bath determines the thickness of the glass sheet. Then these glasses are cooled in a regular and controlled manner to 200ºC in annealing kiln. The float glass surfaces can be described 'tin side' and 'air side' (Cobb, 2009). During this process, the surface of the glass does not make any contact (Goodman & Derby, 2011). Float glass process is shown in Figure 2.2. For using these glasses, they should be free of impurities and discoloration (Cobb, 2009). The amorphous structure of soda-lime-silica float glass (SLSFG) is shown Figure 2.1.

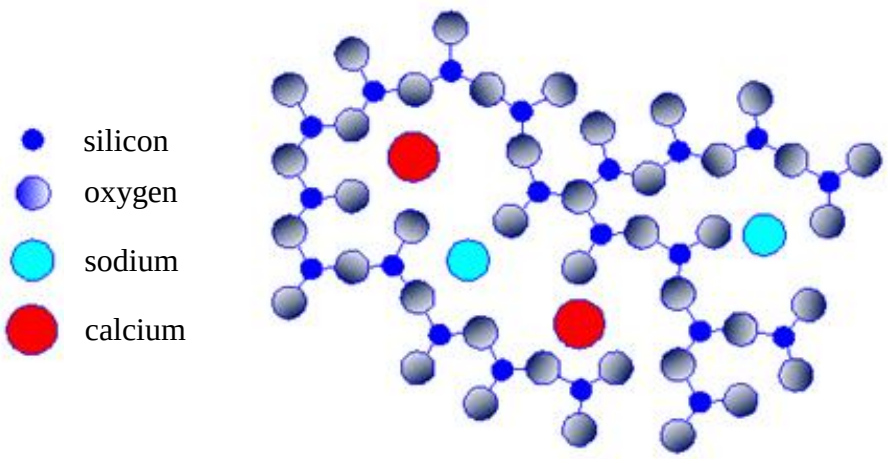

Figure 2.1. The soda-lime-silica float glass structure
(Source: Haldimann, et al., 2008)

Table 2.1. Properties of soda-lime-silica float glass
(Source: Patterson, 2008)

Soda-Lime-Silica Float Glass Properties		
Modulus of Elasticity (Young's Modulus)	72 GPa	10.4×10^6 psi
Modulus of Rigidity (Shear)	30 GPa	4.3×10^6 psi
Bulk Modulus	43 GPa	6.2×10^6 psi
Poission's Ratio		0.23
Density	2530 kg/m^3	158 Ib/ft^3
Coefficient of Thermal Stress	0.62 MPa/ºC	50 psi/ºF
Hardness (Moh's Scale)		5-6
Softening Point (ASTM C338)	715 ºC	1319 ºF
Annealing Point (ASTM C336)	548 ºC	1018 ºF
Strain Point (ASTM C336)	511 ºC	952 ºF
Index of Refraction	0.5893 µm 1 µm 2 µm	1.523 1.511 1.499

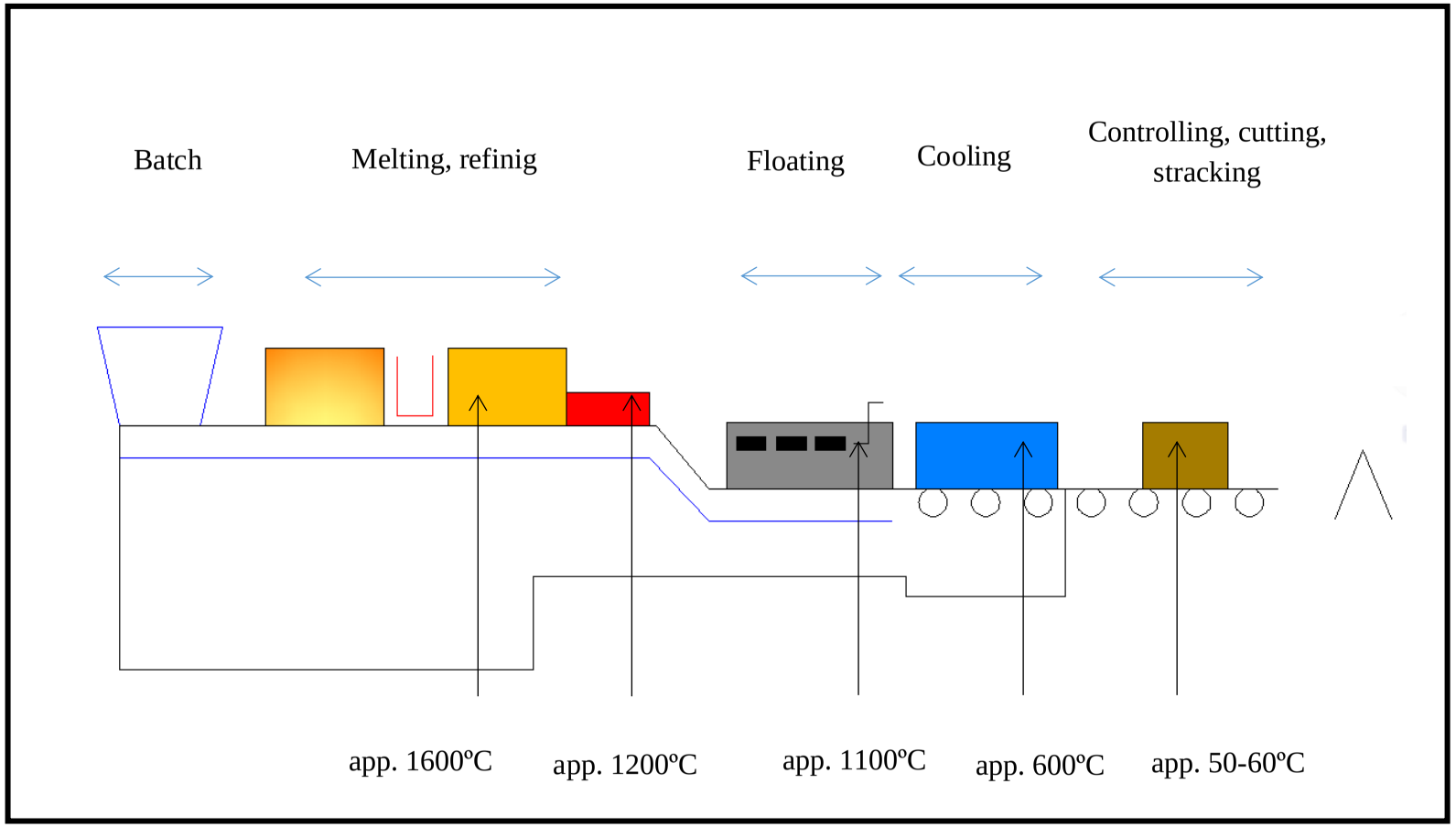

Figure 2.2. Schematic diagram of float process
(Source: Greiner & Rinkens, 2013)

2.2. Glass Weathering and Corrosion

Glass corrosion is one of the big problems for the glass producing industry (Palenta, et al., 2013). In fact, glass is a durable material. However, glasses are known to be corroded with various reasons, such as water, humidity, oxygen, weak acids, and weak bases (Varshneya, 1994). In this study, it is important to corrosion by water and humidity. Water has important effects on the glass surface, and when glass is in contact with an aqueous solution, chemical and structural changes occur on the glass surface. Si-O bonds in the glass network are destroyed during the corrosion. Glass corrosion has been studied for many years (Palenta, et al., 2013, Soares, et al., 2011). Several researchers have indicated that glass-water reaction in two stages (Clark, et al., 1979). Stage 1 and stage 2 shown in Figure 2.3. Commercial flat glasses are produced by float method. Two faces of the glass produced by float method different chemical and mechanical properties because the upper surface of the glass when exposed to a reducing gas atmosphere bottom surface of the glass is in contact with the molten tin, so diffusion of Sn are available on the bottom surface (Soares, et al., 2011). The formation of a hydrated layer of Si–OH as a result of the ion exchange reaction between sodium and hydrogen ions as the aqueous corrosion is described by Hayashi et al. This layer is more difficultly created on the tin side than on the air side. Also the formation of Si-OH is found to be controlled by the concentration of tin on the glass surface. Air side has a lower hardness because the surface hydrate layer is thick (Hayashi, et al., 2001, Hayashi, et al., 2002). Correspondingly, the air-side surface is less fragile than tin-side surface, and offers more strength to crack propagation (Soares, et al., 2011).

In the stage 1, there is an exchange of sodium ions from the glass and hydrogen ions from the solution, in the meantime, the residuary components of the glass are not modified (Soares, et al., 2011).

In the stage 2, a disruption process of the silica structure take place, and surface degradation and dissolution of the leached surface occurs (total dissolution) (Soares, et al., 2011).

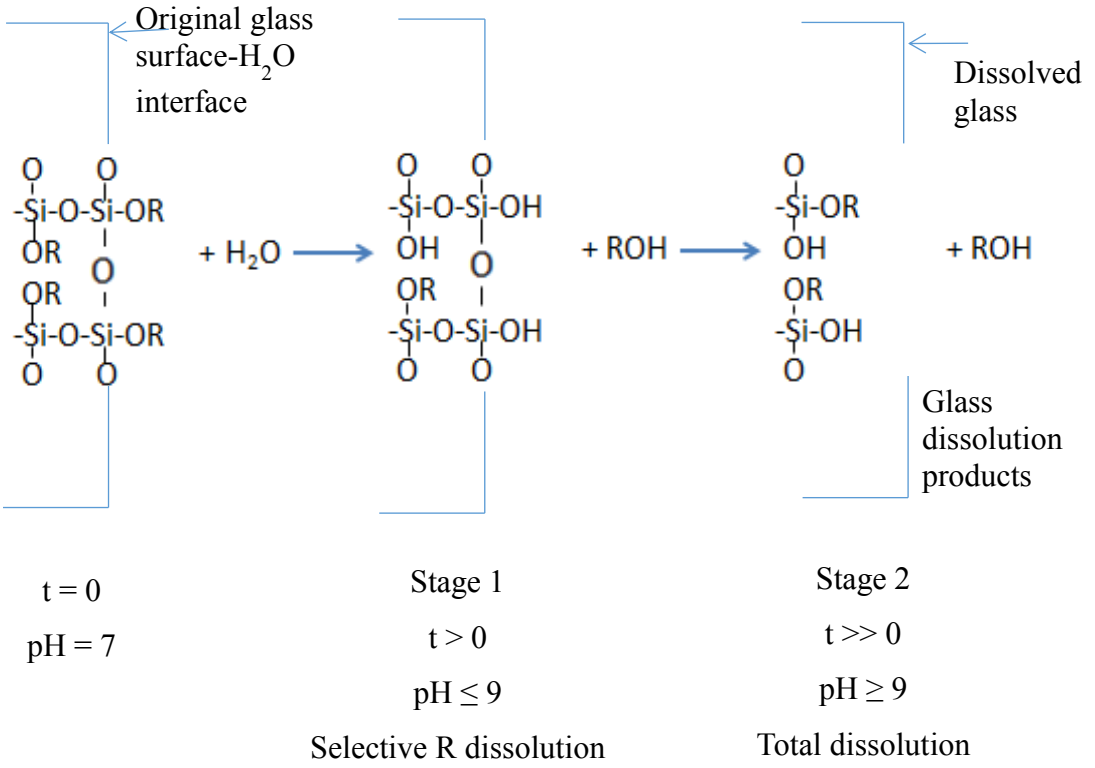

t= duration of experiment

Figure 2.3. Glass corrosion mechanism for a alkali glass
(Source: Clark, et al., 1979)

Leaching encompasses the exchange of mobile ions, such as sodium ions and calcium ions from the glass network, with hydrogen and/or hydronium ions in the aqueous solution. Exchange of mobile ions from glass network with smaller size hydrogen and/or hydronium ions causes tensile stress on the glass surface. Leaching causes the porosity on the glass surface, so leaching increases the corrosion reaction (Sharma, 2002).

According to Shama and Jain, the glass morphology does not change if the glass surface is uniformly dissolving. On the contrary, if the glass surface non-uniform dissolving the glass morphology changes. Therefore, corrosion can cause structural and chemical changes in the glass surface (Sharma, 2002).

Interaction glass-water vapor:

Water vapor can be adsorbed on the glass surface, and a silica gel structure on the glass surface can occur with water vapor effect.

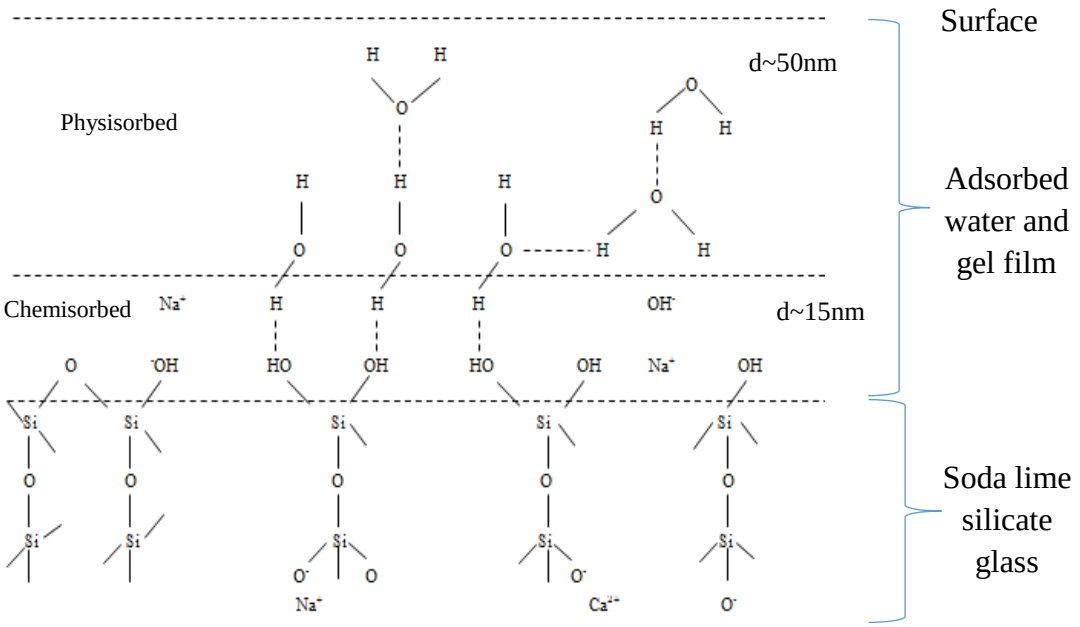

Figure 2.4. Schematic representation of the formation of a water film on glass surface by adsorption of water vapor
(Source: Pantano, 2015, Melcher, et al., 2010)

The effect of humidity on the glass surface:

Results of surface layer formation by humidity, water adsorption and condensation on the surface, leaching ion exchange, and water reaction, and accumulation of reaction products on the surface (such as sulphate, carbonate) can occur.

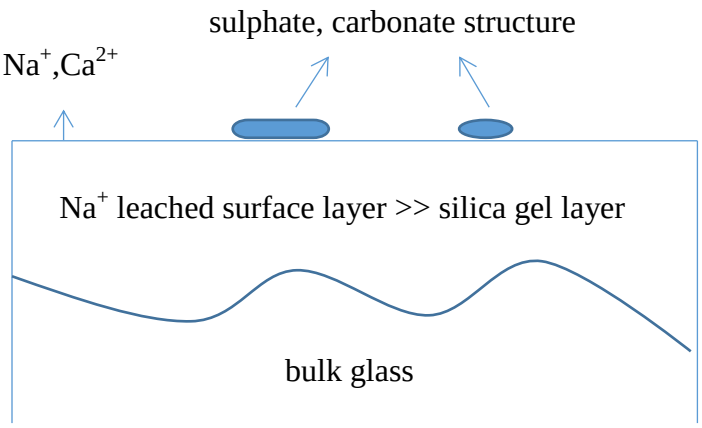

Figure 2.5. Schematic representation of humidity effect
(Source: Pantano, 2015)

Durability and corrosion of glasses are mainly affected by surface composition, solution pH, and conditions during manufacturing, fabrication, storage and service (such as temperatures, homogeneity) (Franz, 1980). In general, factors affecting degradation of glass objects:

- Raw materials - homogeneity, degree of sorting, mixing.
- Glass composition - differences between surface and bulk, impurities.
- Manufacturing technology - materials preparation; processing, forming and finishing, surface treatment, thermal treatment (annealing).
- Environment - humidity, temperature, solution pH, structure of environment, external energy factors.
- Re-use, surface alteration, conservation, storage (Ryan, 1995).

The some factors influencing the glass corrosion:

Composition effects: Alkalis are the most common modifiers used for silicate glasses, addition of alkalis into the atomic network breaks bridging oxygen bonds (BO) and led to the emergence ionically bonded non-bridging oxygen atoms (NBO). Sodium is most commonly used alkaline. Alkali earth oxides are added for increasing the chemical resistance of alkali silicate glass. Calcium, it is alkaline earth metal, is commonly used in sodium silicate glasses structure, and for such glass is called soda lime silicate glass. Ca would undermine the glass network significantly at high temperatures. That is why, minor components are intercalary from transform non-bridging oxygen atoms to the bridging ones such as Al_2O_3, TiO_2 and Fe_2O_3. Mechanical abrasion resistance of the glass increases by adding them. Alkali and alkaline earth oxides are added together for the high mechanical strength of the glass. Therefore, minor components Al_2O_3, MgO, SO_3, TiO_2, Fe_2O_3 and K_2O are added for commercial soda-lime-silicate glass (Sharma, 2002) (Morey, 1925) As shown in Table 2.2. All compositions in our study are very similar for specimens, so it has not effect on glass surface in this work.

Table 2.2. Chemical analysis of a typical SLS float glass
(Source: Patterson, 2008)

Chemical Analysis of a Typical Clear Float Glass							
SiO_2	**Na_2O**	**CaO**	**MgO**	**Al_2O_3**	**K_2O**	**SO_3**	**Fe_2O_3**
Silica	Soda	Calcium oxide	Magnesium oxide	Alumina	Potassium oxide	Sulfur trioxide	Iron oxide
72.6%	13.9%	8.4%	3.9%	1.1%	0.6%	0.2%	0.11%

pH effects: pH and content of environment significantly affect glass corrosion. The pH is less than 9 encourage leaching of mobile ions, otherwise, the pH is greater than 9, take place compatible glass dissolution but this is not always true (Sharma, 2002).

Manufacture processing effects: During manufacture process, like temperature of medium, humidity %, sulfur containing gases in environment, washing water, storage of glass all these factors causes changes the glass surface, and they affect the surface stress (compressive stress and tensile stress). The freshly formed glass surface is react with water and sulfur containing gases, and is produced NaOH and Na_2SO_4 on glass surface. The structure on the surface is removed by washing with water, however, it affects the surface corrosion. In our study, relation of glass corrosion to the ambient conditions will be investigated in detail.

2.3. Reaction with SO_2/SO_3 Gases at High Temperatures

Dealkalization of glasses by SO_2/SO_3 gases at high temperatures is known for too many years, however, the glass surface had been treated at annealing temperatures in the early 20th century. Attribute of the annealing process was decided according to bloom, and the bloom means is a surface film formed on the glass surface, and the main component of the bloom is sodium sulphate. Pyrosulphate can occur if SO_3 gas is used (Şentürk, 1992). Additionally, according to Rancoule and friends, when humidity in air is mixed to the SO_2 gases in oven, $Na_2S_2O_7$ phase can be created in the medium temperature before Na_2SO_4 phases at higher temperature (Rancoule, et al., 2006). After glasses are treated with SO_2, sulphate layer of glass surface can be eliminated washing with water (Shimin, et al., 2007). Surface layer with SO_2-treated is chemically more stable, and stronger when compared with non-treated glass surface. We understand that

the SO_2 treatment enhances the chemical, physical and mechanical properties of the float glass surface by elimination of alkali oxide. Additionally, heat treatment without SO_2, treatment atmosphere and temperatures has a significant impact on the chemical resistance of float glass surface. For this reason, the treatment conditions are very important to create a new surface.

The formation of bloom for structure containing sodium:

$$Na_2O_{(glass)} + SO_2 + ½\ O_2 \longrightarrow Na_2SO_{4\ (glass\ surface)} \quad (2.1)$$

Reaction 2.1 is applicable to dry atmosphere, and the rate of diffusion is low under this condition. There is need relatively high temperature for reaction kinetics to release Na^+ and O^{2-} together in the glass structure.

$$2Na^+_{(glass)} + SO_2 + ½\ O_2 + H_2O \longrightarrow 2H^+_{(glass)} + Na_2SO_{4\ (glass\ surface)} \quad (2.2)$$

If the atmosphere contains water, reaction 2.2 occurs. For this reaction needs the water and mobility of Na^+ ions, and high temperatures may not be required (Şentürk, 1992).

SO_3 gas is formed when the SO_2 gas reacts with O_2 gas, and dealkalization process can applied with SO_3 gas on the glass surface like SO_2 at dry and containing water atmospheres. SO_3 is more reactive than SO_2, and increases the reaction kinetic (Anderson, et al., 1975).

Reaction mechanisms for SO_3 gas:

$$2SO_2 + O_2 \longrightarrow 2SO_3 \quad (2.3)$$

$$Na_2O + SO_3 \longrightarrow Na_2SO_4 \quad (2.4)$$

$$2Na^+_{(glass)} + SO_3 + H_2O \longrightarrow 2H^+_{(glass)} + Na_2SO_4 \quad (2.5)$$

Reaction 2.4 for dry atmospheres, reaction 2.5 for atmospheres containing water (Şentürk, 1992).

2.4. Overview of Glass Surface Analysis Methods

A summary of some of the methods used for surface analysis are given in Table 2.3. It will only described techniques that we use, all of these techniques will not be discussed. Fourier transform infrared (FTIR) spectroscopy is an analytical technique used to obtain infrared spectra that is analysis of solids, liquids and gases. Infrared spectroscopy techniques and Raman spectroscopy technique are commonly used method for the glass surface structure analysis, and AFM is used for the surface topography analysis.

The air-side surfaces of the weathered glass surfaces were analyzed using XPS (x-ray photoelectron spectroscopy) by Smith and Pantano. In addition, the relative extent of glass surface leaching was evaluated using FT-IRRS (fourier transform infrared reflection spectroscopy), and the topography of weathered and unweathered glass surfaces was evaluated by means of AFM (atomic force microscopy). Experiments were performed in cyclic and static conditions -with or without acid. It is understood that the research of Smith and Pantano, the final leached layer depends on many interrelated factors associated with the interleave coating (acid concentration, uniformity of coating, and bead diameter) and with the weathering conditions (emperature, humidity, runoff, and time) (Smith & Pantano, 2008).

Juliane Hopf and EM Pierce, they used a different technique for the AFM surface topography analysis which is PF-QNM-AFM (Quantitative Nanomechanical Peak Force Atomic Force Microscopy). This technique allows for topography and mechanical property information to be measured simultaneously at each pixel. Their study show that X analysis results readily provides images of elastic modulus, adhesion, height, and deformation correlated with surface topography (Hopf & Pierce, 2014).

Table 2.3. Experimental techniques for analysis of glass surfaces (Source: Doremus, 1994, Reviere & Myhra, 1998, Woodruff & Delchar , 1994)

Chemical Analysis		
Rutherford back scattering	RBS	1 μm
Resonant nuclear reaction	RNR	1 μm
Secondary-ion mass spectroscopy	SIMS	1 μm
Electron microprobe		1 μm
Ion beam spectrochemical analysis	IBSCA	1 μm
Electron energy dispersion	EDS	1 nm
Chemical and Bonding Analysis		
Auger electron spectroscopy	AES	5 nm
Electron spectroscopy for chemical analysis	ESCA	5 nm
X-ray photoelectron spectroscopy	XPS	
Low-energy ion scattering	LEIS	
High energy ion scattering	HEIS	
Surface Observation		
Scanning electron microscopy	SEM	100 nm
Transmission electron microscopy	TEM	100 nm
Atomic force microscopy	AFM	
Diffraction Techniques		
Small-angle X-ray diffraction	SAXS	
Low-angle electron diffraction	LEED	
Optical		
Infrared absorption and reflection		
Raman spectroscopy		
Ellipsometry		

Another study was conducted by Amma and his colleagues. They investigated water and hydroxyl species in soda lime glass surfaces using attenuated total reflection (ATR)-IR spectroscopy. The results of their studies are as follow; the peaks lie on the range between 3600 and 2200 cm^{-1}, which is due to the variation of hydrogen bonding interactions in H_2O and OH. 2800 cm^{-1} band is expected to be evident in the IR spectra of the soda-lime-silica float glass because of nonbridge oxygen. The peak at 2750 cm^{-1} to the SiOH-stretching vibration with strong hydrogen bonding to the nonbridging oxygen and the 3600 cm^{-1} to the SiOH-stretching vibration with weak hydrogen bonding to an oxygen from the neighboring hydroxyl group. The band at 1650 cm^{-1} to bending vibration and the band near 3400 and 3200 cm^{-1} to symmetric stretching of interstitial molecular H_2O. SO_2-treated in samples are expected to increase SiOH peaks (Amma, et al., 2016).

Soda-lime-silicate glass infrared bands assignments are given in Table 2.4 for ATR-FTIR and Table 2.5 for SR-IR.

Smets examined the glass surface with different techniques (Smets, 1985). Leached layer on the glass surface has explained. According to this and other studies, surface layer can be explained as follow (Yamamoto & Yamamoto, 2011):

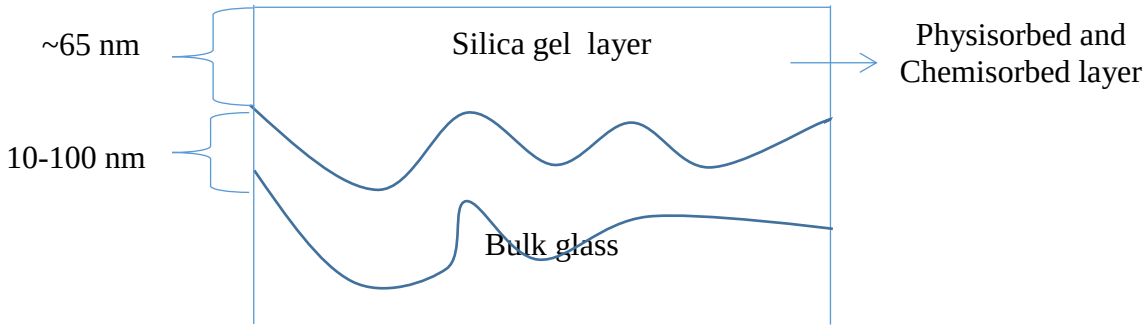

Figure 2.6. Schematic representation of surface layer

Table 2.4. ATR-FTIR- Infrared band assignments of soda-lime-silicate glass (Source: Amma, et al., 2016, Amma, et al., 2015, Uchino, et al., 1989, Şentürk, et al., 1995, Şentürk, 1992)

Wavenumber (cm^{-1})	Assignment	Type of vibration
4500	OH Si-OH	From the combination the OH stretch and the Si-OH bending vibrations
3600-2200	OH	Stretching of X-OH (X=Si,H)
1650	H-O-H	Bending vibration of the molecular water
1160-1140	SiO_4^{4-}	Polymerization
1120-1050	Si-O-Si	Antisymmmetric stretching ("S" band)
970-950	$Si\text{-}O^{-}(modifier\ ion)^{+}$	Stretching of $Si\text{-}O^{-}Na^{+}/Ca^{+}$ ("NS" or "NSX" band)
900-870	Si-O Si-OH	Stretching of Si-OH Bending
770-730	Si-O-Si	Symmetric stretching
600	Si-O-Si	Bending

Table 2.5. SR-IR- Assignments of infrared band of soda-lime-silicate glass (Source: Amma, et al., 2015, Lefèvre, 2004, Lee, et al., 1997, Geotti Bianchini, et al., 1991, Smith & Pantano, 2008)

Wavenumber (cm^{-1})	Assignment	Type of vibration
~3500	OH-type	OH-type vibrations
1050-1120	Si-O-Si	Stretching vibration of the Si-O-Si (or silicium-bridging oxygen) bonds ("S" peak)
~1050	Si-O	Si-O asymmetric stretching (AS) mode
~950	Si-O	Si-O stretching mode of non-bridging oxygens (NS) (Si-O stretching band)
~766	Si-O	symmetric stretching (SS) or bending mode
~510	Si-O-Si	Bending

ATR-FTIR spectra investigated for SO_2-treated soda-lime-silicate float glass by Şentürk et. al. (Şentürk, et al., 1995). In this study, ATR-FTIR penetration depth is given with equation 2.1. The depth of penetration is an important factor for infrared spectroscopy analysis. Penetration depth can be calculated using the below equation:

$$d_{P=} \frac{\lambda}{2\pi n_1[\sin^2\theta-(n_2/n_1)^2]^{1/2}}$$

Equation 2.1.
(Douglas & Isard , 1949)

Where,

n_1= the refractive indices of the denser media

n_2= the refractive indices of the rarer media

θ= angle of incidence

λ= wavelength of light

Equation 2.1. suggests that the penetration depth of the incoming light onto a surface is effected by the angle of incidence, incident wavelength and the difference between the refractive index of the two media (Şentürk, 1992).

According to Affatigato, penetration depth is 0.7 μm for micro-Raman laser at 532 nm (Affatigato, 2015).

CHAPTER 3

EXPERIMENTAL PROCEDURES

3.1. Organization of Samples and Their Analysis

The production, preparation and analysis of the samples throughout this study were carried out at three different sites, as further explained in the following sections of this chapter. Below is an overview of the organization of the sample production and their analysis:

1. Production of the glass samples were done during the routine manufacturing of commercial float glass at Sisecam's manufacturing facilities,
2. Aging of the manufactured samples were done at Şişecam Science and Technology Center while the preparation (scoring, cutting, packaging, and storing) of both unaged and aged samples for further analysis were carried out either at the manufacturing facility or at the laboratories of Sisecam and Izmir Institute of Technology (Iztech),
3. Sample analysis were carried out at Şişecam Science and Technology Center and at Iztech according as follows:
    a. Grazing incidence X-ray diffraction, ATR-FTIR and SR-FTIR were conducted at Şişecam Science and Technology Center
    b. AFM and micro-Raman analysis were conducted at Iztech

3.2. Sample Preparation

Commercial soda-lime-silica float glass was used in this study. The glass samples were provided by Şişecam from four of their different manufacturing sites. These samples have been labeled as F1-L1, F1-L2, F2-L5, F3-L7, F4-L1, and F4-L2, where F denotes the different sites and L denotes the production line from each site. A generic composition of the glasses is shown in Table 3.1 as provided by the manufacturer. Glasses that have been treated with SO_2, SO_3, and no gas treatment have been identified as shown in Table 3.2. The measurements on the surface properties were conducted only on one side of glass, which is the surface that has not been in

contact with the tin bath during the production. This surface will be referred to as the "air side". The analysis was conducted in five separate and sequential groups. These groups are labeled as G1, G2, G3, G4 and G5.

Glasses were received in 10x10 cm plates from the manufacturing facilities. Samples for groups G1, G2, G3 and G4 were stacked such that their surfaces were not in contact with each other and transferred in a regular package from the manufacturing site to the laboratory. Samples for groups G1 and G2 were placed in a desiccator after their receipt in the laboratory. Samples for groups G3 and G4 were unpacked and thereafter wrapped with an aluminum foil followed by a paper napkin, packaged into vacuum sealed plastic liners and placed into a desiccator after their receipt at the laboratory. Samples for Group G5 were wrapped with an aluminum foil followed by a paper napkin and packaged into vacuum sealed plastic liners immediately after sampling at the manufacturing site. Group G5 samples were transferred to the laboratory in this condition.

Samples for AFM analysis were scored and cut to a size of 1x1 cm. No further scoring or cutting was employed for samples used in Raman, ATR-IR and SR-IR analysis.

Table 3.1. A generic composition of the SLSFG in this study

Compositions (wt %)					
SiO_2	Na_2O	CaO	MgO	Al_2O_3	Others
71-72	13.5-14.5	8-9.5	4-4.5	0.9-1.5	0.3-0.7

Table 3.2. SO_2/SO_3-treated and untreated glass surfaces

Set name	Factory-Line	Dealkalization
G1	F1-L2	-
	F2-L5	SO_2
	F3-L7	-
	F4-L1	SO_3
	F4-L2	-
G2	F1-L2	-
	F2-L5	SO_2
	F3-L7	-
	F4-L1	SO_3
	F4-L2	-
G3	F1-L2	-
	F2-L5	SO_2
	F3-L7	-
	F4-L2	SO_2
G4	F1-L2	-
	F2-L5	SO_3
	F3-L7	SO_2
	F4-L2	-
G5	F1-L1	-
	F2-L5	SO_3
	F3-L7	SO_2
	F4-L2	-

3.2.1. Sample Cleaning

All of the samples used in the analysis were subjected to a laboratory cleaning process before an analysis. Different cleaning procedures have been evaluated in order to determine the optimum procedure and formulation. Accordingly, samples for each group were prepared and cleaned as per below explained procedures:

Sample Preparation for sample set G1: The samples were analyzed in their as sampled condition (i.e. in its condition as sampled from the manufacturing facility, without the use of any vacuum or other surface and environmental exposure protection) with ATR-IR and were placed in the same condition into the humidity cabinet. For AFM analysis, however, a cleaning procedure using ethanol and demineralized water (DM H_2O) in an ultrasonic bath (UB) (Bandelin Elektronic/RK Serie-Sonerex-Digitec) for 5 minutes followed by drying with nitrogen gas was applied.

Sample Preparation for sample set G2: Two different sample preparation procedures were applied on this set:

1. Samples were prepared in the same way as sample set G1.
2. The samples for this set were cleaned in various ways where the effects of cleaning were specifically examined. The factors evaluated for cleaning are: drying using nitrogen gas and ultrasonic bath (UB) treatment in demineralized water (DM H_2O), isopropyl alcohol (IPA), and ethanol. 6 different combinations of these factors were evaluated for the effect of cleaning. Unwashed samples were placed in the humidity cabinet. Table 3.3. provides a summary of the cleaning procedures used in this sample set.

Table 3.3. Sample cleaning procedures used in the sample set G2

	F1-L2	F2-L5	F3-L7	F4-L1	F4-L2
As-Received	√	√	√	√	√
DM H_2O (in UB for 5 minutes) + N_2 gas	√	√	√	√	√
DM H_2O (in UB for 5 minutes) + IPA (in UB for 5 minutes) + N_2 gas	√	√	√	√	√
IPA (in UB for 5 minutes) + DM H_2O (in UB for 5 minutes) + N_2 gas	√	√	√	√	√
DM H_2O (in UB for 5 minutes) + Ethanol (in UB for 5 minutes) + N_2 gas	√	√	√	√	√
Ethanol (in UB for 5 minutes) + DM H_2O (in UB for 5 minutes) + N_2 gas	√	√	√	√	√

Sample Preparations for G3, G4, G5: Samples for this set were cleaned with demineralized water and isopropyl alcohol in an ultrasonic bath (Bandelin Elektronic / RK Serie-Sonerex-Digitec) for 10 minutes. The cleaned samples were dried with nitrogen gas followed by a heat treatment in an oven at 180-200°C for 15 minutes. Figure 3.1. provides a flow chart of the cleaning and drying procedure used for the samples in G3, G4 and G5.

An overall summary of the samples, their surface treatments, where applicable, and corresponding cleaning procedures used in this study is provided in Table 3.4.

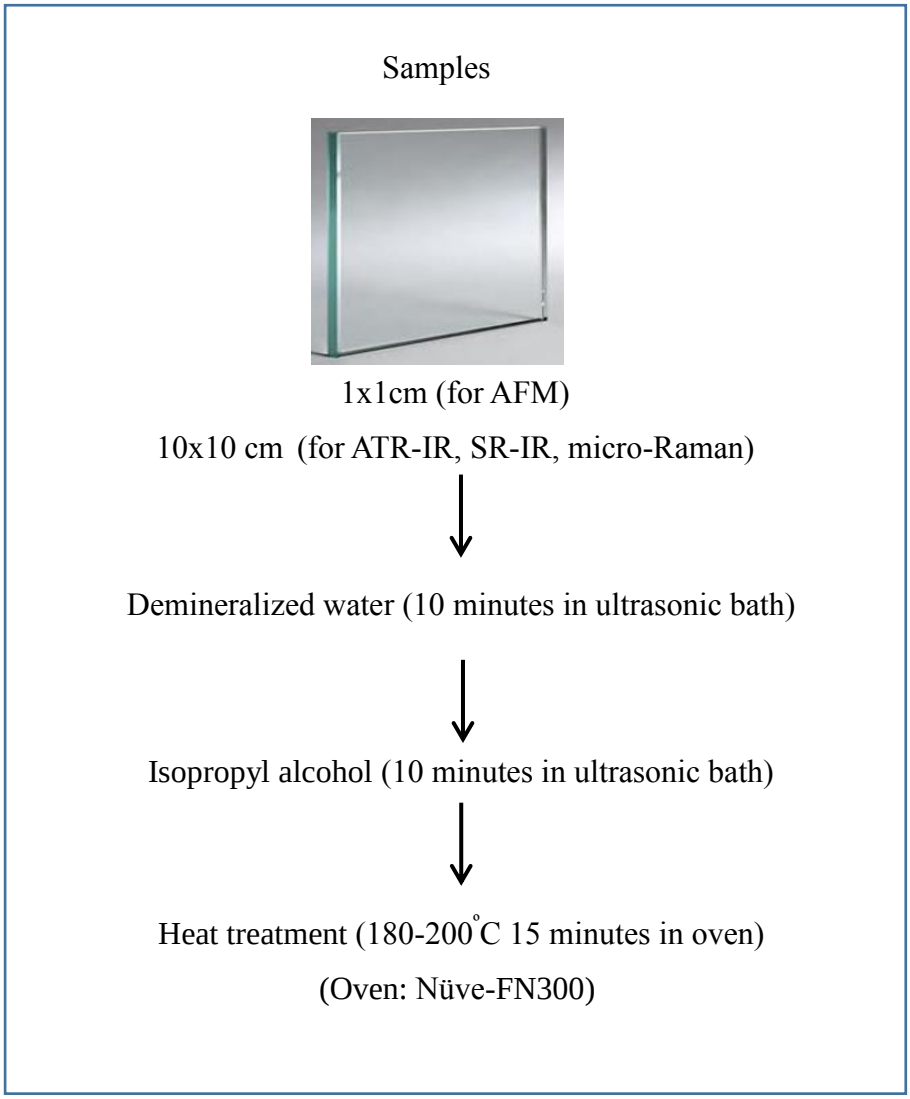

Figure 3.1. Schematic representation of the cleaning procedure for sample sets G3, G4 and G5

Table 3.4. Summary of the samples properties

Set name	Factory-Line	Dealk.	Thickness (mm)	Cleaning procedures
G1	F1-L2	-	4	The SLS float glass samples were cleaned with ethanol and demineralized water in an ultrasonic bath for 5 minutes, and they were dried with nitrogen gas for AFM analysis.
	F2-L5	SO_2	4	
	F3-L7	-	4	
	F4-L1	SO_3	3	
	F4-L2	-	4	
G2	F1-L2	-	4	Various cleaning procedures applied. (Shown in Table 3.3)
	F2-L5	SO_2	4	
	F3-L7	-	4	
	F4-L1	SO_3	4	
	F4-L2	-	4	
G3	F1-L2	-	4	Before the analysis, the surfaces were cleaned with demineralized water and isopropyl alcohol in an ultrasonic bath for 10 minutes. The cleaned samples were dried with nitrogen gas, then they were heated in an oven at 180-200°C for a period of 15 minutes.
	F2-L5	SO_2	4	
	F3-L7	-	4	
	F4-L2	SO_2	4	
G4	F1-L2	-	4	
	F2-L5	SO_3	4	
	F3-L7	SO_2	4	
	F4-L2	-	4	
G5	F1-L1	-	4	
	F2-L5	SO_3	4	
	F3-L7	SO_2	4	
	F4-L2	-	4	

3.3. Weathering of Glass Samples

Weathering of the manufactured glass samples were carried out at Şişecam Science and Technology Center facilities, where the samples were subjected to 40°C and 95% of humidity inside a humidity test cabinet (Ascott-H450T CTG 060) for 7, 14 and 21 days. Figure 3.2. shows a picture of the humidity test cabinet during this study. Glass samples G1 to G4 were aged in the humidity chamber placed at equal spacing and

at an incline with their air sides facing the same direction and angle supported on a plastic frame, as shown in Figure 3.3. Weathering of the G5 samples were carried out with the samples stacked inside a pressure supported (pressure of 1 torr using screws) wooden cabinet with samples separated using a commercial polymer powder as shown in Figure 3.4. It should be noted that samples G1 and G2 were placed into the cabinet in their as sampled condition while samples G3 to G5 were cleaned according to the procedure explained in section 3.2 and 3.2.1 before placing into the cabinet.

Upon completion of the respective weathering period of either 7, 14 or 21 days, the samples were removed from the humidity test cabin and dried by blowing nitrogen gas on both surfaces. G1 and G2 were maintained in a desiccator while G3, G4 and G5 were maintained in vacuum sealed packages for further analysis.

Figure 3.2. Humidity test cabinet at Şişecam (Ascott-H450T CTG 060)

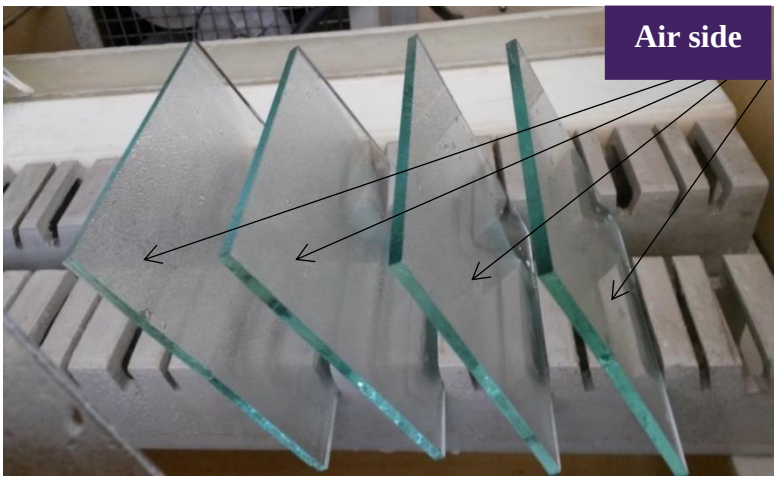

Figure 3.3. The shape of the sample placed in the humidity cabinet for sample sets G1, G2, G3 and G4

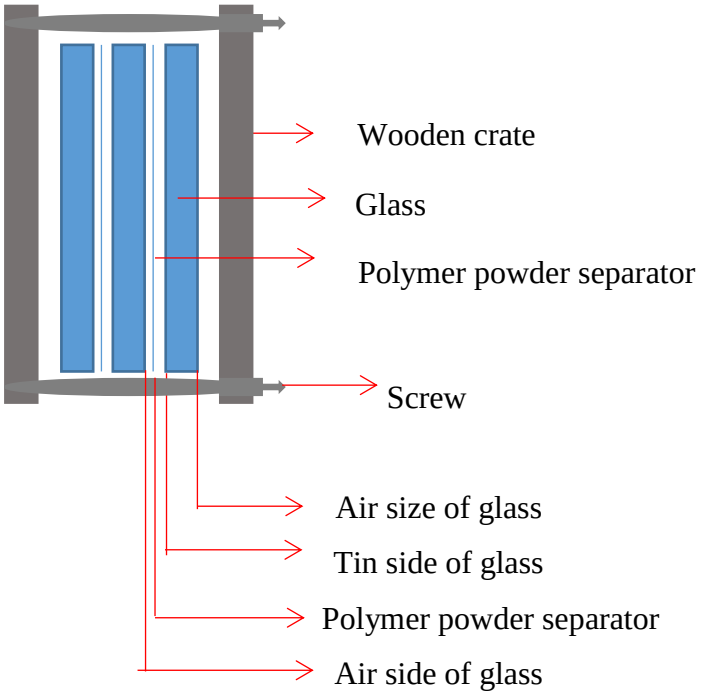

a) Side view of the stacked samples

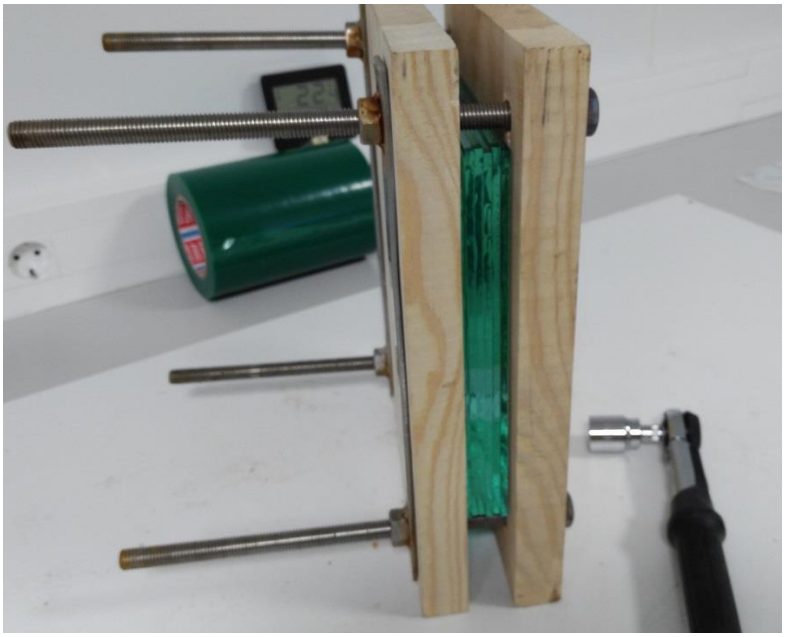

b) Side view of the stacked samples

Figure 3.4. Representation of stacked sample of G5 a) schematically from the side b) side view of the stacked samples

3.4. Analysis methods

3.4.1. Surface Structure using Infrared Spectroscopy

Glass surfaces were studied using a Bruker Hyperion 3000 micro-FT-IR system equipped with a mid-band MCT detector (liquid-N_2 cooled with preamplifier) (Figure 3.5). Two different infrared methods were used, attenuated total reflectance (ATR) and specular reflectance (SR). A gold mirror was used as reference for all FTIR measurements. Spectra were acquired for three spots per sample in 200 scan. The following sections will give the experimental details for the infrared spectroscopy techniques.

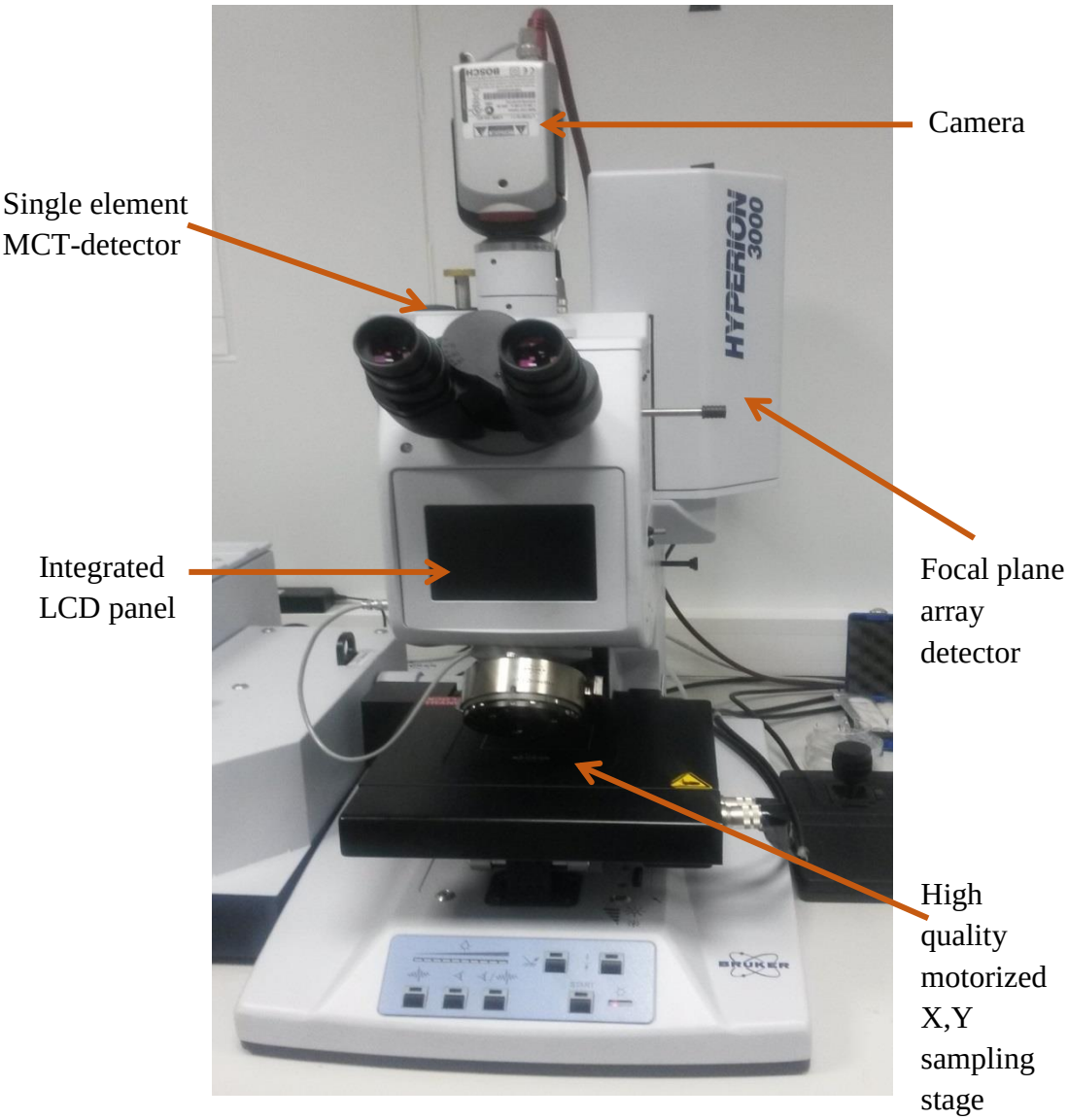

Figure 3.5. Bruker-Hyperion 3000 microscope at Şişecam

3.4.1.1. Attenuated Total Reflection Fourier Transform Infrared (ATR-FTIR) Spectroscopy Measurements

The glasses for the analysis were cut to a size of 10x10 cm from 4-thick plates. Before the ATR analysis, samples were washed with demineralized water (for 10 minutes) and isopropyl alcohol (for 10 minutes) in an ultrasonic bath. The cleaned samples were dried with nitrogen gas, then they were heated in an oven at 180-200ºC for a period of 15 minutes. ATR analysis was performed on the air side after the glass samples were cooled to room temperature in a desiccator.

The ATR-Objective of Bruker Hyperion 3000 FTIR equipment with 45º incident angle was used for the analysis of the glass surfaces. Below conditions were applied during the measurement:

- Objective: 20x mirror objective (Figure 3.6)
- Numerical aperture: 0.6
- Working distance: 6 mm
- ATR crystal material: Germenium Diameter of the ATR crystal tip 100 μm, Measurement spot of the ATR crystal is about 32 μm
- Pressure: 0.5 N over 1 μm^2 sampling area ($5x10^5$ N/cm^2)

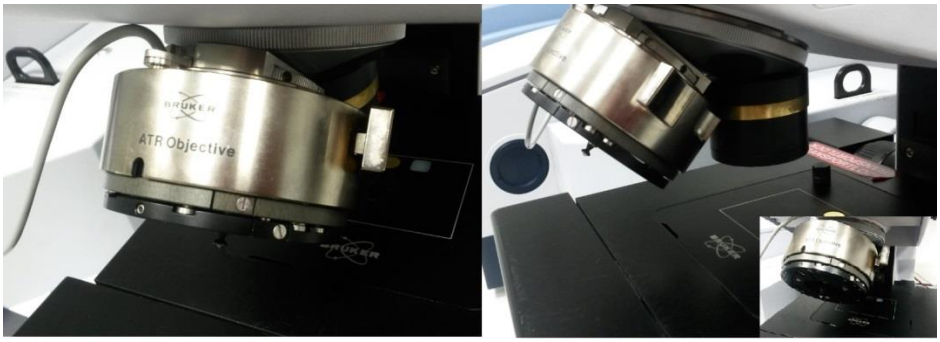

Figure 3.6. Image of the Ge-ATR objective

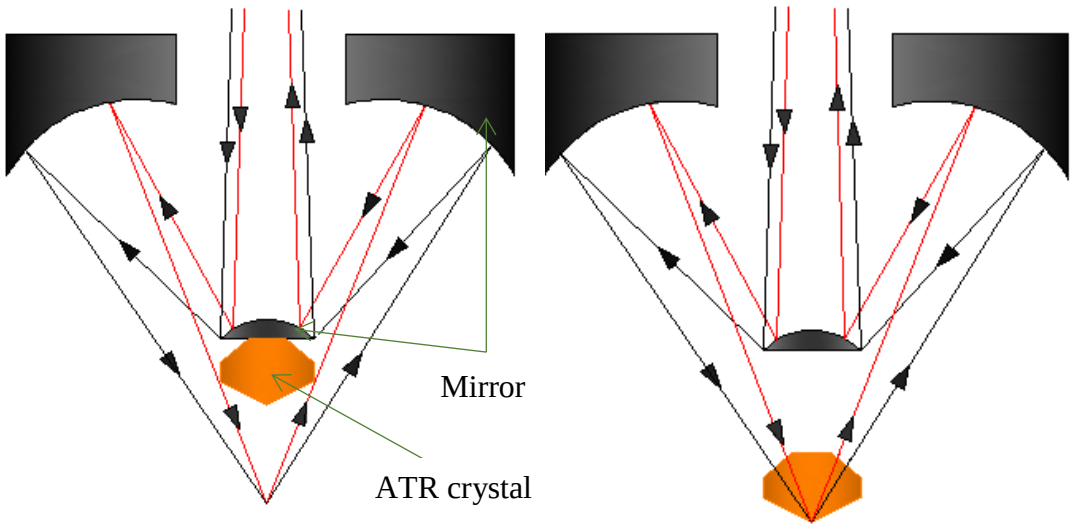

Figure 3.7. ATR-FTIR objective beampath

The FTIR spectra obtained from three separate locations on each sample surface was collected in the 4000 cm^{-1} to 400 cm^{-1} range.

3.4.1.2. Specular Reflectance Infrared (SR-IR) Spectroscopy Measurements

The radiation reflected from a surface is utilized in external reflectance techniques. External techniques is shown in Figure 3.8.

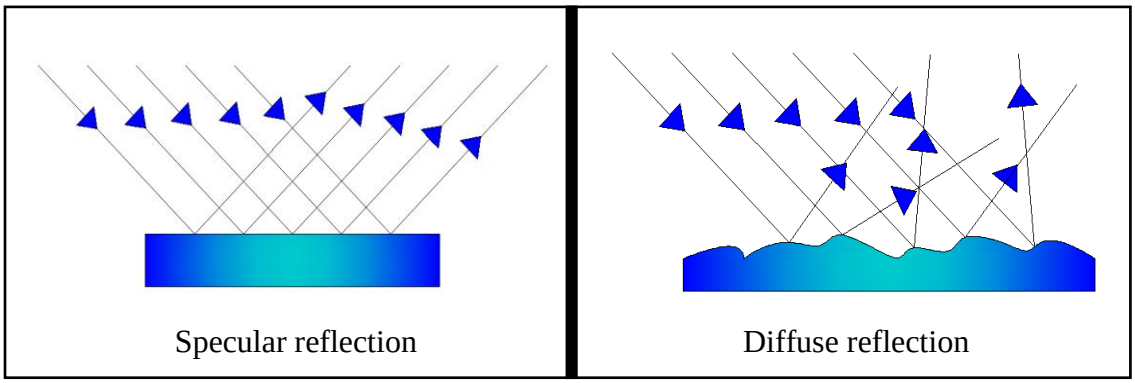

Figure 3.8. Representation of external reflection

In this study, specular reflectance technique was used, diffuse reflectance technique was not. Specular reflectance occurs when the reflection angle equals the

angle of incident radiation, and specular reflectance technique is used for samples which have reflective smooth surface (Khoshhesab, 2012).

This analysis was conducted immediately after ATR-FTIR analysis of the glass surface. SR-IR spectra with NA (numerical aperture of the objective) 0.4: 23.6º (shaded NA 0.17:9.8º) incidence angle from the surface normal direction was obtained (Figure 3.9). The SR-IR spectra were obtained, using a Bruker Hyperion 3000 micro-FTIR system equipped with a 15x infrared microscope objective lens (Bruker Optics Inc.) in the 4000 - 400 cm^{-1} wavenumber region.

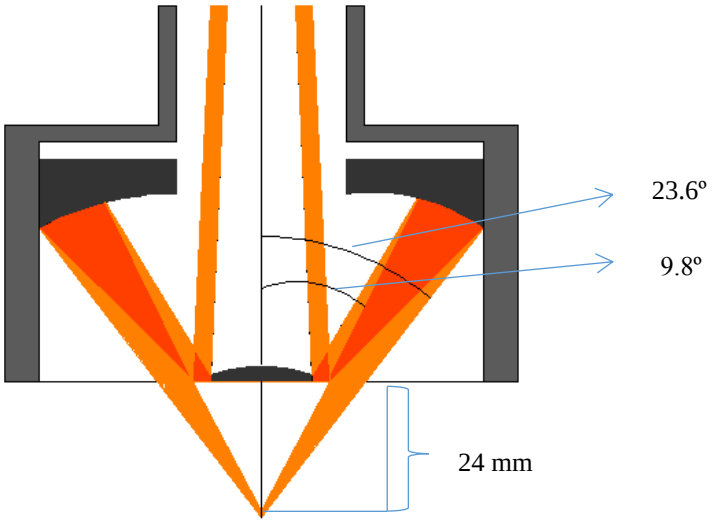

Figure 3.9. SR-IR objective beampath

3.4.2. Micro-Raman Spectroscopy Measurements

Micro-Raman analysis was conducted on the same samples used in conducting the ATR-FTIR and SR-IR analysis. The analysis was done using an XploRA Plus Horiba (Ltd.) system with the laser wavelength at 532 nm, laser power at ~80 mW and spectral resolution (according to measurement parameters) at 2 cm^{-1}, and signal. The measurements were taken from three different locations on the sample surface with a collection time set a 35 seconds.

3.4.3. Grazing Incidence X-Ray Diffraction (GIXRD) Measurements

PANalytical Empyrean was used for GIXRD analysis. The device is set as follows: step size 0.05, time per step 1, time 45 min., in the range of 10-80^0, omega/ entrance angle 0.25^0.

During the manufacturing process, the samples were the unwashed after dealkalization process, and structures on the surface was analyzed. These structures were analyzed without any operation on the glass surface.

3.4.4. Atomic Force Microscopy (AFM) Measurements

The SLS float glass samples were used for surface topography studies using a Bruker MultiMode 8 AFM. The samples were scanned in the PeakForce tapping mode, and a silicon AFM probe tip was used for AFM analysis (nominal tip radius of 10 nm; cantilever length 140-110 μm resonance frequency in the range of 230–410 Hz). Images were obtained by scanning 5μm x 5μm and 15μm x 15μm areas. Prior to AFM investigation, the surfaces were further cleaned by using N_2 gas, demineralized water, IPA and heat treatment (Figure 3.1).

CHAPTER 4

RESULTS AND DISCUSSIONS

4.1. Effect of Sample and Surface Preparation

The importance of preparing the surface of a sample for a surface specific analysis has been discussed for glasses (Kolluru, et al., 2010, Bradley, et al., 2013, Amma, et al., 2015), which suggest that a controlled sample preparation method is needed to represent the true surface of the material. In this study, the need for a careful surface preparation is also considered keeping in mind that the cleaning and surface preparation process should not modify the surface structural changes that have taken place due to the dealkalization and weathering processes on the sample surfaces. Surface preparation methods applied for sample sets G1 through G5 reflect the procedural modifications that have been used throughout this study. There were two critical guides used in deciding the changes in the procedures:

(1) Achieving consistent peak shifts in ATR-FTIR spectra, specifically the shifts in the 950-970 cm^{-1} wavenumber region, was used as one guide.

(2) Obtaining a clean and uncontaminated surface image from AFM analysis. A clean and uncontaminated surface would constitute an image with no foreign particles and no surface residue or film.

Below sub sections will discuss the sample preparation procedures based on the above two criteria.

a) Surface Preparation Based on ATR-FTIR Spectral Analysis:

The results obtained from sample set G1 and G2 show the peak shifts to be highly inconsistent. The results can be found in Table 4.1. This inconsistency highlighted the need for a better and consistent sample surface preparation method. Accordingly, various cleaning procedures were applied as described in detail in section 3.2.1. Table 4.2 shows effects of the various cleaning procedures on the ATR-FTIR spectral peak position in the 970-950 cm^{-1} wavenumber range. These results show no significant changes in the peak position by applying the different cleaning procedures.

The results further show that the sequence of the liquids used in the cleaning process is not important on the surface spectral shifts. The author attributes this to the ATR-FTIR penetration depth of the IR beam, which has been calculated to be in the 0.63-0.65 μm range (Equation 2.1), which is higher than silica gel layer (10-100 nm) on surface (Pantano, 2015, Melcher, et al., 2010) (Table 4.3).

Following the surface washing and cleaning procedures explained above, samples in sets G3 through G5 were prepared by washing only using the procedure given in Figure 3.1. Sample collection and storage was significantly altered for G3-G5 where samples for sets G3 and G4 were taken into vacuum as soon as the samples were received in the research center while samples for set G5 were taken into vacuum as soon as they were picked up from the production line. All of the samples in sets G3-G5 were kept in vacuum until sample analysis.

Results provided in Table 4.1 and Table 4.2 will be presented in the below sub sections to show the effects of surface and sample preparation process, surface dealkalization and weathering on the surface structural changes.

It should be noted that the key differences between the samples prepared in groups G1 and G5 are the cleaning process, the sample stroge condition, the transfer of the samples between sites and the condition of sample stacking in the weathering chamber. These procedures are described in detail in sections 3.2.1 and 3.3.

Based on the data provided in Table 4.1, samples evaluated in sets G1 and G2 show inconsistencies: a key inconsistency can be noted in the shift in band positions between G1 and G2 although both sample sets were prepared identical. Based on this unexpected and unexplained behavior a new cleaning procedure, sample storage and sample transfer method was used to generate samples in groups G3 and G4. Both groups were prepared in a similar way. An additional sample set G5 was also prepared in a similar way G3 and G4 were prepared but this set included the use of polymer beads to help separate glass surfaces from each other during storage and weathering testing.

Table 4.1. ATR-FTIR shifts in peak positions of all sample sets

Samples			AR			AW			7 days			14 days			21 days		
G1	F1-L2	—	966	775	583	—	—	—	961	775	584	966	776	583	979	776	584
	F2-L5	SO_2	964	775	583	—	—	—	962	775	583	966	776	583	977	776	583
	F3-L7	—	964	774	583	—	—	—	962	776	583	966	775	583	975	775	583
	F4-L1	SO_3	962	775	582	—	—	—	960	776	583	964	775	584	971	776	583
	F4-L2	—	964	775	582	—	—	—	962	776	582	964	776	583	968	776	583
G2	F1-L2	—	973	776	583	—	—	—	968	777	584	967	777	583	969	778	582
	F2-L5	SO_2	974	775	582	—	—	—	971	776	583	969	776	582	969	776	583
	F3-L7	—	971	775	582	—	—	—	967	776	583	960	775	582	967	776	582
	F4-L1	SO_3	977	775	583	—	—	—	969	776	583	970	775	582	969	776	582
	F4-L2	—	970	776	582	—	—	—	966	776	583	966	776	582	966	777	581
G3	F1-L2	—	960	775	583	960	775	584	959	775	584	958	776	583	958	776	584
	F2-L5	SO_2	961	776	583	962	775	585	959	775	583	960	776	583	960	776	583
	F3-L7	—	955	774	583	954	774	583	955	774	583	954	775	583	953	775	583
	F4-L2	SO_2	967	776	583	966	776	583	965	776	583	964	776	583	963	776	583
G4	F1-L2	—	961	776	582	961	776	582	961	777	584	959	777	583	959	778	582
	F2-L5	SO_3	957	775	582	956	775	583	956	776	583	955	776	582	954	776	583
	F3-L7	SO_2	955	775	582	954	775	582	953	776	583	952	775	582	952	776	582
	F4-L2	—	959	776	582	959	776	583	959	776	583	957	776	582	957	777	581
G5	F1-L1	—	953	777	580	953	777	581	952	778	581	951	777	582	951	778	581
	F2-L5	SO_3	953	776	583	954	777	581	952	777	579	952	776	580	952	777	582
	F3-L7	SO_2	950	776	580	950	776	581	949	777	579	948	777	580	948	777	580
	F4-L2	—	954	777	581	954	777	581	954	778	580	952	778	580	953	778	581

Table 4.2 shows the ATR-FTIR spectra of group G2, as mentioned above, where the effects of cleaning procedures are provided. Surface cleaning was done using demineralized (DM) water, DM water with IPA, IPA with DM water, DM water with ethanol and ethanol with DM water. The results of the ATR-FTIR peak position changes for each washing condition indicate no significant differences for all the cleaning processes applied in this study. The reason for this is attributed to the penetration depth of the IR beam into the surface, where this penetration has been calculated to be 0.63-0.65 μm (Table 4.3), which is higher than the surface modifications achieved with surface dealkalization and surface weathering.

Table 4.2. Effect of sample surface washing procedure on the ATR-FTIR peak position on set G2 samples

Samples		Dealk.	AR	Only H_2O	H_2O – IPA	IPA - H_2O	H_2O-Ethanol	Ethanol - H_2O
G2	F1-L2	—	973	974	974	974	973	973
	F2-L5	SO_2	974	974	974	975	975	975
	F3-L7	—	971	971	972	972	972	972
	F4-L1	SO_3	977	978	978	977	977	978
	F4-L2	—	970	970	970	970	970	970

Table 4.3. Penetration depth for ATR-FTIR

	θ	n_1	n_2	λ	d_P microns
Ge-ATR	45º	4.01	1.52	950	~0.63
Ge-ATR	45º	4.01	1.52	975	~0.65

b) Surface Preparation Based on AFM Analysis:

The samples that were analyzed for ATR-IR were also examined for their surface morphology using atomic force microscopy (AFM) analysis. As with the ATR-FTIR study, the effects of surface cleaning and preparation were investigated for the AFM evaluations. Figure 4.1 and 4.2 show the AFM image obtained for F2-L5 samples of G2 and G5, respectively. One can notice the presence of white particles, some images showing these at significant amounts, that are of varying size and size distribution. The presence of these particles are thought to have formed as a result of sample handling and are not due to the controlled dealkalization or surface weathering effects investigated in this study. For the cleaning procedure, the effects of washing the surface with demineralized (DM) water, ethanol and isopropyl alcohol (IPA) were investigated. All the samples were subjected to a low pressure nitrogen gas application using a hand held gun in order to dry and remove any physically attached surface debris. Figure 4.1 shows the effects of cleaning the surface using DM water and ethanol and Figure 4.2 shows the effects of cleaning with DM water and IPA. A comparison of these images shows a significant reduction in the white particles after the DM water and IPA treatment, which has not been observed for DM water and ethanol. The comparison suggests that the white surface features have remained after washing, causing the author to think these have been fixed on the surface due to the application of ethanol. Although not shown here, a surface film was also observed with the ethanol

cleaning that was not found with IPA. This was noticed with the scans showing blurry features when this surface film was present. Overall, the findings for an effective cleaning of the sample surfaces for AFM analysis point towards the use of DM water followed by IPA. Accordingly, combination of DM water followed by IPA was determined as the optimal cleaning liquids for this study.

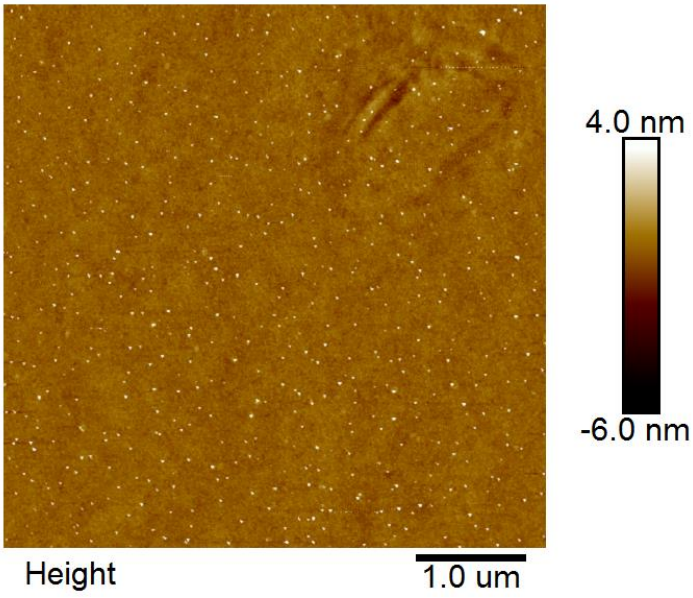

(a)

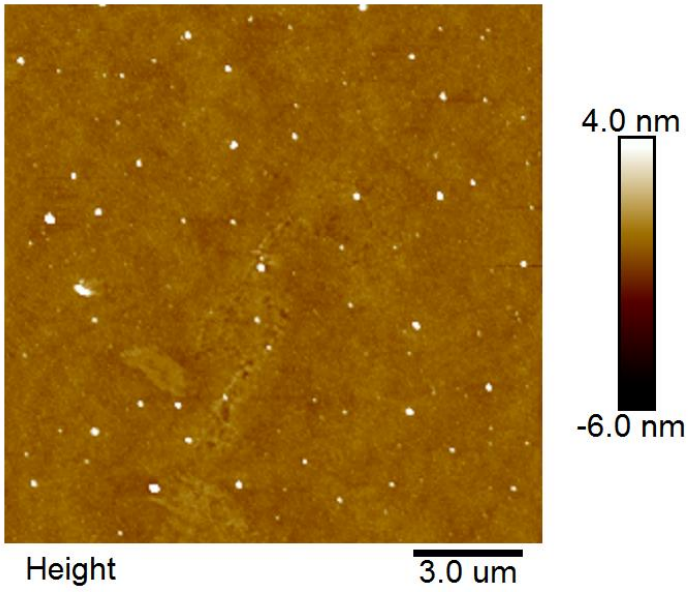

(b)

Figure 4.1. AFM images showing the surface morphology of sample G2_F2-L5 where the sample surface was cleaned using the use of DM water and ethanol: (a) AFM scan size at 5µm x 5µm (b) AFM scan size at 15µm x 15µm

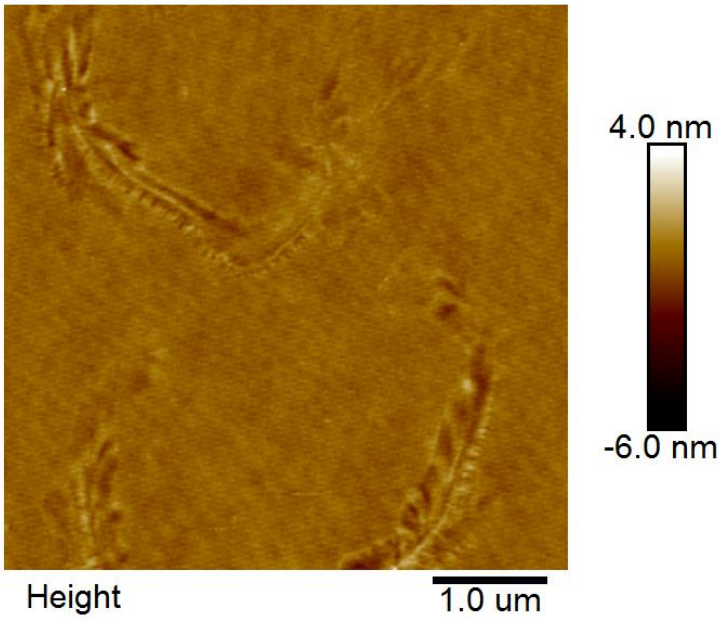

(a)

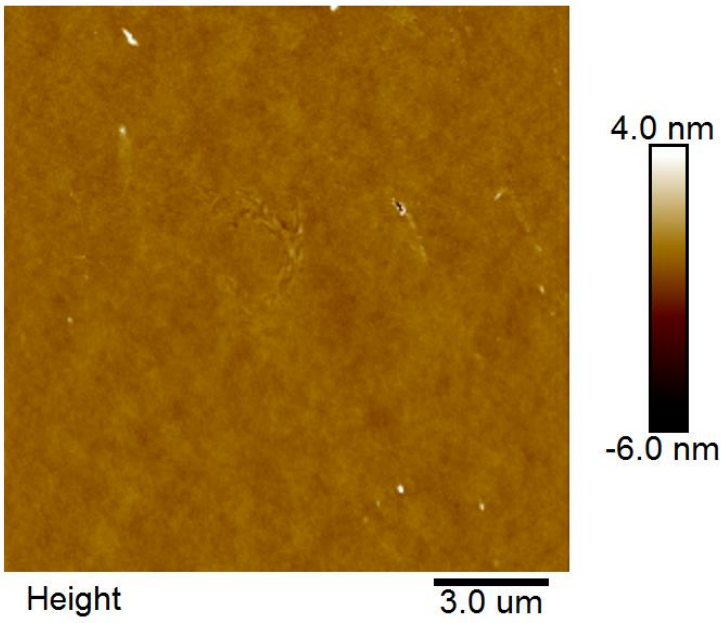

(b)

Figure 4.2. AFM images showing the surface morphology of sample G2_F2-L5 where the sample surface was cleaned using the use of DM water and IPA:
(a) AFM scan size at 5µm x 5µm (b) AFM scan size at 15µm x 15µm

4.2. Characterization of the Surface Features and Structure

The characterization of the surface structure and morphology will be presented in this section. The first section will present the findings on the structural changes using infrared (attenuated total reflection-Fourier transform infrared – ATR-FTIR – and specular reflection – SR – infrared spectroscopy) and Raman spectroscopy analysis results. The second section will present the surface morphology of the glasses. Surface morphology will be reviewed regarding two aspects: (1) characterization and morphology of the surface residue formation after SO_2/SO_3 gas dealkalization using scanning electron microscope (SEM) and grazing incidence x-ray diffraction (GIXRD) and (2) findings on the effects of weathering and dealkalization using atomic force microscopy (AFM)

4.2.1. Characterization of Surface Features

4.2.1.1. Effects of SO_2 and SO_3 Gas Dealkalization on Surface Morphology

It is known that a layer of sodium sulfate forms on the surface of the glass after it has been treated with a sulfur containing gas at elevated temperatures (Şentürk, 1992) (Rancoule, et al., 2006). Figure 4.3 and 4.4 shows this formation after the glass has been subjected to a heat treatment below its glass transition temperature in an SO_2 gas and SO_3 containing atmosphere, respectively. Both gas treatments show the surface formations to be formed of particles that have been clustered together. The surface, therefore, does not appear to have been completely covered with a layer. This clustering versus a lack of a covered layer formation may have implications on the nature of the dealkalization and the corresponding structural modifications that has taken place on the surface layers of the glass. The morphology of the surface residue also appears to be different when treated with SO_2 or SO_3 containing gases. It should be mentioned here that the images provided for the two cases may not be representative and further investigation into such potential difference, if any, needs to be conducted and verified. In common industrial practice, this layer is removed by washing leaving a pristine surface.

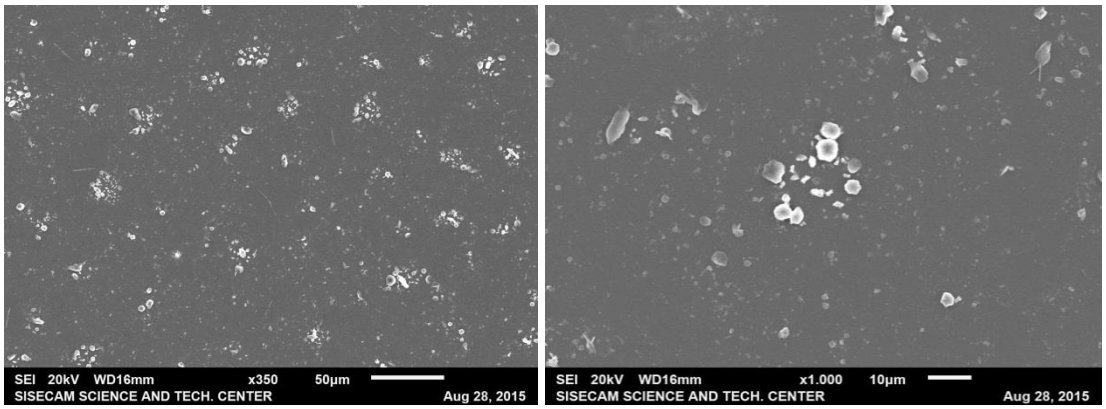

(a) (b)

Figure 4.3. SEM image of unwashed G2_F2-L5(SO_2) sample: (a) x350 magnification and (b) x1,000 magnification (SEM: JEOL – JSM 6010 LV)

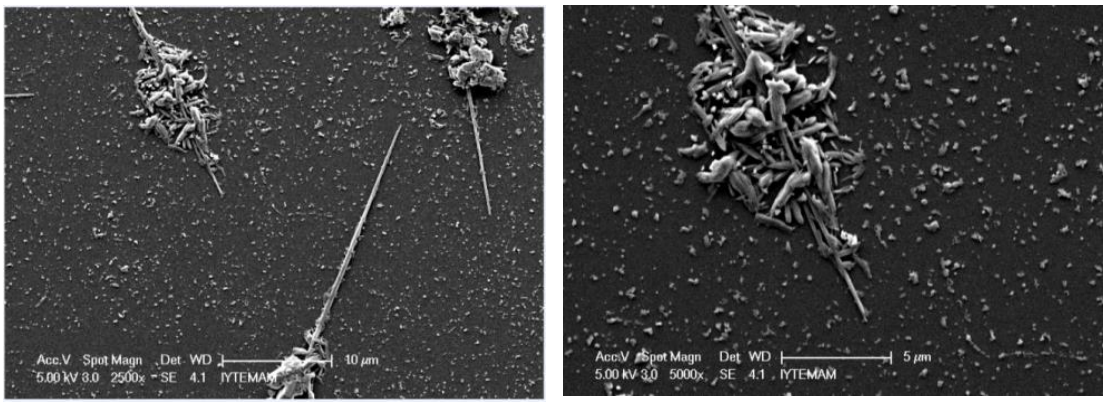

(a) (b)

Figure 4.4. SEM image of unwashed G2_F4-L1(SO_3) sample: (a) x2,500 magnification and (b) x5,000 magnification (Philips XL 30SFEG)

The analysis of the form and crystal structure of the formations on the dealkalized glass surfaces was conducted using GIXRD measurement. Figure 4.5 shows the results of this analysis. The spectral peaks and crystal phase match analysis show that the surface formations are of a disodium sulphate (Na_2SO_4) structure. Pyrosulphate and others sulphate structure, as shown by Rancoule et. al. (Rancoule, et al., 2006), was not observed on the surfaces. Na_2SO_4 phase is found at different rates in both samples. It can be said that this salt layer formation is relatively more on the G5_F2-L5 sample due to the presence of more intense peaks obtained from its spectra.

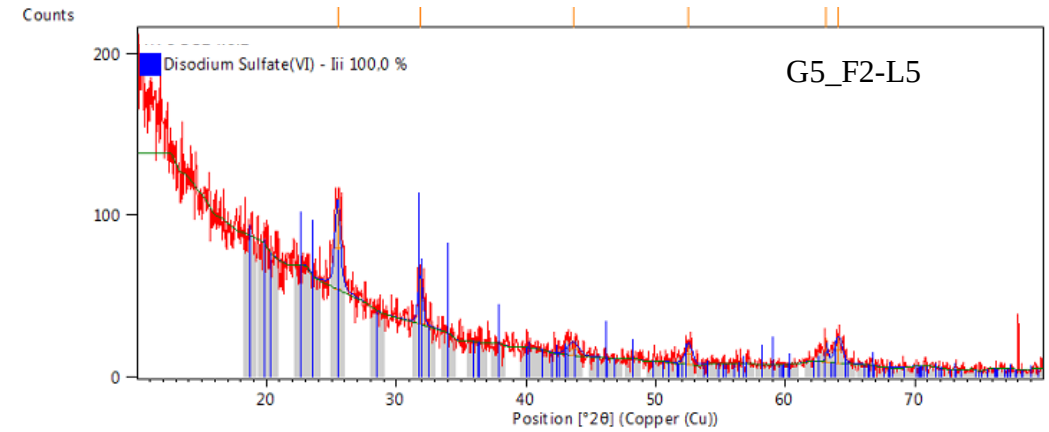

(a)

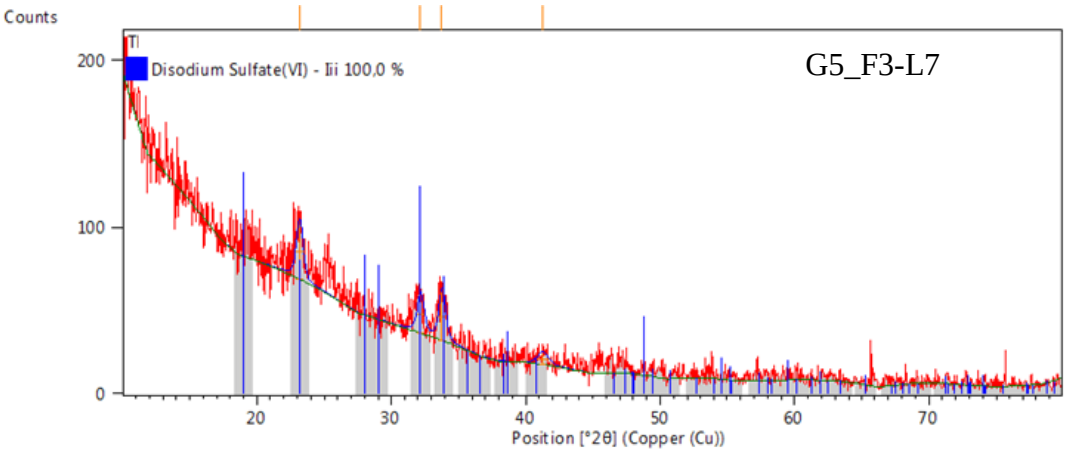

(b)

Figure 4.5. GIXRD analysis result for (a) G5_F2-L5 and (b) G5_F3-L7

The surface morphology of the gas dealkalized samples after washing the surface residue was determined using atomic force microscope (AFM) analysis. Each sample was analyzed from at least three different locations. Figure 4.6. shows the formation of what appears to resemble micro-cracks on the SO_2/SO_3-treated and washed surface. It is important to note that these micro-cracks were not observed on surfaces that have not been subject to sulfur containing gas heat treatment. Accordingly, these formations are attributed to the dealkalization reactions associated with the sulfur containing gases. Although there is no side by side evidence, these micro-cracks like features are thought to be associated with the sulfate salts formed on the surface (see Figure 4.3. and 4.4.) and that they may have developed below these clusters at some point during the heat treatment process. Figure 4.6.d shows the surface of a glass treated with SO_3 containing gas, which illustrates that the surface dealkalization with

sulfur containing gases can develop smaller and highly populated micro-crack like formations. While we have not shown the results in this write-up, other SO_3 treated glass surfaces have shown these cracks to be of similar nature to SO_2 gas treated surface formation. Accordingly, these smaller and densely populated micro-crack formations seen in Figure 4.6.d. are not attributed to SO_3 gas treatment but to other unexplained factors.

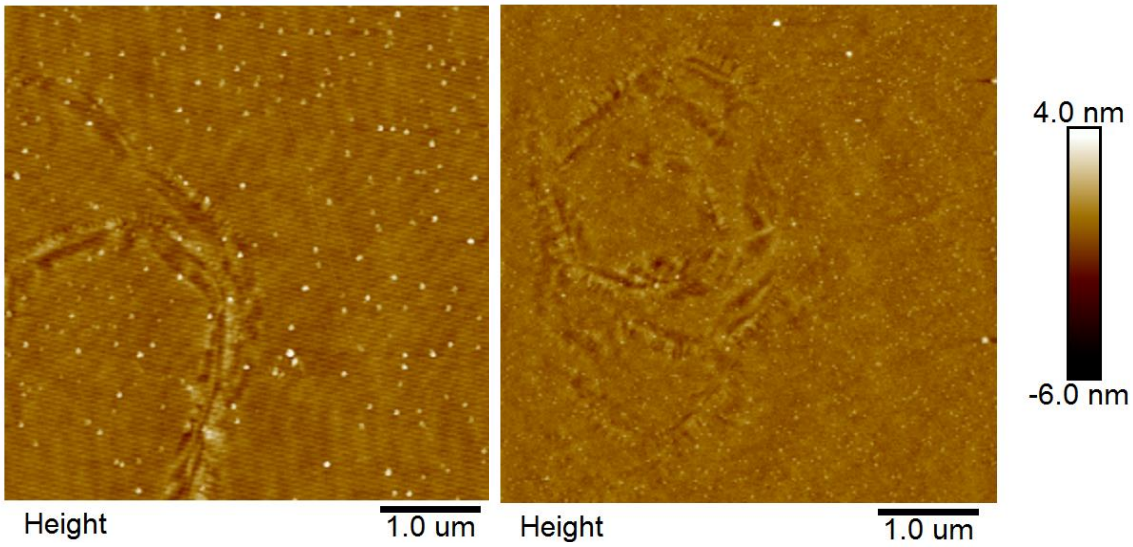

(a) SO_2-treatment air side of G1_F2-L5 (b) SO_2-treatment air side of G2_F2-L5

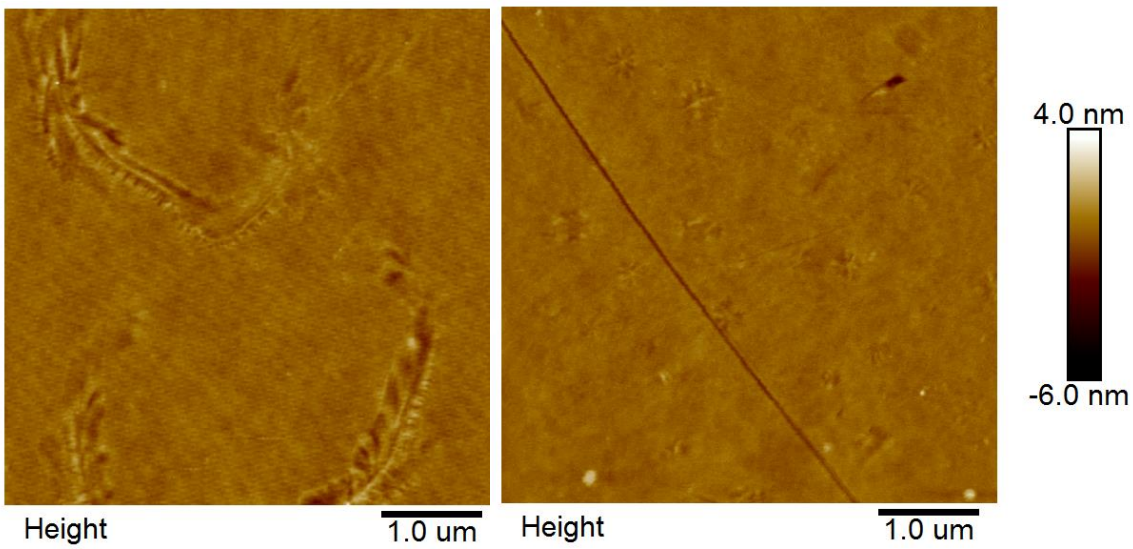

(c) SO_2-treatment air side of G3_F2-L5 (d) SO_3-treatment air side of G4_F2-L5

Figure 4.6. 5µm x 5µm AFM image of air side of F2-L5 (a) G1_F2-L5 (b) G2_F2-L5 (c) G3_F2-L5 (d) G4_F2-L5 (e) G5_F2-L5

(cont. on next page)

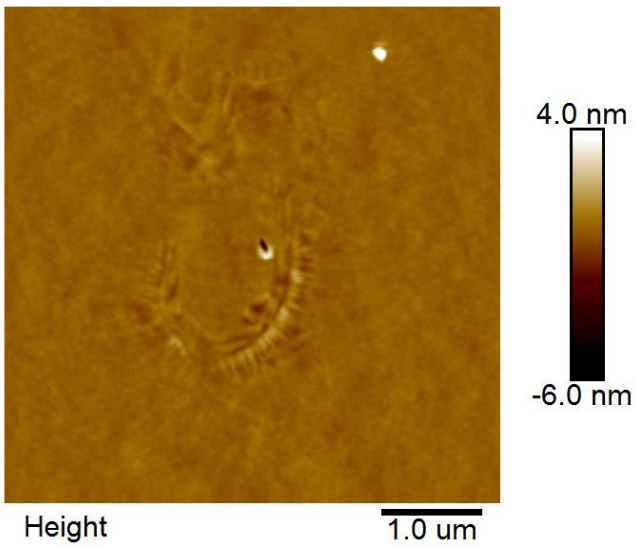

(e) SO_3-treatment air side of G5_F2-L5

Figure 4.6. (cont.)

4.2.1.2. Effects of Weathering on Surface Morphology

Samples with and without any dealkalization using a sulfur containing gas were exposed to 95% relative humidity at 40°C for periods of 7, 14 and 21 days. The effects of this weathering treatment at 21 days on the surface morphology for sample set G5 are shown in Figure 4.7. The figure also shows the non-weathered surfaces to allow for a comparison. The figures include the roughness values measured on images collected at 15x15µm size. Although one may conclude that the roughness of the surface increases with weathering, it will be difficult to come to this conclusion based on the analysis and results provided in these figures. This is because of the difficulty in finding an exact comparison of the surface features, especially the micro-crack like formations, to show the difference between the before and after weathering. Accordingly, based on the results from this evaluation it is not possible to explain the effects, if any, of weathering on surface topography and morphology.

Roughness R_q: 0.140 nm

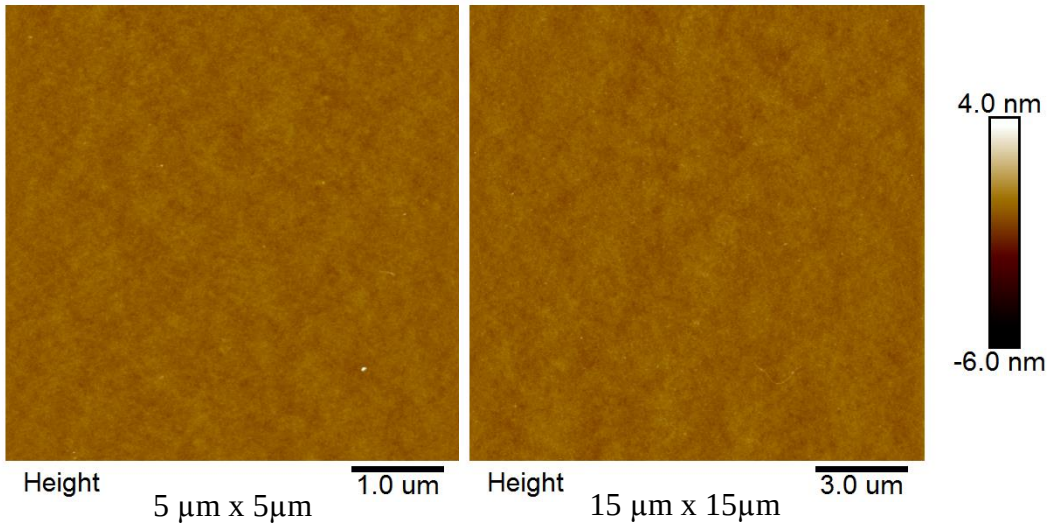

(a) F1-L1 AR

Roughness R_q: 0.190 nm

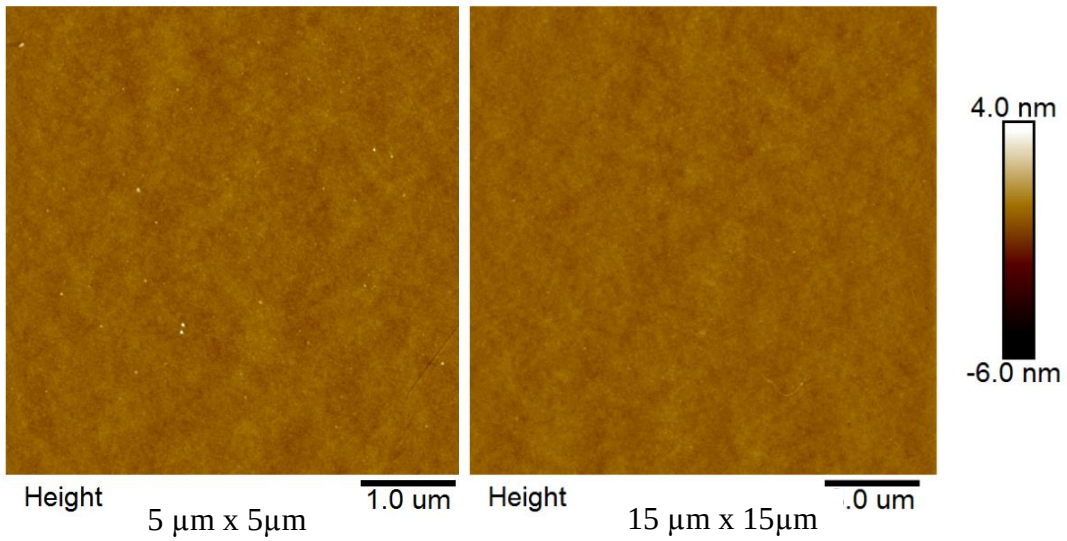

(b) F1-L1 21 days

Figure 4.7. AFM images of the G5-AR and G5-21 days samples (a) F1-L1 AR (b) F1-L1 21 days (c) F2-L5 AR (d) F2-L5 21 days (e) F3-L7 AR (f) F3-L7 21 days (g) F4-L2 AR (h) F4-L2 21 days

(cont. on next page)

Roughness R_q: 0.166 nm

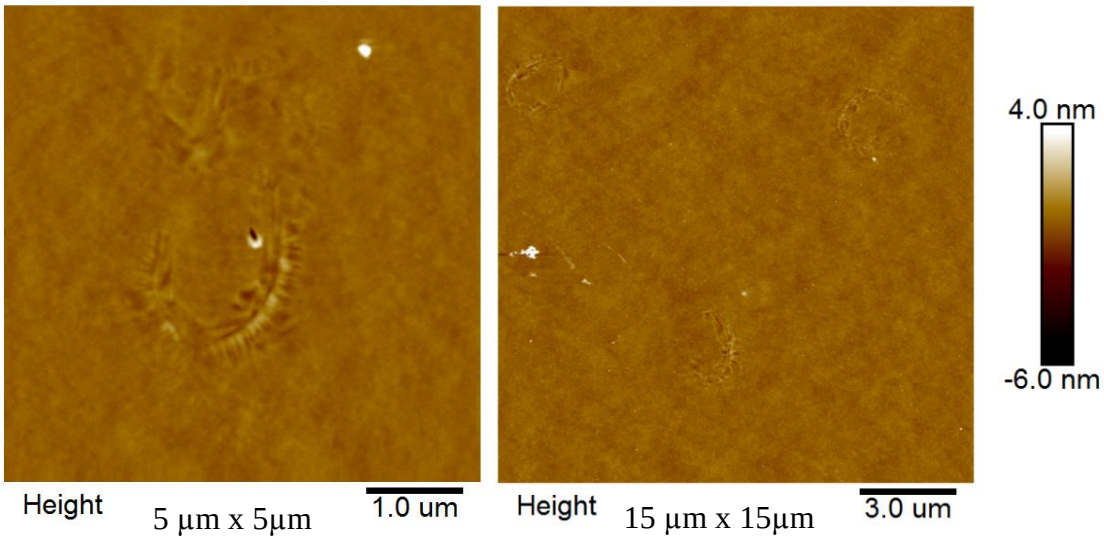

(c) F2-L5 AR

Roughness R_q: 0.170 nm

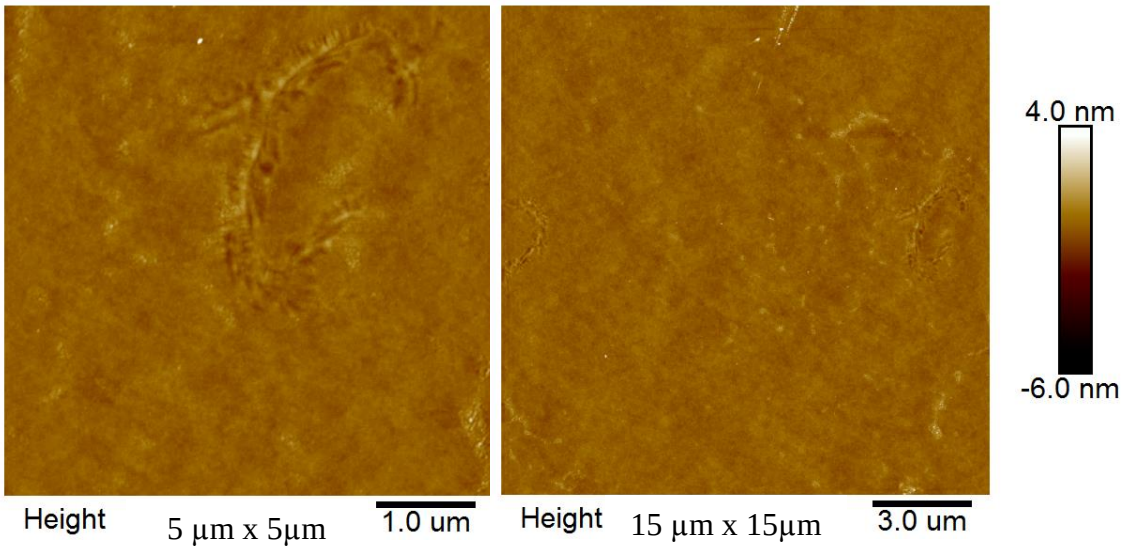

(d) F2-L5 21 days

Figure 4.7. (cont.)

Roughness R_q: 0.156 nm

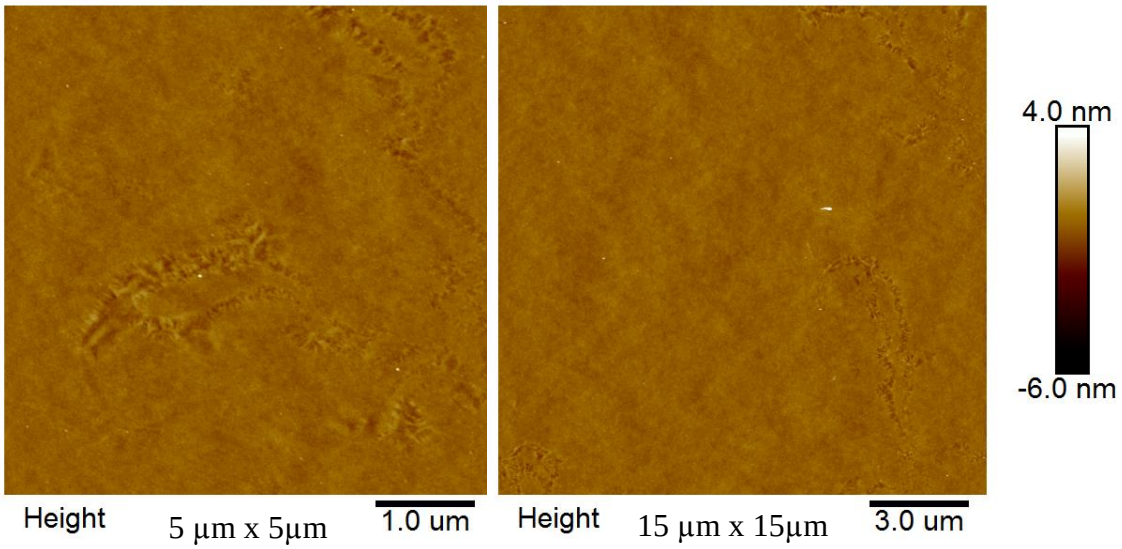

(e) F3-L7 AR

Roughness R_q: 0.177 nm

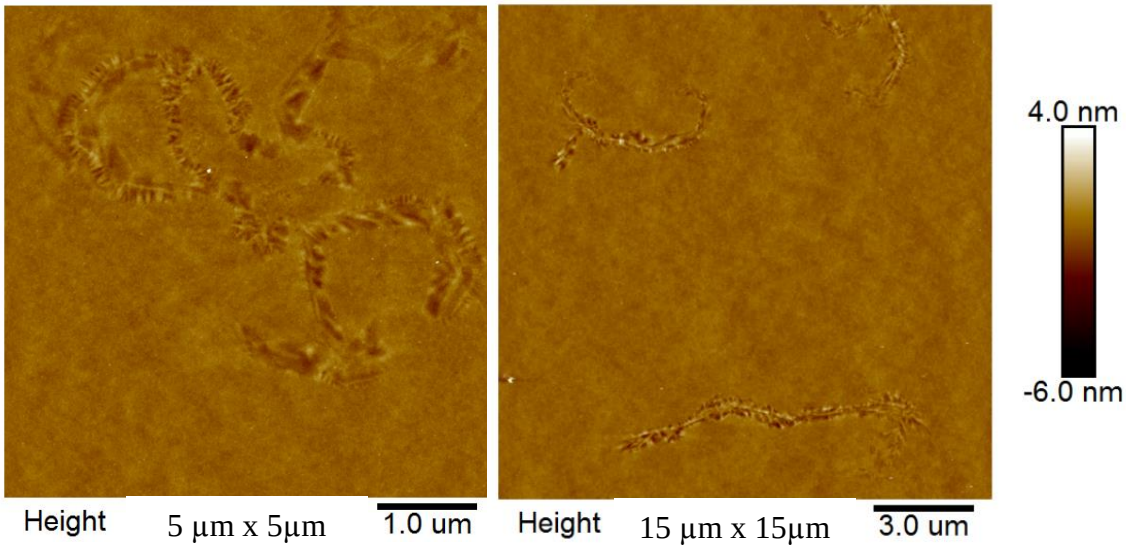

(f) F3-L7 21 days

Figure 4.7. (cont.)

Roughness R_q: 0.157 nm

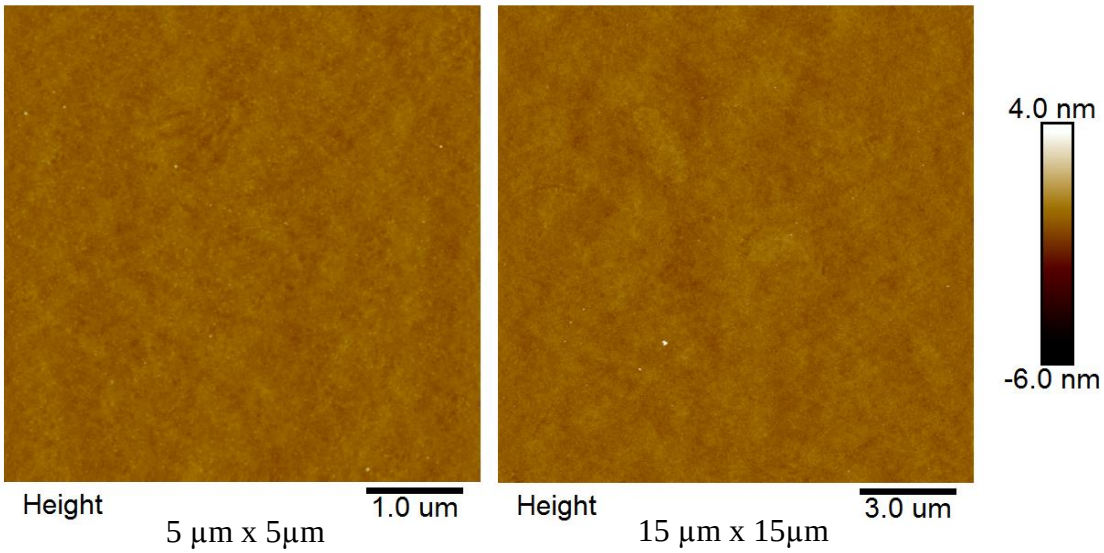

(g) F4-L2 AR

Roughness R_q: 0.177 nm

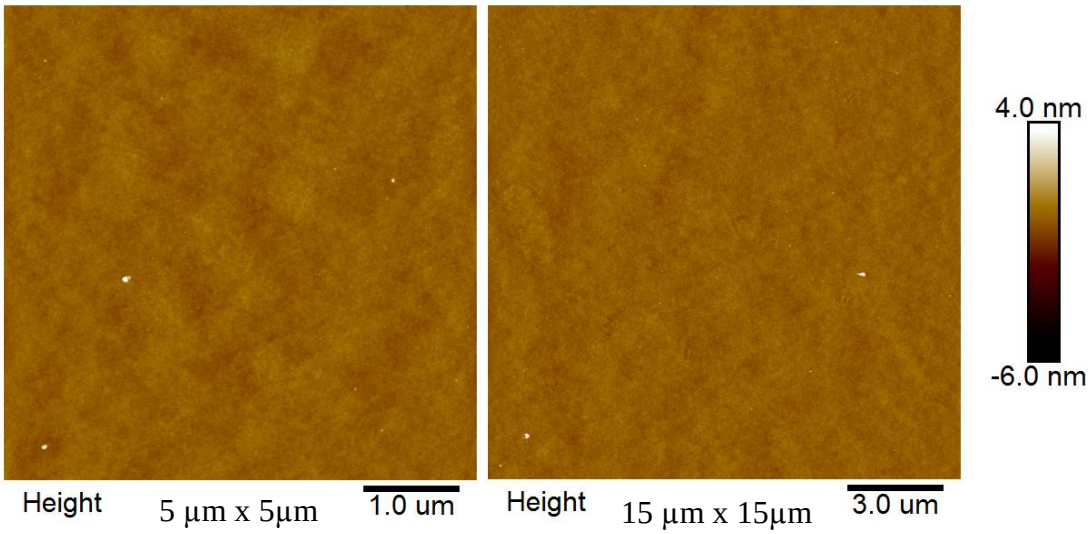

(h) F4-L2 21 days

Figure 4.7. (cont.)

4.2.2. Characterization of Surface Structure

4.2.2.1. ATR-FTIR Analysis:

ATR-FTIR results from the spectra will be discussed in two sections: analysis between 3800 – 1550 cm^{-1} range and between 1000 – 400 cm^{-1} range.

Analysis of spectra between 1000 – 400 cm^{-1}

The peaks in this spectra region correspond to the structural formation of glass network. There are three critical peak positions that appear in this region: peaks between the 970-950 cm^{-1} corresponding to the $Si\text{-}O^{-}(\text{modifier ion})^{+}$, at 600 cm^{-1} corresponding to Si-O-Si bending and at 760 cm^{-1} corresponding to Si-O-Si symmetric stretching vibrations (Table 2.4). Table 4.1 gives a complete listing of the wavenumber positions of the peaks for the different set of samples and weathering treatments. It can be seen from this table that of the three vibrational bands, 970-950 cm^{-1} is the only structural formation that shows variation in the form of a shift in the peak position. The inserts in Table 4.4 illustrate the changes in the peak position corresponding to the 970-950 cm^{-1} range for G3, G4 and G5. Accordingly, any changes in the surface structure due to the effects of dealkalization and weathering condition is therefore discussed based solely on the shifts in the 970-950 cm^{-1} region. Results suggest that the lowest wavenumber positions belong to samples obtained from F3-L7 evaluated for sets G3, G4 and G5, which show the position to be between 955-950 cm^{-1}.

Figure 4.8 show representative ATR-FTIR spectra that have been selected from a collection of surface spectral analysis results obtained for sample set G5. These spectra have been measured on the air surface of the glasses in their as-received (AR), after washing (AW), and after weathering treatments at 7, 14 and 21 days for sample set G5. The spectra for sample sets G3 and G4 are not shown here to help the reader follow the context and are given in Appendix A.

Table 4.4. Illustrate the changes in the peak position at 970-950 cm^{-1} for sample sets G3, G4 and G5

Samples			AR	AW	7 days	14 days	21 days
G3	F1-L2	—	960	960	959	958	958
	F2-L5	SO_2	961	962	959	960	960
	F3-L7	—	955	954	955	954	953
	F4-L2	SO_2	967	966	965	964	963
G4	F1-L2	—	961	961	961	959	959
	F2-L5	SO_3	957	956	956	955	954
	F3-L7	SO_2	955	954	953	952	952
	F4-L2	—	959	959	959	957	957
G5	F1-L1	—	953	953	952	951	951
	F2-L5	SO_3	953	954	952	952	952
	F3-L7	SO_2	950	950	949	948	948
	F4-L2	—	954	954	954	952	953

Analysis of spectra between 3800 – 1550 cm^{-1}

The spectral peaks in this range indicate presence of water (Table 2.4): peaks between 3800 and 2450 cm^{-1} is attributed to the variation of hydrogen bonding interactions in H_2O and OH and peaks between 1650-1550 cm^{-1} show the bending vibration of the molecular water. The spectra at 3800-3500 cm^{-1}, 2600-2450 cm^{-1}, 1650-1550 cm^{-1} for the five sets of samples for the as-received glasses do not show a defined pattern to allow for a correlation or a trend. Accordingly, the results suggest that it is not possible to determine any significant effect of sample preparation and especially sample transfer from one location to another regarding the nature and relative amount of pyhsisorbed water on the surface.

Amma et al. (Amma, et al., 2016) note the presence of a peak at 2800 cm^{-1} band attributed to the strong bonding of Si-OH stretching vibrations to the non-bridging oxygens. These peaks were not observed in this study. As for the weathered samples, while the 21 day treatment appears to show increased intensity, the results do not show a clear trend from as-received to 21 days of treatment.

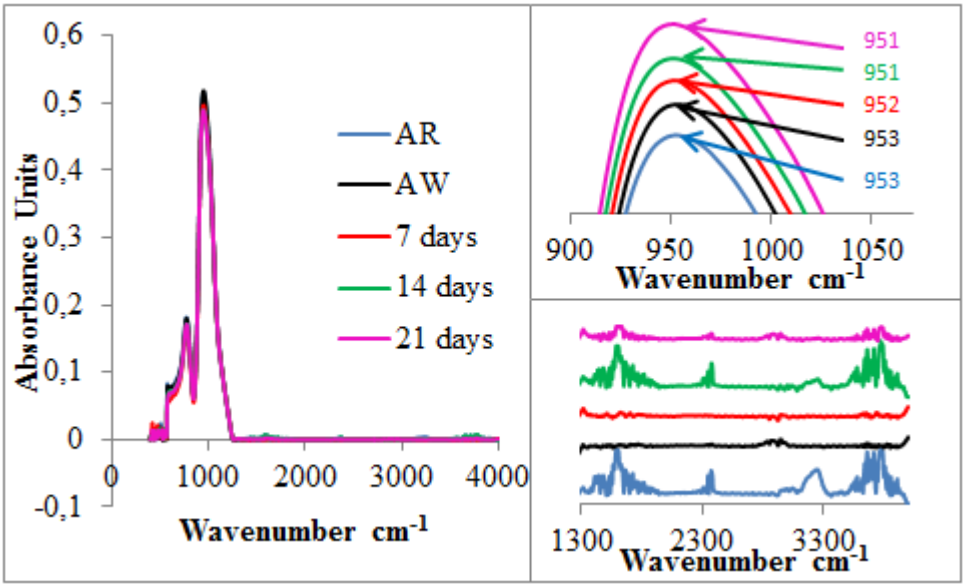

(a) G5_F1-L1

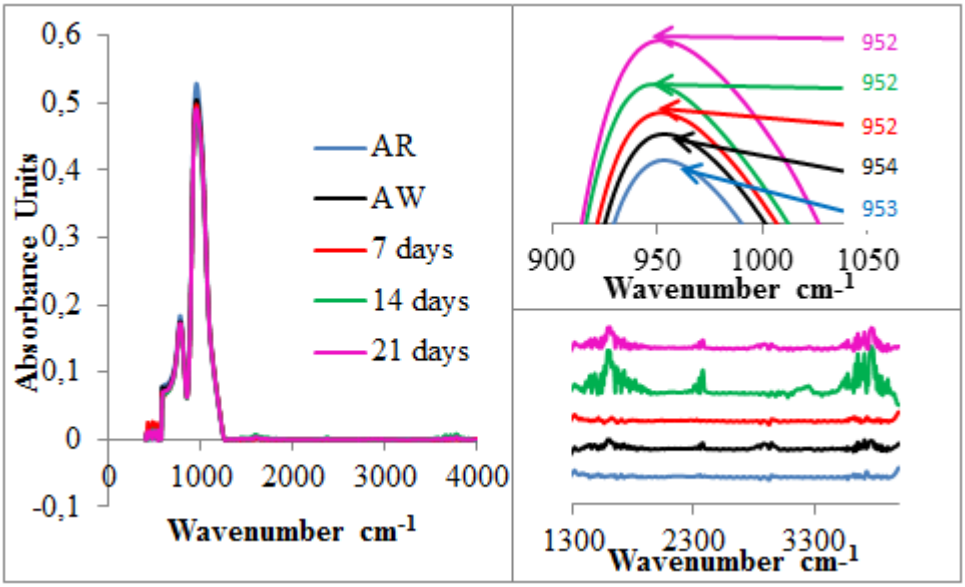

(b) G5_F2-L5

Figure 4.8. Representative ATR-FTIR spectra for sample set G5

(cont. on next page)

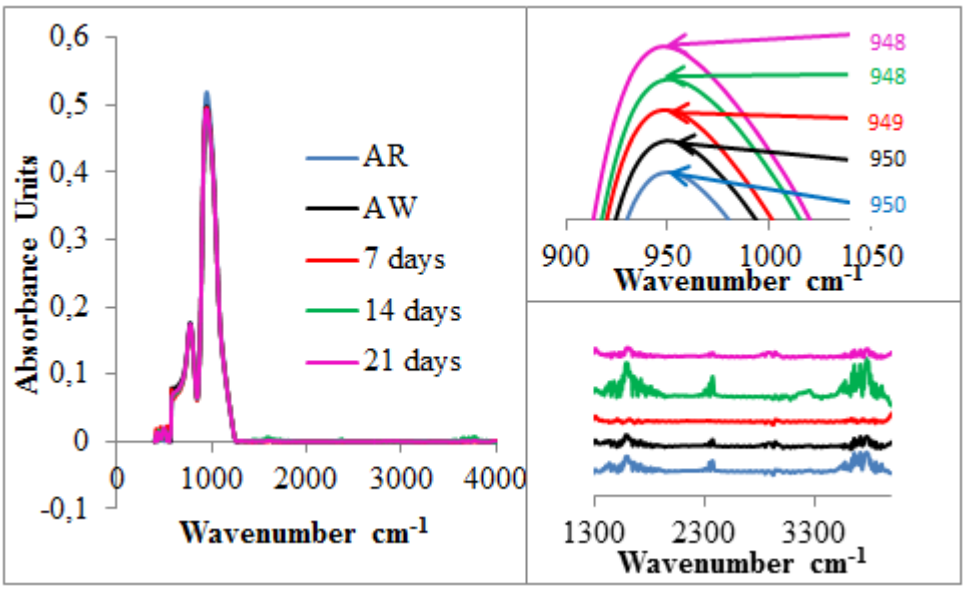

(c) G5_F3-L7

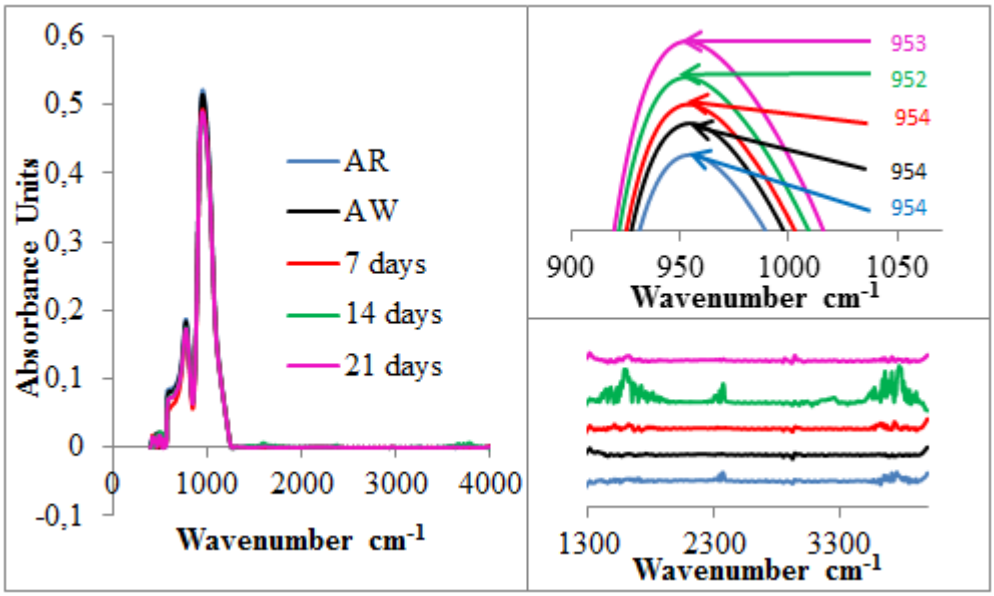

(d) G5_F4-L2

Figure 4.8. (cont.)

4.2.2.1.1. Effects of Dealkalization on ATR-FTIR:

Figure 4.9. shows the effects of SO_2, SO_3 and no sulfur gas treatment on the peak positions obtained from ATR-FTIR spectra discussed in the previous section. The overall comparison of the effects of peak position with and without sulfur gas treatment suggests a wide scatter within each group. This scatter implies that sulfur gas treatment does not have any statistically significant effects. However, when one looks further into the data sets, it can be realized that for sample set G4 and G5, the peak position shifts to lower wavenumber with SO_2 gas treatment while this is the reverse for sample set G3. Considering the fact that sample preparation is different between sets G5 and G3 and G4 combined, it can be argued that there seemingly may be an effect of SO_2 treatment. However, the opposite finding from set G3 negates this conclusion, leaving us to state that the ATR-FTIR results show so effect of sulfur gas treatment on the structure of the surface layer. This conclusion may, indeed, have logical grounds as we know that the penetration depth of the IR beam is further than the depth of the surface modified layer.

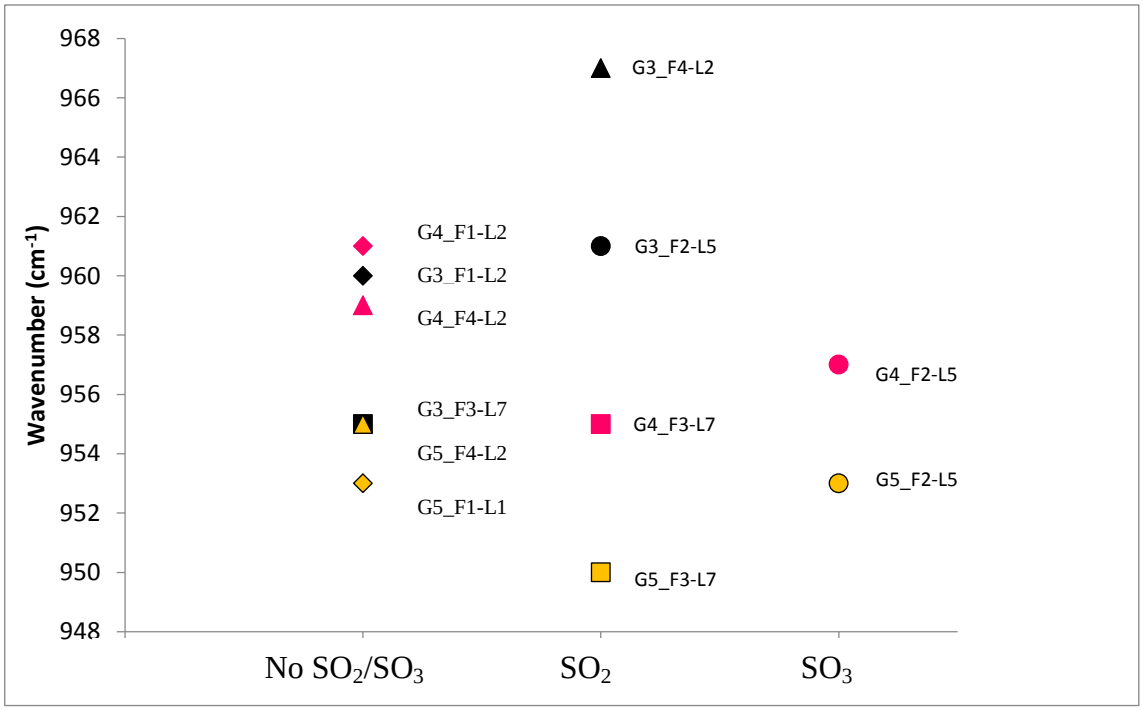

Figure 4.9. ATR-FTIR peak positions for sample sets G3, G4 and G5

4.2.2.1.2. Effects of Weathering on ATR-FTIR:

Figure 4.10 shows the change in the ATR-FTIR peak positions as a function of weathering periods of 7, 14 and 21 days for the band at the 950-970 cm^{-1} wavenumber range. The peak positions for the as-received surfaces are also shown for comparison purpose. These results are shown for sample sets G3, G4 and G5 where sample preparation protocols for sets G3 and G4 were different than for set G5. Results in each set are given for samples originating from four different locations. The change in peak positions shown in the figures do not appear point to a significant trend, i.e., there is no clear evidence of a decreasing or increasing peak position as the weathering period is increased. That said, the data appears to shows a slight decreasing trend as the surface is exposed to increasing weathering treatment period. Weathering is expected to cause the surface alkali ions to exchange with the protons from the water molecules thereby causing a dealkalization to take place. Because this dealkalization involves the presence of water and because the weathering treatment takes place at 40ºC (relatively low temperature compared with high temperature gas dealkalization), one can expect the dealkalized surface layer to be in the form of hydrated silica.

The results from Figures 4.10 also show a difference in peak position when comparing the origin of the samples. This appears to hold true regardless of whether the sample has been exposed to weathering or not. A common finding from all three sets of results shows that samples originating from source F3-L7 are at a lower peak intensity position versus the other three locations. The positions of the remaining three sources show a dependence on the sample set: set G3 suggests a wider gap between source F1-L2 compared with source F2-L5 and F4-L2; set G4 shows sources F2-L5 and F4-L2 to also separate in the peak position. The decreased peak positions suggest lower alkali association with the silica tetrahedra, indicating a larger degree of dealkalization and silica cross linking. The same decrease in the peak position can also be attributed to the formation of compressive stresses limiting the frequency of vibrations associated with the $Si\text{-}O^{-}(\text{modifier ion})^{+}$ stretching vibrations. With these two possible causes in mind, we expect the probable surface structural differences between the four sources to be caused by the differences in the processing parameters applied to the glass during manufacturing at the four locations.

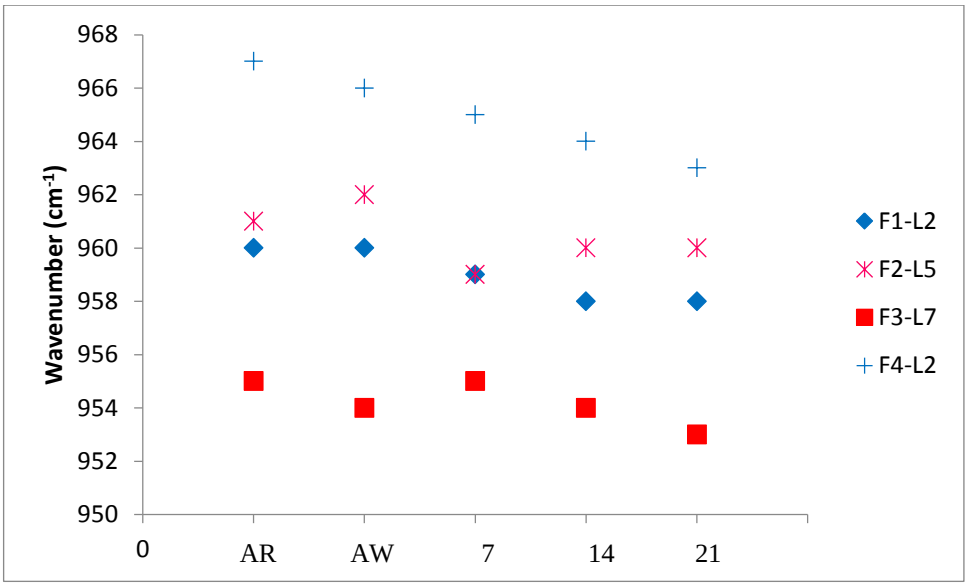

(a) G3

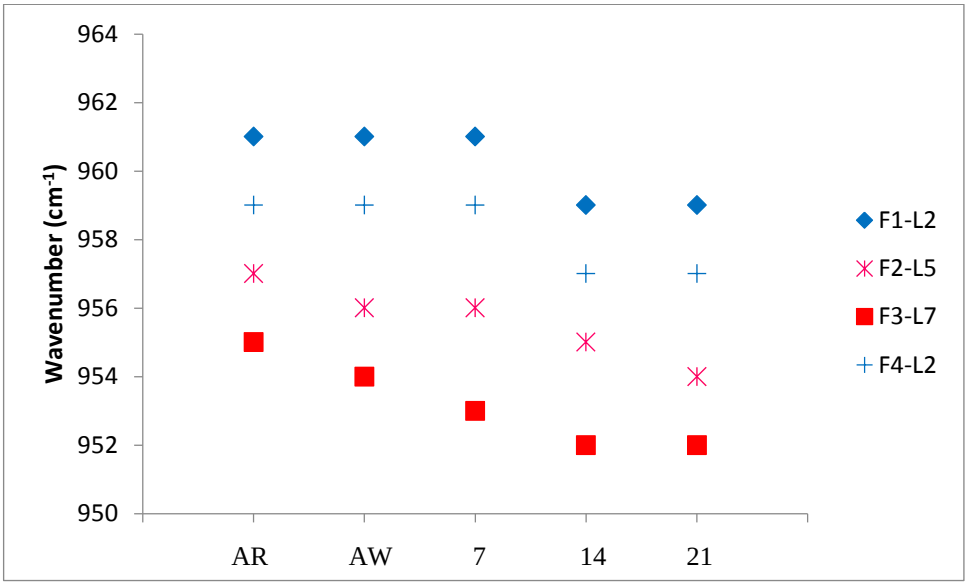

(b) G4

Figure 4.10. Peak positions for sample sets G3, G4 and G5

(cont. on next page)

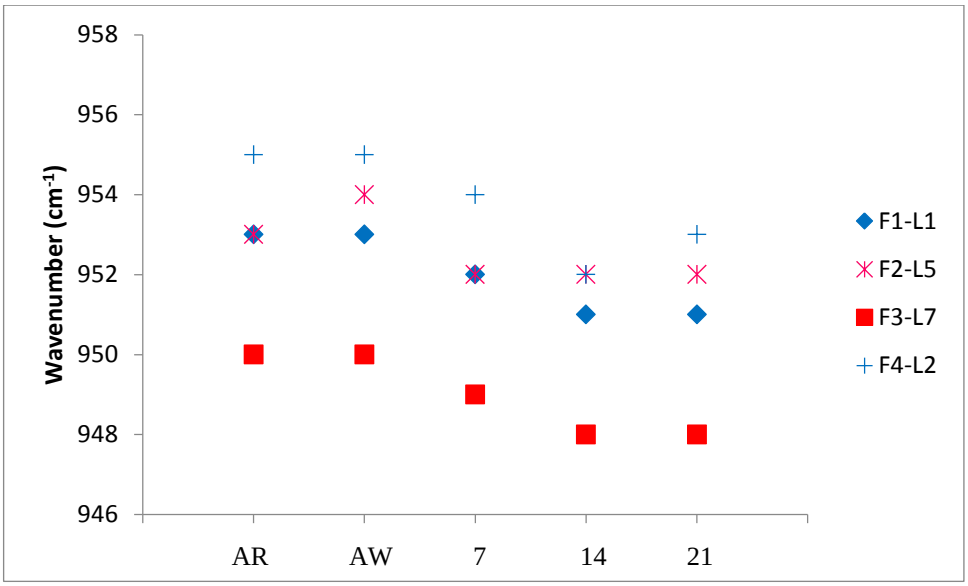

(c) G5

Figure 4.10. (cont.)

4.2.2.2. Specular Reflectance Infrared (SR-IR) Spectroscopy Analysis Results

Figure 4.11 shows the specular reflectance spectra for sample set G5, and Table 4.5 shows the specular reflectance infrared (SR-IR) spectroscopy analysis results for sample sets G3 to G5. The results show that the surfaces of the glass have peaks, at ~1064 cm^{-1} and ~766 cm^{-1} which correspond to asymmetric and symmetric mode of vibration of the Si-O-Si (BO) network. There is also a peak position at ~950 cm^{-1}, which Amma et. al. (Amma, et al., 2015) attributes to the stretching vibration of the $Si\text{-}O^{-}$ (NBO) group in the glass structure. These peaks do not clearly appear in the results obtained during this study. They are believed to be hidden the ~1060 cm^{-1} band. Smithw and Pantano (Smith & Pantano, 2008) show that the 950 cm^{-1} band penetration depth of the IR beam as well as the duration and significance of the corrosion on the glass results in the appearance of the 950 cm^{-1} peak. These findings compared with the results from this study would indicate that the 21 days of weathering has been a short duration for a strong corrosive effect to take action on the glass surface. The peak at ~513 cm^{-1} corresponds to the Si-O-Si bending vibration. ~3500 cm^{-1} range weak reflectance band observed OH-type vibrations (Smith & Pantano, 2008). The peaks indicate the presence of water molecules. The effects of the washing procedures, the transferring and the storing were not observed because of high penetration depth

(Affatigato, 2015). The water peaks with effect of aging was observed for all groups samples. Although the peak of water was observed, the peak shift at ~1060 was not observed for samples.

F3-L7 compared with the other samples was observed to show the lowest wavenumber positions for groups G3, G4 and G5 (Table 4.5). The penetration depth is greater than ATR-FTIR for this analysis (see Section 2.4). The results of ATR-FTIR and SR-IR do not disclose why F3-L7 peak has low wavenumber band than the other sample.

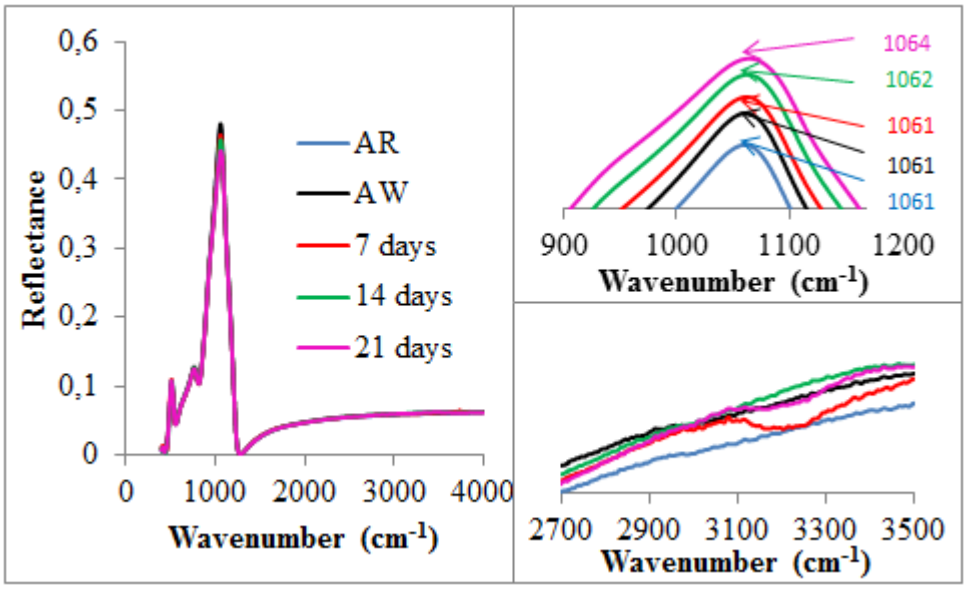

(a) G5_F1-L1

Figure 4.11. SR-IR spectra of sample set G5 (a) F1-L1 (b) F2-L5 (c) F3-L7 (d) F4-L2

(cont. on next page)

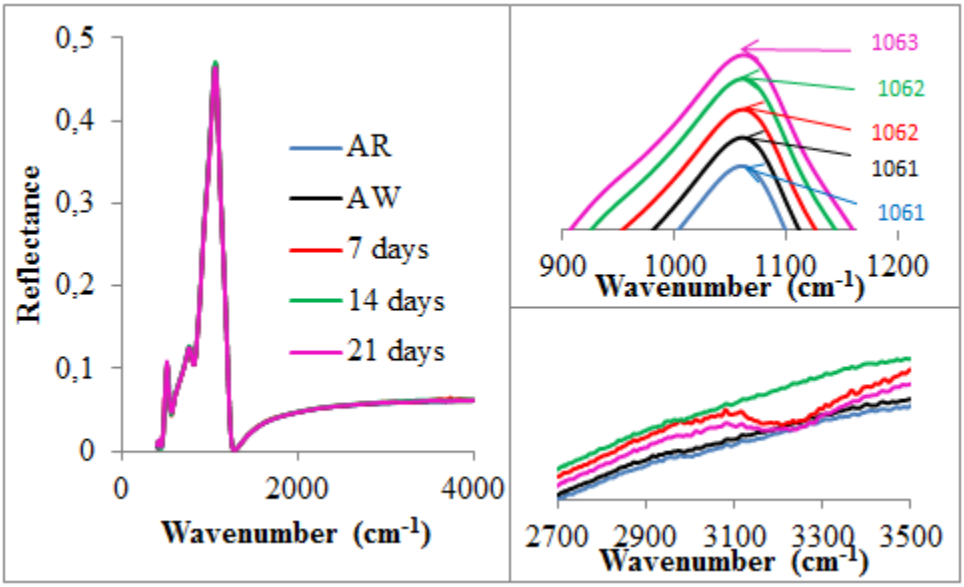

(b) G5_F2-L5

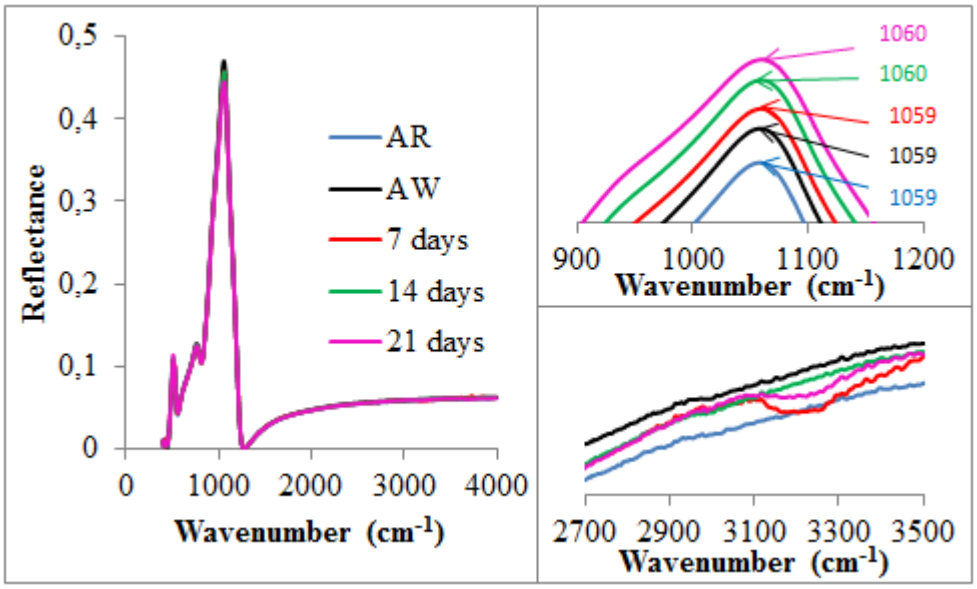

(c) G5_F3-L7

Figure 4.11. (cont.)

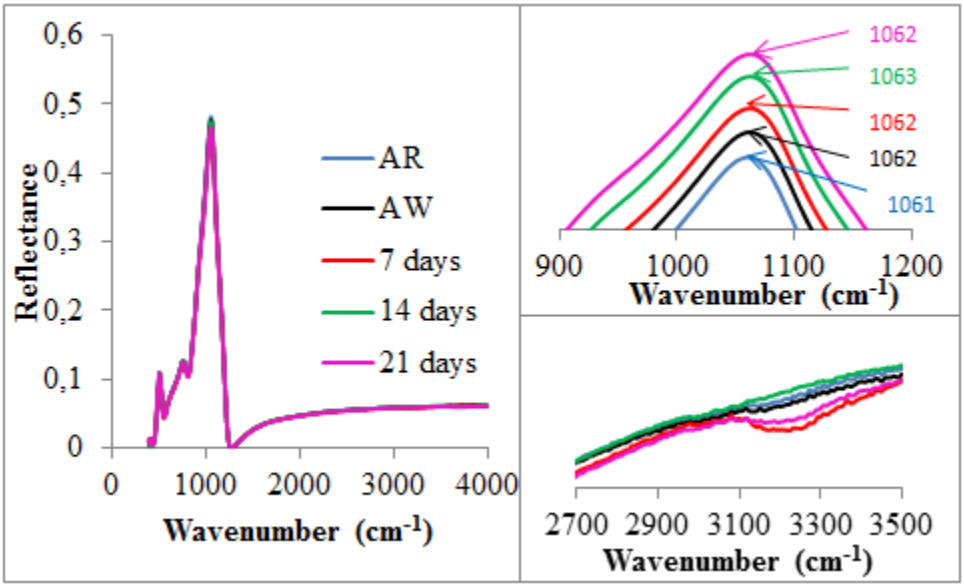

(d) G5_F4-L2

Figure 4.11. (cont.)

Table 4.5. SR-IR shifts in peak positions of sample sets G3, G4 and G5

Samples			AR			AW			7 days			14 days			21 days		
G3	F1-L2	—	1061	766	513	1061	766	511	1062	766	501	1064	766	516	1063	766	513
	F2-L5	SO_2	1062	766	513	1062	766	511	1063	767	503	1062	766	513	1063	762	511
	F3-L7	—	1059	764	515	1059	766	511	1059	766	502	1059	764	517	1061	766	515
	F4-L2	SO_2	1065	767	515	1064	765	515	1065	767	503	1062	766	511	1064	767	512
G4	F1-L2	—	1064	766	511	1064	765	517	1064	766	513	1065	766	509	1064	765	511
	F2-L5	SO_3	1061	765	511	1061	765	512	1061	764	512	1061	765	509	1061	765	511
	F3-L7	SO_2	1059	765	513	1059	765	511	1061	765	511	1061	766	515	1059	764	513
	F4-L2	—	1063	766	511	1063	766	513	1062	766	515	1063	765	511	1063	765	511
G5	F1-L1	—	1061	765	516	1061	765	515	1061	766	512	1062	767	511	1064	766	512
	F2-L5	SO_3	1061	766	513	1061	765	516	1062	765	512	1062	765	511	1063	765	512
	F3-L7	SO_2	1059	765	511	1059	765	508	1059	765	510	1060	764	514	1060	765	512
	F4-L2	—	1061	766	511	1062	766	513	1062	766	511	1063	766	512	1062	767	510

4.2.2.2.1. Effects of Dealkalization and Weathering on SR-IR:

Figure 4.12. shows the effects of SO_2, SO_3 and no sulfur gas treatment on the peak positions obtained from SR-IR spectra. Figure 4.13 shows the SR-IR peak position results plotted as a function of weathering periods of 7, 14 and 21 days. Similar to the findings from ATR-FTIR data and its analysis, a clear difference and trend is not found when comparing the peak positions for surfaces. This is true for both the heat treated glasses using a sulfur containing gas or not as well as for surfaces that have been exposed to weathering. We, therefore, hesitate to discuss and conclude any information on the structural changes based on the SR-IR results and attribute this to the increased

penetration depth (see Section 2.4) of the IR beam compared with the possible surface modifications.

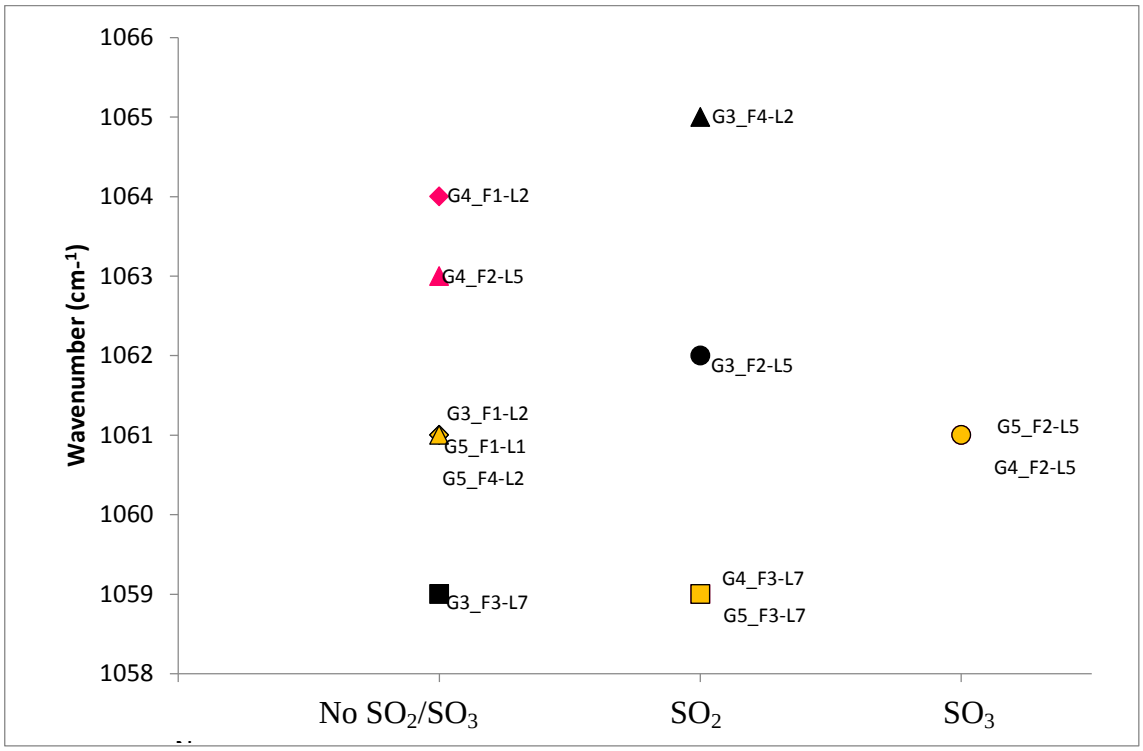

Figure 4.12. SR-IR peak positions for sulfur treated and untreated samples of sets G3, G4 and G5

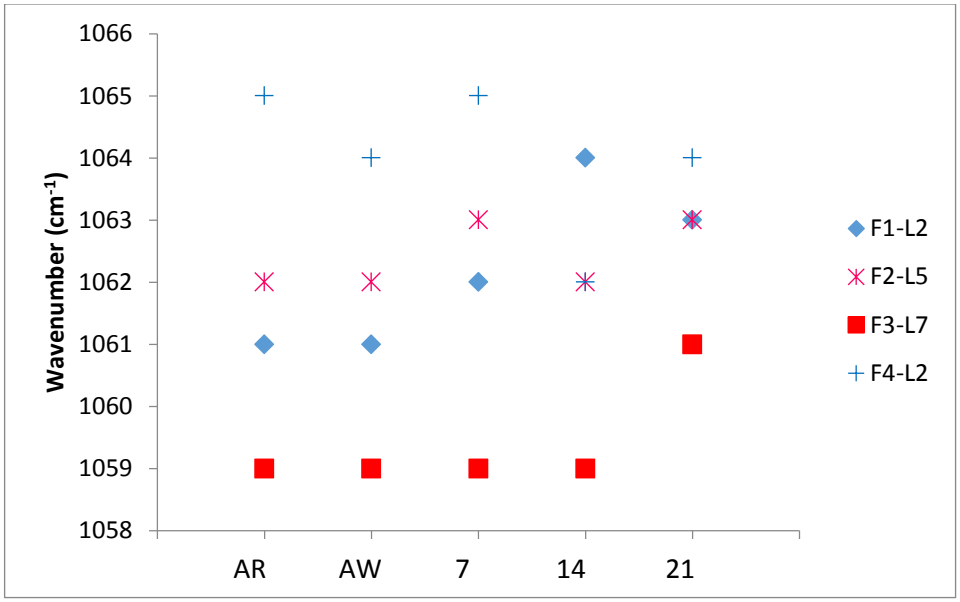

(a) Sample set G3

Figure 4.13. SR-IR peak positions for sample sets G3, G4 and G5

(cont. on next page)

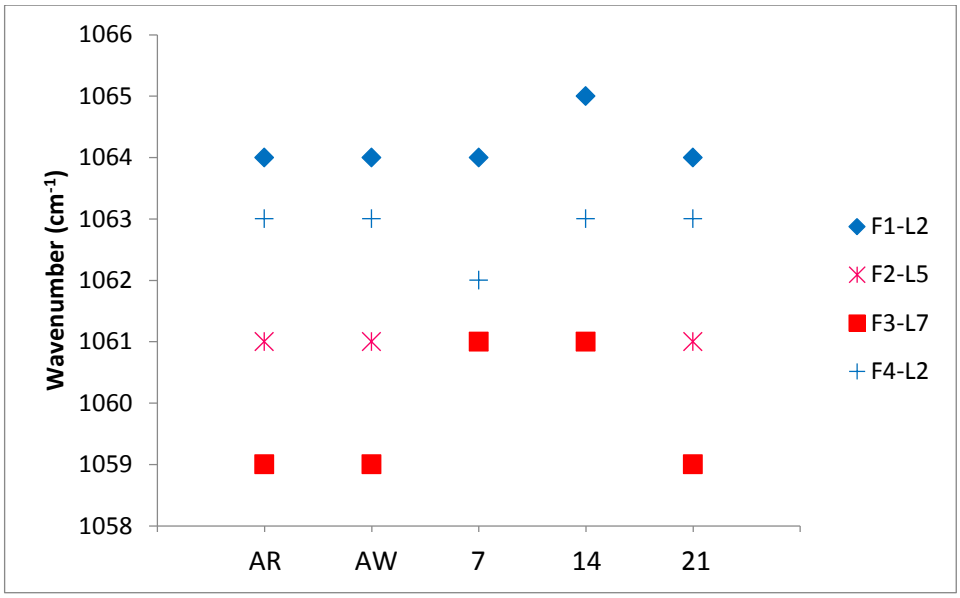

(b) Sample set G4

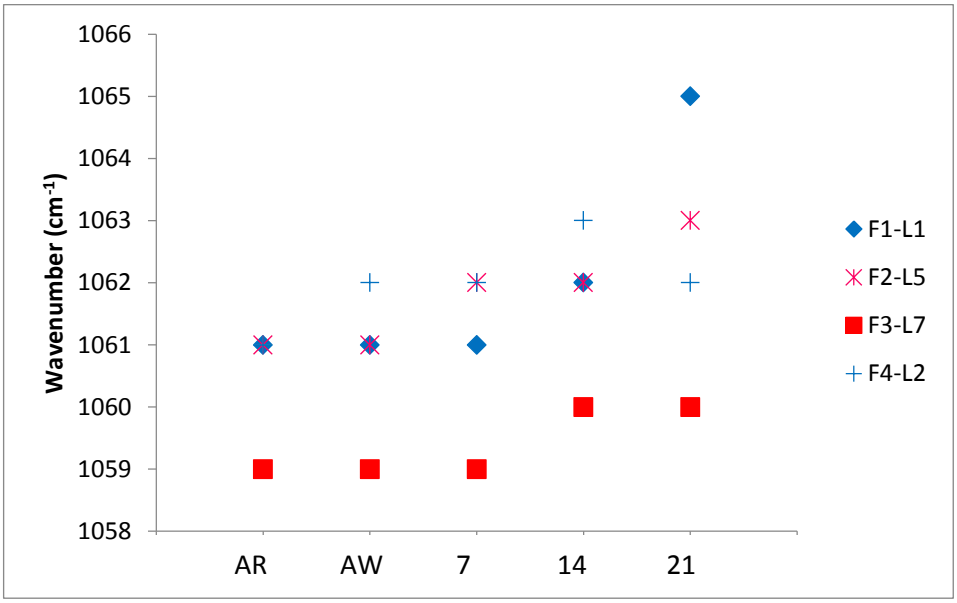

(c) Sample set G5

Figure 4.13. (cont.)

4.2.2.3. Micro-Raman Analysis Results

In addition to the IR techniques discussed above, the possible changes on the surface structure were analyzed using micro-Raman technique. This technique utilizes a built in microscope allowing for a focused analysis on targeted areas on the specimen surface. As explained in Section 3.4.2, analysis was conducted on three different locations on the glass surface. Figure 4.14 shows results obtained from the surface of sample set G4_F2-L5, where the effects of weathering is provided. The peak positions and their corresponding structural units from this spectra are given in Table 4.6.

Table 4.6. Raman peak positions
(Source: Deschamps, et al., 2011, Wang, et al., 2011)

Raman shift (cm^{-1})	Assignment	Type of vibration
1100-950	Si-O	Asymmetric stretching vibration modes of Q_2 and Q_3 species
790	Si-O-Si	Symmetric stretching
600	Si-O-Si	Symmetric stretching mode of Q_2
560-450	Si-O-Si	Symmetric stretching vibration modes of Q_4 and Q_3 species

Results for sample set G4_F2-L5 is given only with the other sample sets omitted in this write-up. This is because the spectra for all the other sets showed no significant difference from what is shown in this section. These results did not show any significant effects of sample surface preparation, dealkalization and weathering when the peak shifts between the samples were compared. In a similar manner to what was discussed for SR-IR results in Section 4.2.2.2 the lack of correlation is attributed to be due to the penetration depth of the laser beam. The calculated penetration depth is found to be ~1 μm, which is significantly higher than the structural changes taking place on the surface due to dealkalization and weathering (Affatigato, 2015).

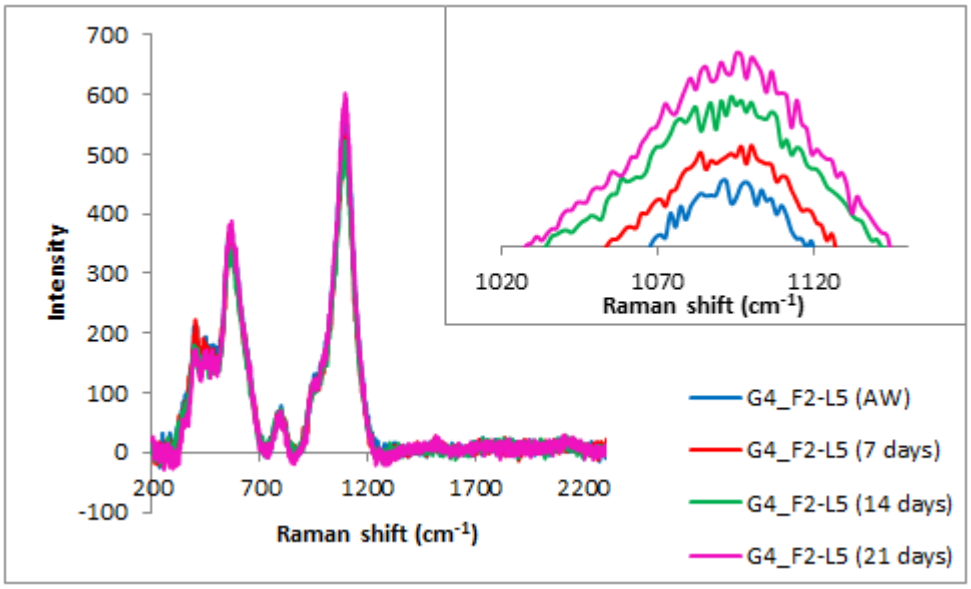

Figure 4.14. micro-Raman spectra of G4_F2-L5

4.3. Discussion

This thesis work, as its name implies, has focused on the investigations related to the surfaces of dealkalized and weathered float glasses. The surface related investigations have been focused on the structure and morphology changes as a result of the dealkalization and weathering treatments. The surface analysis throughout this work was conducted only on the atmospheric side (referred to as the air side) of the glass. The experimental procedures and their associated results provided in the prior sections of this thesis, therefore, have been concentrated on the following four main topics:

1. Effects of high temperature sulfur containing gas dealkalization on the glass surface,
2. Effects of weathering on the glass surface,
3. The use of surface analysis techniques to characterize the structure and morphology,
4. Sample and surface preparation for an effective surface analysis.

The findings on the high temperature gas dealkalization have found no significant effects of using SO_2 or SO_3 gas on the surface structural changes. This finding has mainly been based on the results obtained from the ATR-FTIR results,

where the shift in 970-950 cm^{-1} $Si\text{-}O^{-}(modifier\ ion)^{+}$ stretching vibration towards a lower wavenumber position was taken as an indication for a dealkalized structural formation (Şentürk, et al., 1995). While the effects of forming a dealkalized layer due to sulfur gas dealkalization has been reported in prior studies (Şentürk, 1992, Anderson, et al., 1975, Temnyakova, et al., 2009), the reason for the lack of such effect found in this study has been attributed to the high penetration depth of the surface analysis techniques used compared with the relatively shallow depth of the surface modified layer formed due to the gas dealkalization reactions. The depth of penetration for the surface spectroscopy techniques used in the study has been calculated as 0.63-0.65 μm for ATR-FTIR, 1 μm for micro-Raman and 1 μm for SR-IR. This compares with a reported gradually alkali depleted layer thickness of 40-60 nm (0.04-0.06 μm), and a fully depleted layer of ~10nm (Yamamoto & Yamamoto, 2011, Brow & LaCourse, 1983, Tadjiev & Hand, 2010, Walters & Adams, 1975). Hence, the techniques used for determining the surface structure is expected penetrate the modified surface layer by at least an order of magnitude higher. The fact that ATR-FTIR results provided a measurable change on the surface structural changes, as mentioned above, can be attributed to the relatively lower penetration depth calculated for this technique compared with micro-Raman and SR-IR methods. The results from the latter two, therefore, have provided no significant guidance for this study.

Contrary to the lack of effects found on the surface structure, the high temperature sulfur containing gas dealkalization suggested a potential change in the morphology of the glasses. The morphology changes have been characterized using AFM. This change has appeared in the form of micro-crack like features. The results from the surface morphology analysis in this study appear to suggest these formations to possibly originate from the high temperature gas dealkalization reaction products, namely the formation of sodium sulfate salts, on the surface. These salts form at the heat treatment temperatures of 300-500ºC and have been shown to deposit in form of clusters of micron sized particulates of sodium sulfate (see Figure 4.3 and 4.4). It is thought that the micro-crack like appearing features may have found its origins under these salt formations. While there is some reasonable evidence from the results of this study to support this theory, further focused work will certainly be in order to prove the concept. It is also worth to note that this theory, to the best of the authors knowledge, has not been discussed in the literature.

Formation of the surface sodium salts due to sulfur gas reactions at high temperatures have been reported in the literature (Şentürk, 1992). While this surface residue is washed at the end of the process it has also been found to provide a lubrication effect on the surface helping to eliminate the contact damage, especially with the side contacting the rollers during transport at the manufacturing site. The clustered type formation of these salts shown in study (see Figure 4.3 and 4.4) raises a potential question about the amount and uniformity of the glass surface-gas reactions. One can speculate that the reactions and salt formation at the heat treatment temperatures may be forming a film layer that is then converted into particulates and clusters. In any case, the low amount and lack of uniformity of the salt formation causes a concern over the uniformity of the dealkalized surface layer due to the potential surface-gas reaction heterogeneities and the duration of the reaction. Based on these arguments, one can then relate the lack of finding any significant effects of the gas reactions on the structural formation to the lack of uniformity and surface reaction content. This can also be related to the variations between the sample sources seen in the results where the conditions of sulfur gas application, where applicable, could be different enough to results in homogeneity issues.

The other important part of this study was to determine the effects of weathering on the surface structure and morphology. The results based on a total of 21 days of exposure to 95% relative humidity at 40ºC conditions of the glass surfaces which have been packed vertically with either a wide gap or a 100-120 μm gap using sized polymeric separator between each glass showed no significant effect of the weathering on the surface structure and surface morphology. These results were determined mainly from the ATR-FTIR spectra due to the lower penetration depth achieved with this method. The exposure of the surface to atmospheric water is expected to result in the formation of a dealkalized layer generating hydrated silica within this dealkalized layer. Similar to what was explained for the effects of sulfur gas treatment on structure, one can attribute this lack of finding a dealkalized and silica gel rich surface to the higher penetration depth of the light source versus the thickness of the layer. The spectroscopy results showed an increase in the presence of molecular water as evidenced from the formation of peaks at ~3800 cm^{-1}, ~1650 cm^{-1}, ~880 cm^{-1} , which is to be expected due to the exposure of the glass to humidity. The results, however, did not show any increasing trend with increased exposure times. The morphology of the weathered glass

surfaces were also found to be uninfluenced by the weathering treatments. Similar to what was found for the effects of sulfur gas treatment, no significant effects of the use of such a treatment was determined on both the structure and the morphology of the surfaces. There was also no solid evidence showing the effects of weathering on the micro-crack like formations found on the sulfur treated surfaces.

Prior studies on the effects of weathering have suggested the surface to be modified at durations longer than 21 days (Stockdale & Tooley, 1950, Smith & Pantano, 2008, Rodríguez, 2015). The findings in this study, therefore, imply that the surfaces studied have not yet started to show any significant degradation. It is therefore thought that longer static or cyclic exposure to humidity and heat may magnify the surface effects.

It would be evident to the reader that obtaining reliable and repeatable results from the characterization techniques that have been used in determining and discussing the surface structure and morphology is critical. During these analyzes, in order to confirm accuracy and repeatability of the results from within each dataset as well as in between datasets the devices were calibrated at regular intervals. Therefore, the error from the device calibration was reduced to a minimum. For each sample, analysis was done at three different locations and it was found that for each of the three measurements taken the results have been consistent with each other. An analysis on the repeatability of the data has been provided in Appendix A and B. Therefore, any changes in the data can mostly be attributed to the sample and the effects of device on the data can be neglected.

The analysis methods used in this study are surface sensitive techniques, requiring the sample to be adequately prepared. It is, therefore, important to address that the surfaces of the samples used in the analysis were prepared properly and represented the true surface rather than any unintended modifications from handling and sample preparations. Many glass surface cleaning procedures are known in the literature. A consistent and surface representative cleaning procedure has been developed for the analysis procedures used in this study. This procedure uses demineralized water as the first rinsing step, followed by a treatment with IPA, both done in an ultrasonic bath. The procedure is completed with a final drying and heat treatment at 200ºC. It is also important to minimize exposure and damage to the surface during the transfer from the manufacturing facility to the laboratory locations for

analysis. After the iterations evaluated on sample sets G1 to G4, the most appropriate sample handling procedure was designated to be with sample set G5. This sample set allowed for the least environmental impact on the surface of the glass.

CHAPTER 5

CONCLUSION AND SUGGESTIONS FUTURE STUDIES

The effects of treating the surfaces of float glass using sulfur containing gas at high temperatures and the effects of weathering on these surfaces have been studied using surface related analysis methods. The surface analysis methods were aimed at understanding the changes on the surface structure, morphology and topography. The results showed that the surface structure of the glass, measured at a calculated penetration depth of 0.63-0.65 μm using ATR-FTIR spectroscopy, was not significantly affected by both the surface dealkalization and subsequent weathering reactions. Similar spectroscopic analysis was done on these surfaces using SR-IR and micro-Raman methods, both of which agreed with the ATR-FTIR findings. While prior studies have shown that surface dealkalization and weathering treatments have an influence in modifying the glass surface, the key reason for the lack of such an observation in this study is attributed to the relatively high penetration depth of the ATR-FTIR as well as SR-IR and micro-Raman methods used in understanding the surface structural changes. In addition, the surface modifications that have developed due to the treatments applied in this study have not been at a significant level to provide the level of changes reported in other similar studies. This has been illustrated with the relatively weak structural and morphology modifications on the surface due to weathering at 21 days of accelerated treatment of this study compared with the effects of such treatments found at longer durations reported in the literature.

The analysis of the surface morphology and topography using AFM technique showed the presence of micro-crack like features on the surfaces of sulfur treated glasses. These features are thought to occur under the sodium sulfate salt residue that is formed during the high temperature dealkalization reactions on the surface. While similar surface features have been reported in the literature, its relation to the high temperature sulfur gas treatment proposed from the findings of this study has not been documented in prior studies.

The study also proposes a methodology for preparing the samples for an effective and representative surface sensitive analysis.

Based on the experiences and findings obtained from this study, below are few suggestions for future work:

- Controlled sulfur gas dealkalization of the glass surface in the laboratory would be helpful in finding the root cause and mechanism behind the micro-crack like features found in this study.
- Weathering effects should be studied for duration longer than 21 days. Use of steady and cyclical weathering conditions should be considered for the next phase.
- Other surface sensitive analysis method should be performed for determining the modifications on the surface layers. Techniques, such as grazing incidence reflection absorption Fourier transform infrared (GIRA-FTIR) spectroscopy, surface-enhanced Raman spectroscopy (SERS), and Peak Force Quantitative Nanomechanical Mapping AFM (PF-QNM-AFM) are suggested as candidates that are within the capability of the scope of this study.

REFERENCES

Affatigato, M., 2015. *Modern Glass Characterization.* Hoboken: The Amirican Ceramic Society and John Wiley & Sons. Inc..

Amma, S., Kim, S. H. & Pantano, C. G., 2016. Analysis of Water and Hydroxyl Species in Soda Lime Glass Surfaces Using Attenuated Total Reflection (ATR)-IR Spectroscopy. *Journal of the American Ceramic Society,* 99(1), p. 128–134.

Amma, S., Luo, J., Pantano, C. G. & Kim, S. H., 2015. Specular Reflectance (SR) and Attenuated Total Reflectance (ATR) Infrared (IR) Spectroscopy of Transparent Flat Glass Surfaces: A Case Study for Soda Lime Float Glass. *Journal of Non-Crystalline Solids,* Issue 428, p. 89–196.

Anderson, P., Bacon, F. & Byrum, B., 1975. Effect of Surface Treatments on the Chemical Durability and Surface Composition of Soda-lime glass Bottles. *Journal of Non-Crystalline Solids,* Volume 19, pp. 251-262.

Bradley, L. C., Dilworth, Z. R., Barnette, A. L., Hsiao, E., Barthel, A. J., Pantano, C. G., Kim, S. H.., 2013. Hydronium Ions in Soda-Lime-Silicate Glass Surfaces. Journal of the American Ceramic Society, 96(2) p. 458-463

Brow, R. & LaCourse, W., 1983. Fluorine Treatments of Soda-Lime-Silicate Glass Surface. *Journal of the American Ceramic Society,* 66(8), p. 123-124.

Clark, D. E., Pantano, J. C. G. & Hench, L. L., 1979. *Corrosion of Glass: Books for I ndustry and The Glass Industry.* New York: Division of Maganizes for Industry, INC..

Cobb, F., 2009. *Structural Engineer's Pocket Book.* 2nd Edition: British Standards Edition ed. USA: Elsevier.

Cummings, K., 2002. *A history of glass forming.* London, USA: A & C Black.

Deschamps, T., Martinet, C., Bruneel, J. & Cham, B., 2011. Soda-Lime Silicate Glass under Hydrostatic Pressure and Indentation: a micro-Raman study. *Journal of Physics : Condensed Matter,* Issue 23, p. 7.

Doremus, R. H., 1994. *Glass Science.* 2nd Edition ed. New York, USA: John Wiley Sons, Inc..

Douglas, R. & Isard , J., 1949. The Action of Sulphur Dioxide and of Water on Glass Surfaces. *Journal of the Society of Glass Technology,* Issue 33, pp. 289-335.

Franz, H., 1980. Durability and Corrosion of Silicate Glass Surfaces. *Journal of Non-Crystalline Solids,* 42(1-3), pp. 529-534.

Goodman, O. & Derby, B., 2011. The Mechanical Properties of Float Glass Surfaces Measured by Nanoindentation and Acoustic Microscopy. *Acta Materialia,* V olume 59, p. 1790–1799.

Greiner, R. & Rinkens, R., 2013. *Guardian Glass Time: Techn. Handbook,* Luxembourg: Guardian Europe S.A.R.

Guo, Y., 2006. *Raman Spectroscopy of Glasses with High and Broad Raman Gain in the Boson Peak Region.* Florida, USA: PhD Thesis.

Haldimann, M., Luible, A. & Overend, M., 2008. *Structural Use of Glass.* Zürih: IABSE-AIPC-IVBH.

Harrick, N., 1967. Internal Reflectance Spectroscopy. In: New York: Wiley Inc., Chapters 2 and 3.

Hayashi, Y., Akiyama, R. & Kudo, M., 2001. Surface Characterization of Float Glass Related to Changes in The Optical Properties After Reheating. *Surface and Interface Analysis,* Volume 31, p. 87–92.

Hayashi, Y., Fukuda, Y. & Kudo, M., 2002. Investigation on Changes in Surface Composition of Float Glass Mechanisms and Effects on The Mechanical Properties. *Surface Science,* Issue 507-510, p. 872-876.

He, H. et al., 2013. *Surface Chemistry of Glass: Interfacial Water and Mechanochemical Properties.* Sicily, Italy, Engineering Conferences International Functional Glasses.

Hopf, J. & Pierce, E., 2014. Topography and Mechanical Property Mapping of International Simple Glass Surfaces with Atomic Force Microscopy. *Procedia Materials Science,* Volume 7, p. 316-222.

Kennedy, R., 1997. *The History and Future of the Flat Glass Industry,* USA: AFG Industries, INC. Glass Processing Days 13–15 Sept. ‘97.

Khoshhesab, Z. M., 2012. Reflectance IR Spectroscopy. In: T. Theophanides, ed. *Infrared Spectroscopy - Materials Science, Engineering and Technology.* s.l.:InTech, p. Chapter 11.

Kolluru, P. V., Green, D. J., Pantano, C. G. & Muhlsteinw, C. L., 2010. Effects of Surface Chemistry on the Nanomechanical Properties of Commercial Float Glass. *Journal of the American Ceramic Society,* 93(3), p. 838-847.

Lee, Y.-K., Peng, Y. L. & Tomozawa, M., 1997. IR Reflection Spectroscopy of a Soda-Lime Glass Surface During Ion Exchange. *Journal of Non-Crystalline Solids* , I ssue 222, p. 125-130.

Lefèvre, G., 2004. In situ Fourier-transform infrared spectroscopy studies of inorganic ions adsorption on metal oxides and hydroxides. *Advances in Colloid and Interface Science,* 107(2–3), p. 109-123.

Melcher, M., Wiesinger, R. & Schreiner, M., 2010. Degradation of Glass Artifacts: Application of Modern Surface Analytical Techniques. *Accounts of Chemical Research,* 6(43), p. 916-926.

Mellott, N. P., Brantley, S. L., Hamilton , J. P. & Pantano, C. G., 2001. Evaluation of Surface Preparation Methods for Glass. *Surface and Interface Analysis,* Issue 31, p. 362-368.

Morey, G. W., 1925. The Corrosion of Glass Surfaces. *Industrial and Engineering Chemistry,* 17(4), p. 389-392.

Palenta, T. et al., 2013. Characterization of Corrosion Effects on Float Glass Coated by CCVD. *Surface & Coatings Technology,* Volume 232, p. 742–746.

Pantano, C. G., 2015. *Glass Surface Treatments: Commercial Processes Used in Glass Manufacture,* USA: IMI NFG.

Park, J., 2008. *Bioceramics Properties, Characterizations, and Applications.* USA: Springer Science+Business Media, LLC..

Patterson, M. R., 2008. *Structural Glass Facades: A Unique Building Technology.* USA: University of Southern California Master Thesis.

Rancoule, G., Niveau, N. & Bucko, D., 2006. SO2 Behaviour and Interaction with Furnace Atmosphere and Glass. *Verre,* 12(3).

Reviere, J. & Myhra, S., 1998. *Handbook of Surface and Interface Analysis: Methods for Problem-Solving.* New York: Marcel Dekker Inc..

Rodríguez, J. A. G., 2015. *The Mechanical Response to Contact of Soda Lime Silica Float Glass and the Effects of Hydration and High Temperature,* England: The University of Sheffield.

Ryan, J., 1995. Chemical Stabilisation of Weathered Glass Surfaces. *Conservation Journal,* Issue 16.

Sharma, A., 2002. *Role of surface defects on the corrosion behavior of commercial soda-lime silicate glasses.* Master Thesis ed. Pensilvanya, USA: Lehigh University.

Shimin, L., Guoqiang, Q. & Dongchun, L., 2007. Use of Sulfur Dioxide in Chinese Float Glass Propuction Lines. *American Ceramic Society Bulletin,* 86(6), p. 9401-9404.

Smets, B., 1985. On the Mechanism of the Corrosion of Glass by Water. *Philips Technical Review*, 2(42), p. 59-64.

Smith, N. J. & Pantano, C. G., 2008. Leached Layer Formation on Float Glass Surfaces in the Presence of Acid Interleave Coatings. *Journal of American Ceramic Society*, 91(3), p. 736–744.

Soares, P. et al., 2011. Aqueous Corrosion of a Commercial Float Glass Studied by Surface Spectroscopies and Nanoindentation. *Physics and Chemisrt of Glasses: European Journal of Glass Science and Technology Part B*, 52(1), p. 25–30.

Stockdale, G. & Tooley, F., 1950. Effect of Humid Conditions on Glass Surfaces Studied by Photographic and Transmission Techniques. *Journal of the American Ceramic Society*, 33(1), p. 11-16.

Synowicki, R. A., Johs, B. D. & Martin, A. C., 2011. Optical Properties of Soda-Lime Float Glass from Spectroscopic Ellipsometry. *Thin Solid Films*, Volume 59, p. 2907–2913.

Şentürk, U., 1992. *Effects of High-Temperature Gas Dealkalization on Surface Mechanical Properties of Float Glass.* Alfred, New York: Alfred University.

Şentürk, U., Lee, D., Condrate Sr., R. & Varner, J., 1995. ATR-FTIR Spectral Investigation of SO2-Treated Soda-Lime-Silicate Float Glass. In: H. Z. Cummins, D. J. Durian, D. L. Johnson & H. E. Stanley, eds. *Disordered Materials and Interfaces.* Alfred: Materials Research Society Symposium Proceedings, p. 337-342.

Tadjiev, D. R. & Hand, R. J., 2010. Surface Hydration and Nanoindentation of Silicate Glasses. *Journal of Non-Crystalline Solids*, Volume 356, p. 102–108.

Temnyakova, N. V., Shitova, L., Yuneva, E. & Zinina , E., 2009. Corrosion Resistance of Float Glass. *Science for Glass Production- Glass and Ceramics*, 66(3), p. 79-81.

Uchino, T., Sakka, T., Hotta, K. & lwasaki, M., 1989. Attenuated Total Reflectance Fourier-Transform Infrared Spectra of a Hydrated Sodium Silicate Glass. *Journal of the American Ceramic Society*, 72(11), p. 2173-2175.

Varshneya, A. K., 1994. *Fundamentals of Inorganic Glasss.* New York, USA: Academic Press, INC..

Walters, H. & Adams, P., 1975. Effects of Humidity on the Weathering of Glass. *Journal of Non-Crystalline Solids*, Volume 19, p. 183-199.

Wang, M., CHeng, J., Li, M. & He, F., 2011. Raman Spectra of Soda–Lime–Silicate Glass Doped with Rare Earth. *Physica B*, Issue 406, p. 3865-3869.

Woodruff, D. P. & Delchar , T. A., 1994. *Modern Tecniques of Surface Science.* New York: Cambridge University Press.

Yamamoto, Y. & Yamamoto, K., 2011. Precise XPS Depth Profile of Soda-Lime-Silica Float Glass using C60 Ion Beam. *Optical Materials,* Volume 33, p. 1927-1930.

APPENDIX A: Results of ATR-FTIR

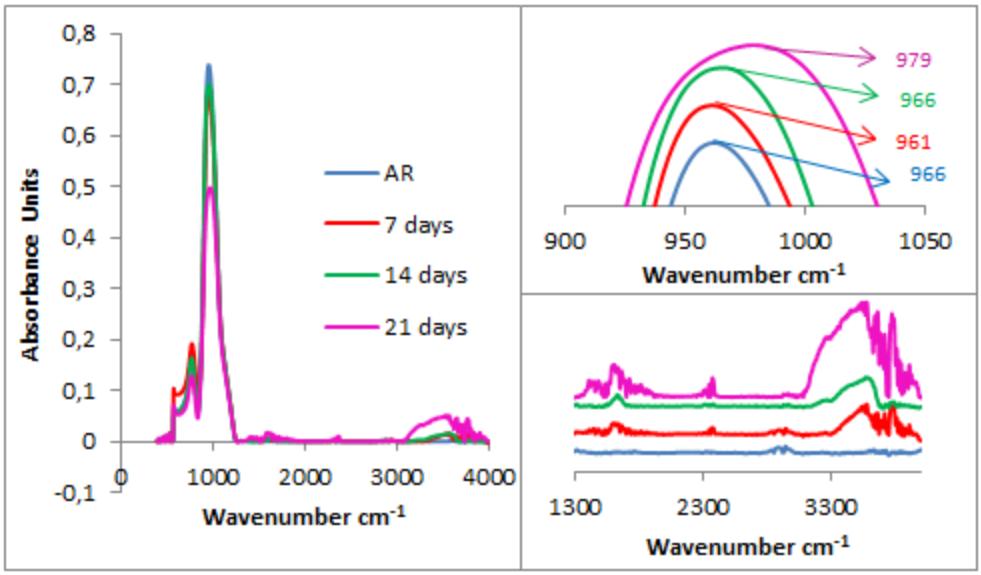

(a) G1_F1-L2

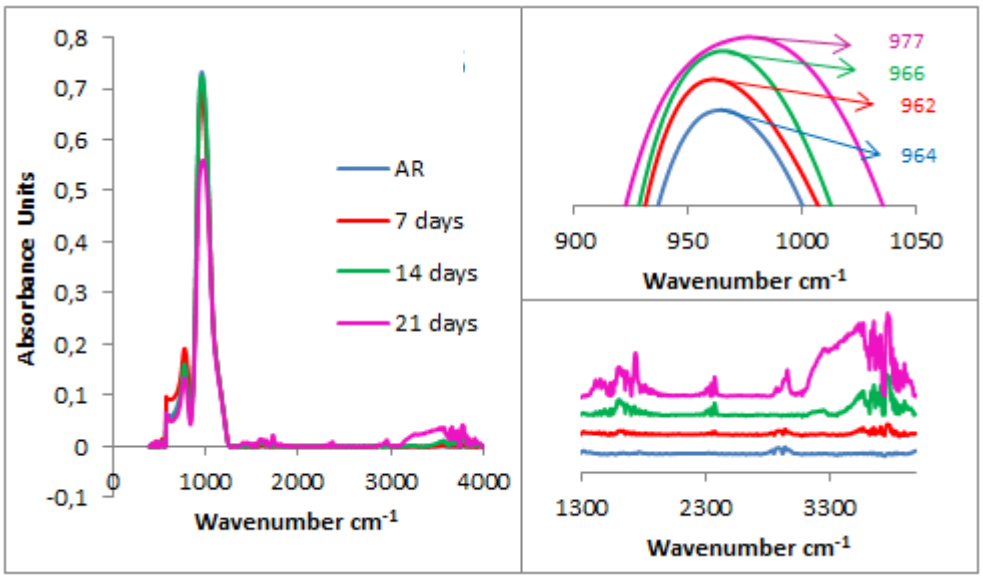

(b) G1_F2-L5

Figure A.1. ATR-FTIR results of sample set G1 (a) F1-L2 (b) F2-L5 (c) F3-L7 (d) F4-L1 (e) F4-L2

(cont. on next page)

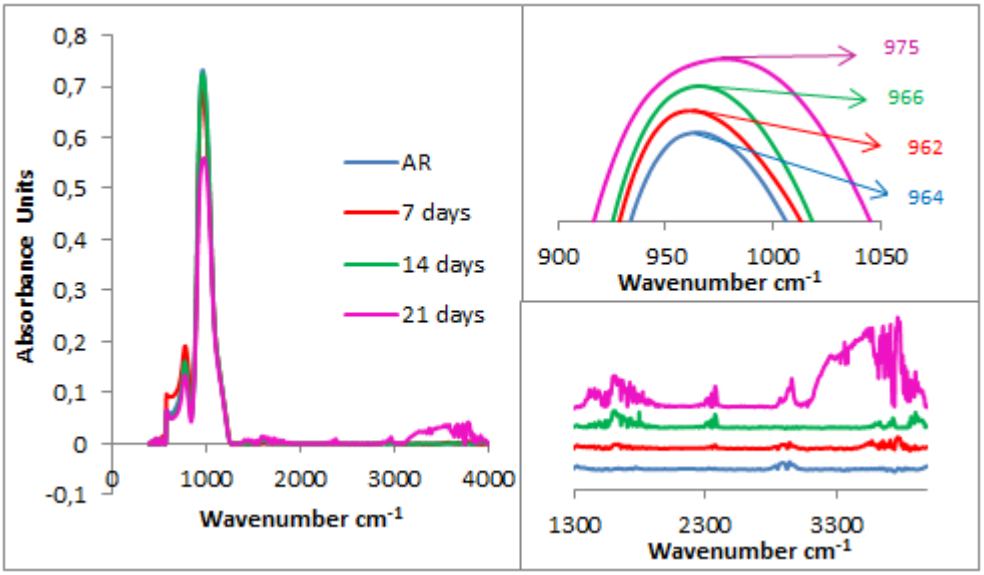

(c) G1_F3-L7

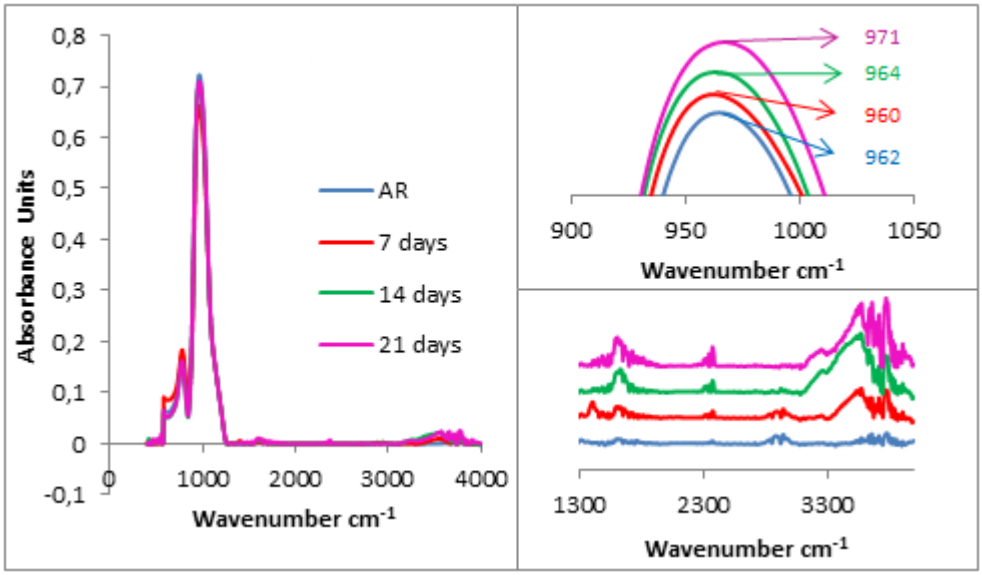

(d) G1_F4-L1

Figure A.1. (cont.)

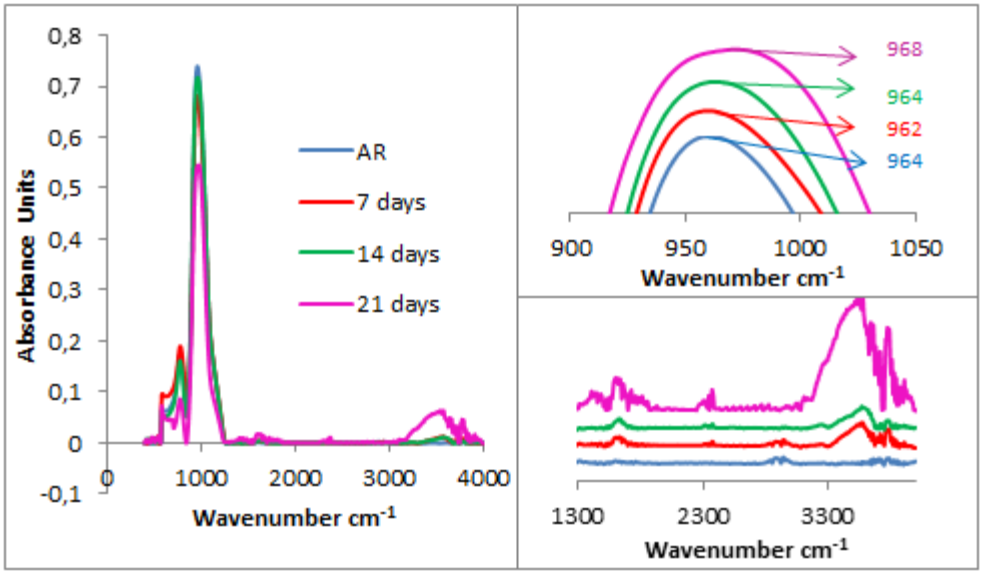

(e) G1_F4-L2

Figure A.1. (cont.)

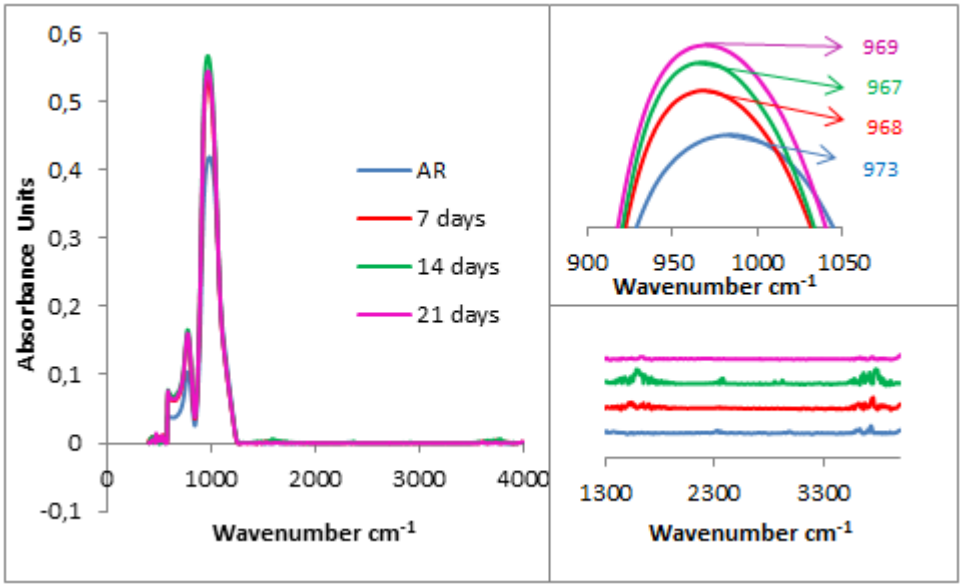

(a) G2_F1-L2

Figure A.2. ATR-FTIR results of sample set G2 (a) F1-L2 (b) F2-L5 (c) F3-L7 (d) F4-L1 (e) F4-L2

(cont. on next page)

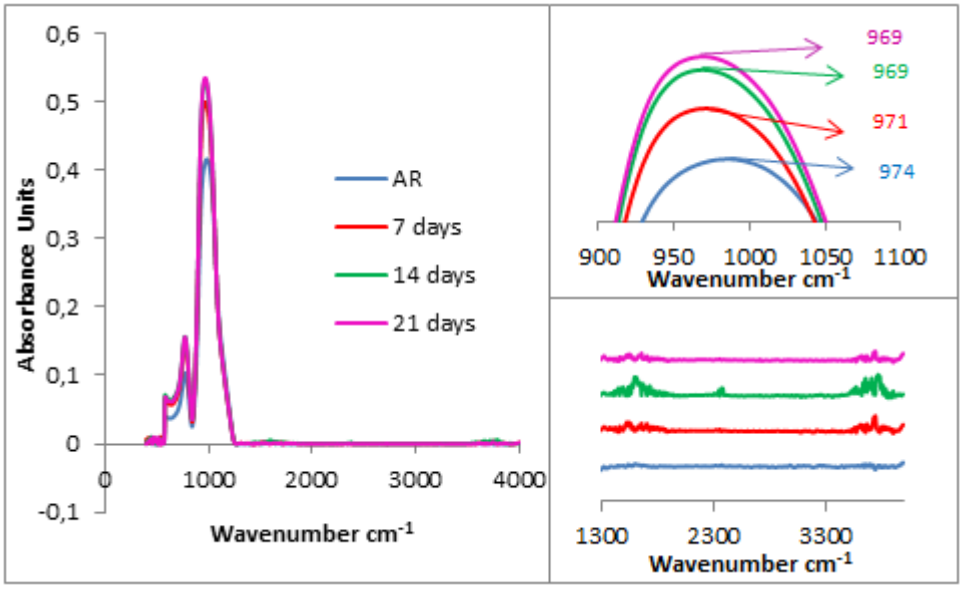

(b) G2_F2-L5

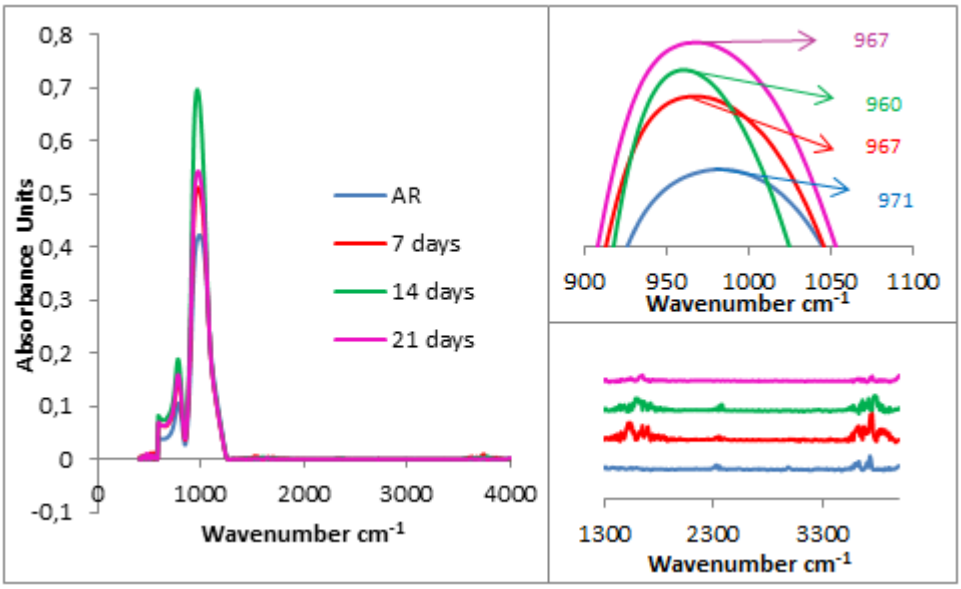

(c) G2_F3-L7

Figure A.2. (cont.)

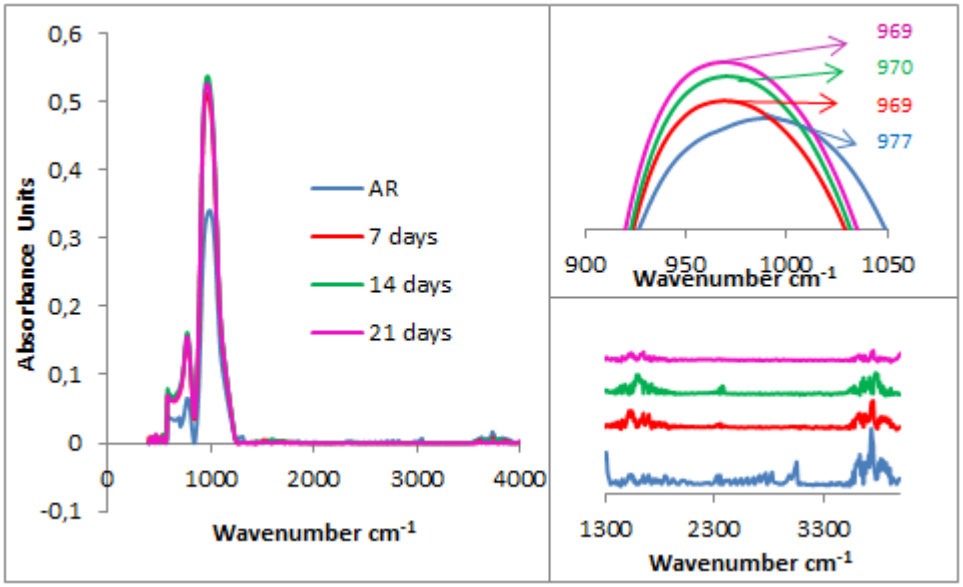

(d) G2_F4-L1

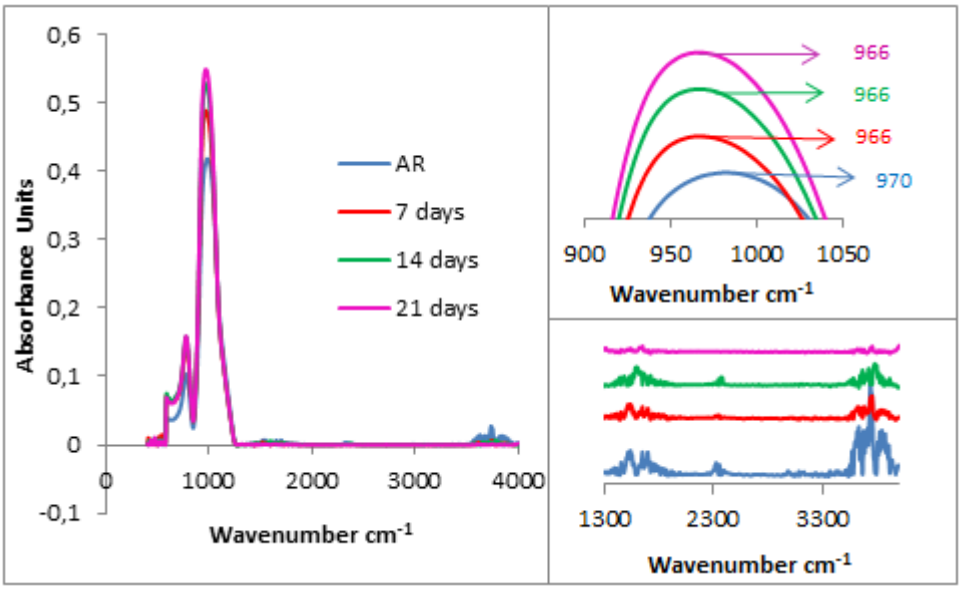

(e) G2_F4-L2

Figure A.2. (cont.)

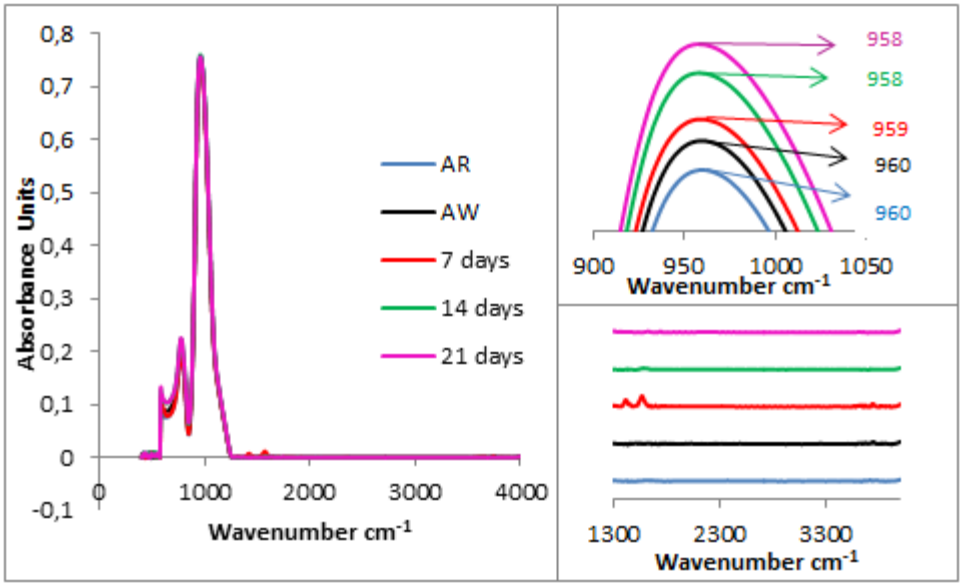

(a) G3_F1-L2

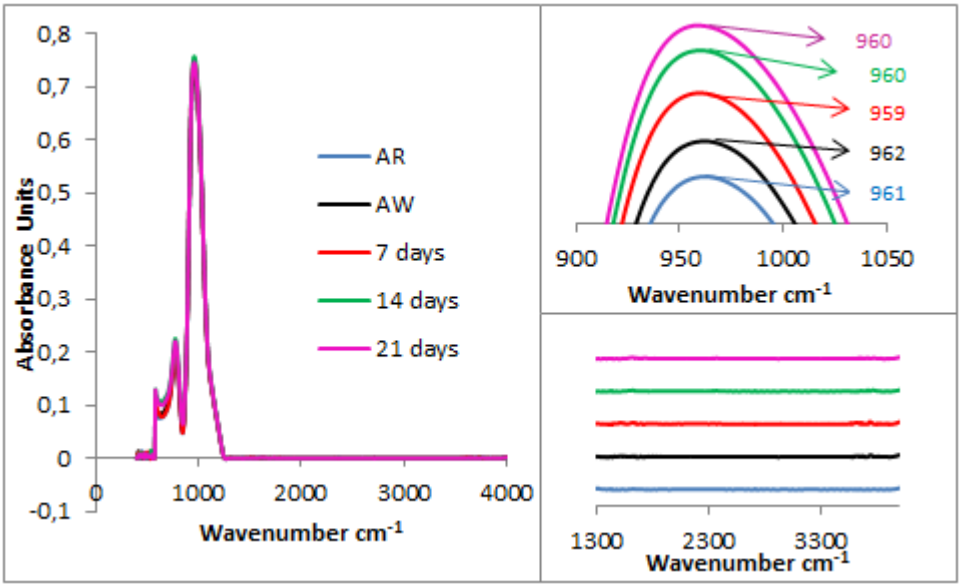

(b) G3_F2-L5

Figure A.3. ATR-FTIR results of sample set G3 (a) F1-L2 (b) F2-L5 (c) F3-L7 (d) F4-L1

(cont. on next page)

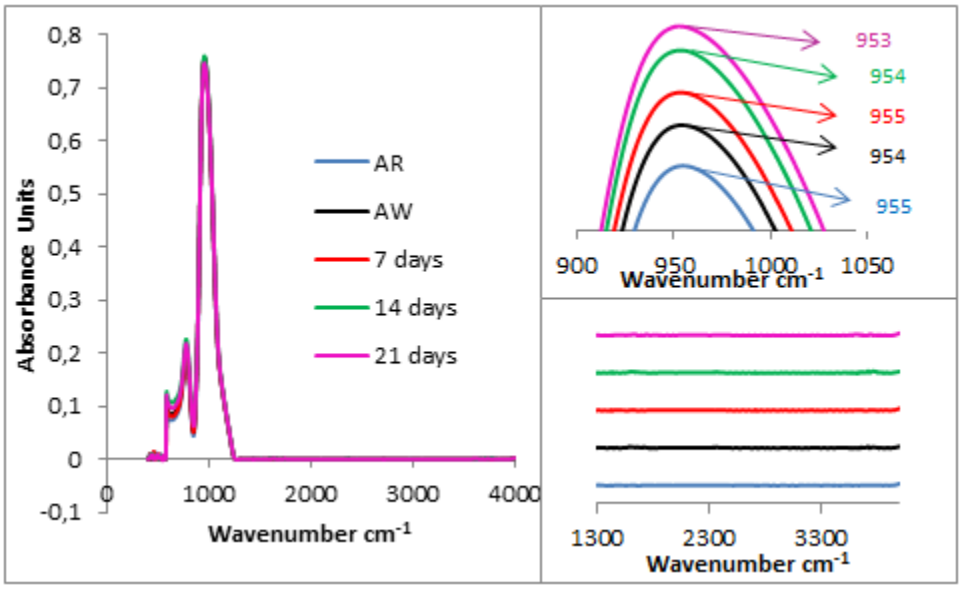

(c) G3_F3-L7

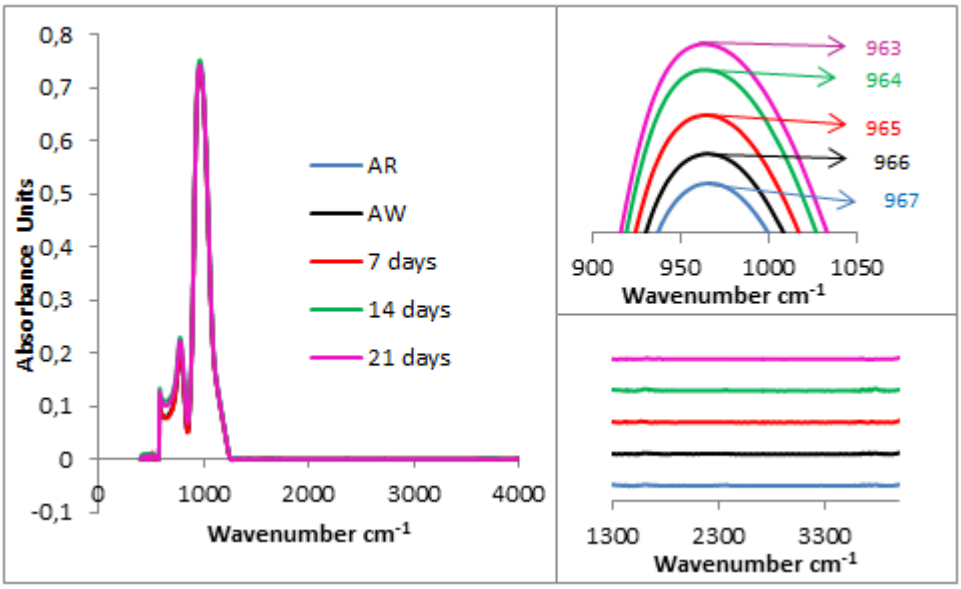

(d) G3_F4-L2

Figure A.3. (cont.)

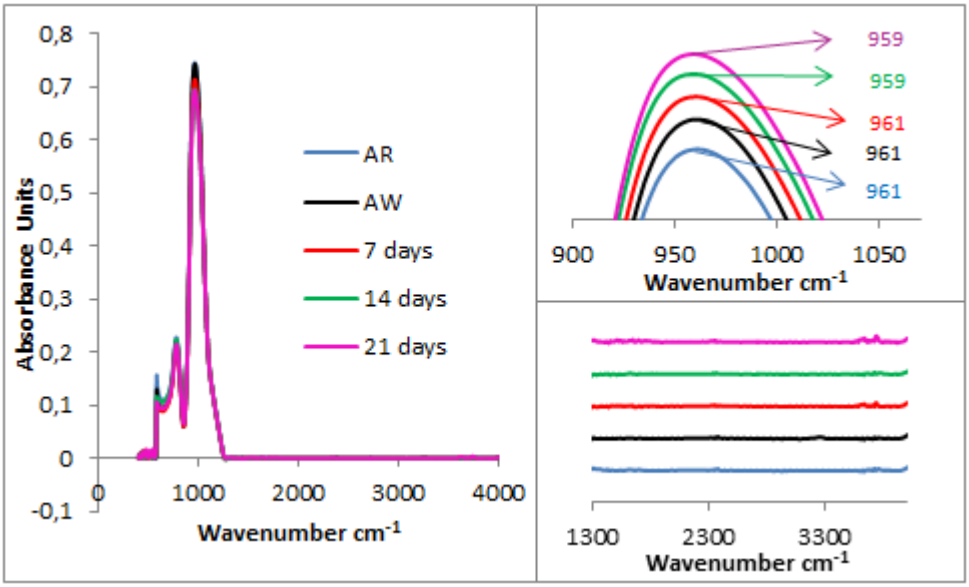

(a) G4_F1-L2

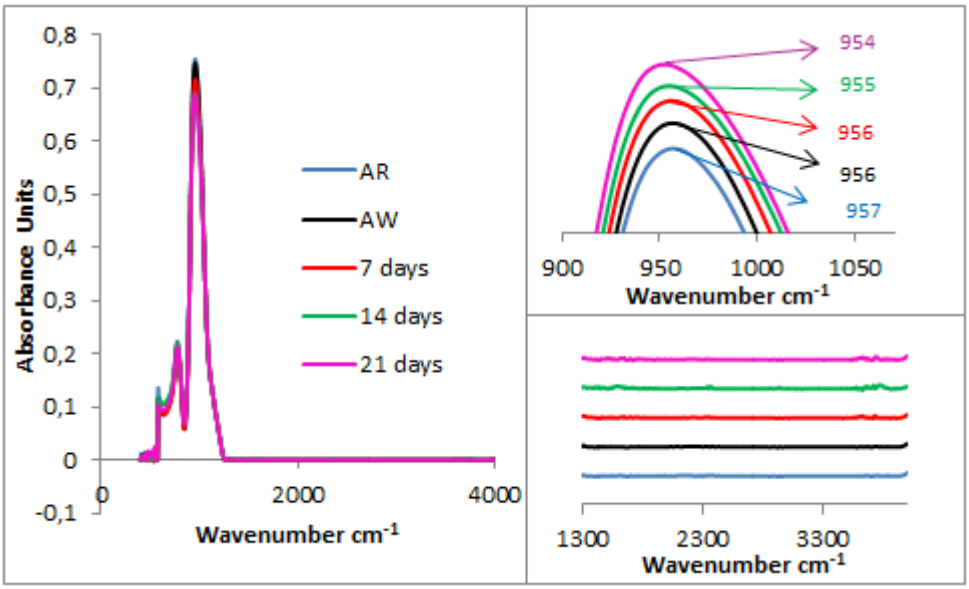

(b) G4_F2-L5

Figure A.4. ATR-FTIR results of sample set G4 (a) F1-L2 (b) F2-L5 (c) F3-L7 (d) F4-L1

(cont. on next page)

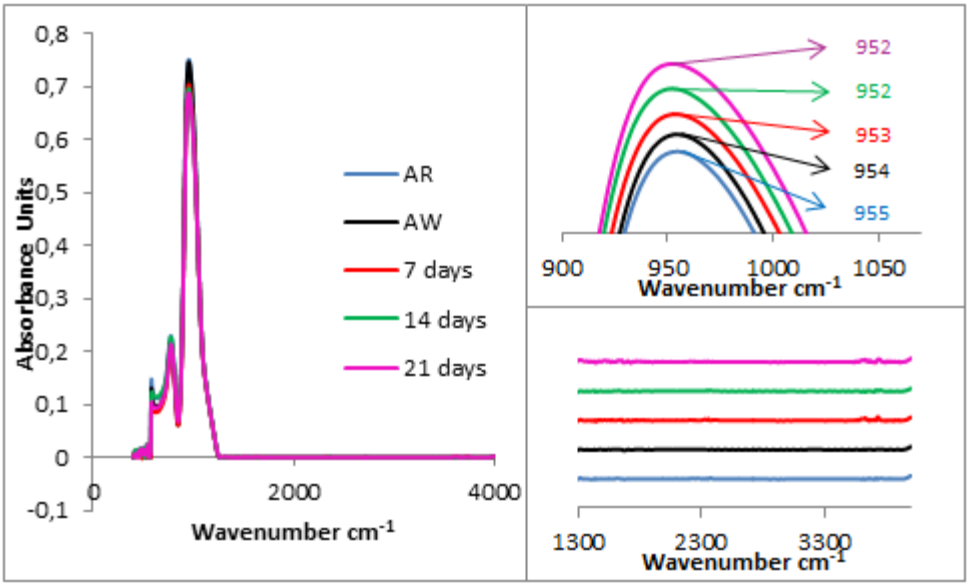

(c) G4_F3-L7

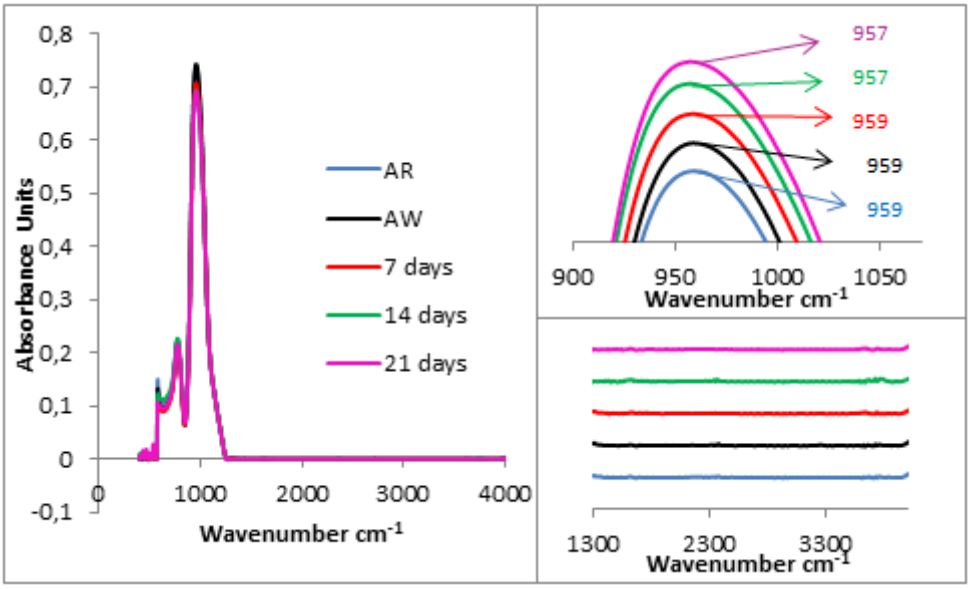

(d) G4_F4-L2

Figure A.4. (cont.)

APPENDIX B. Results of SR-IR

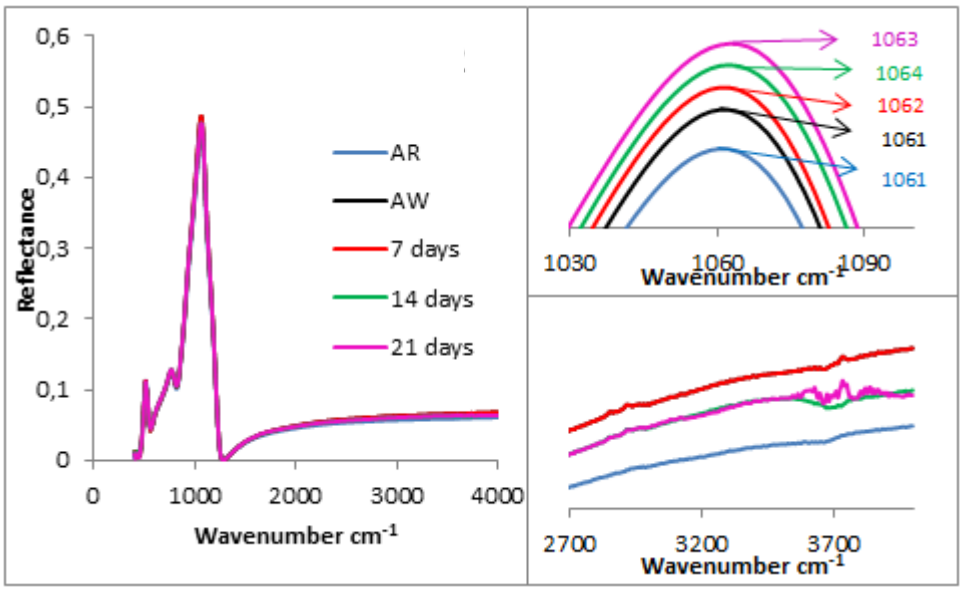

(a) G3_F1-L2

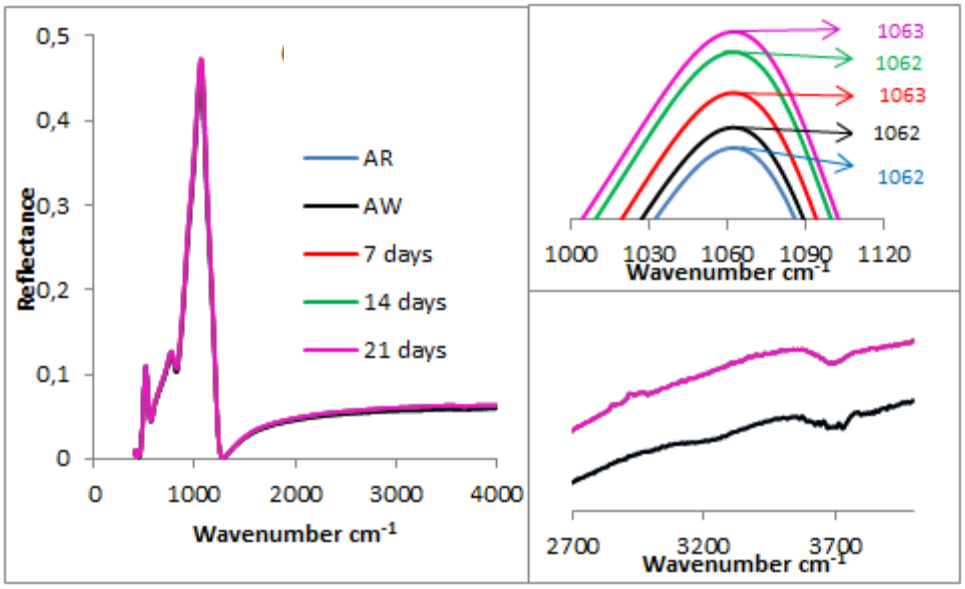

(b) G3_F2-L5

Figure B.1: SR-IR results of sample set G3 (a) F1-L2 (b) F2-L5 (c) F3-L7 (d) F4-L2

(cont. on next page)

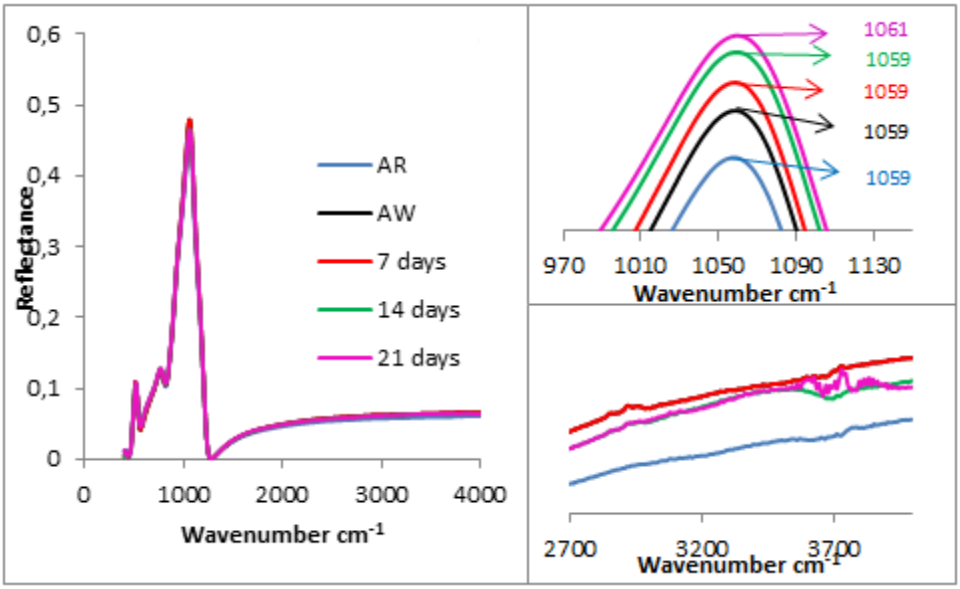

(c) G3_F3-L7

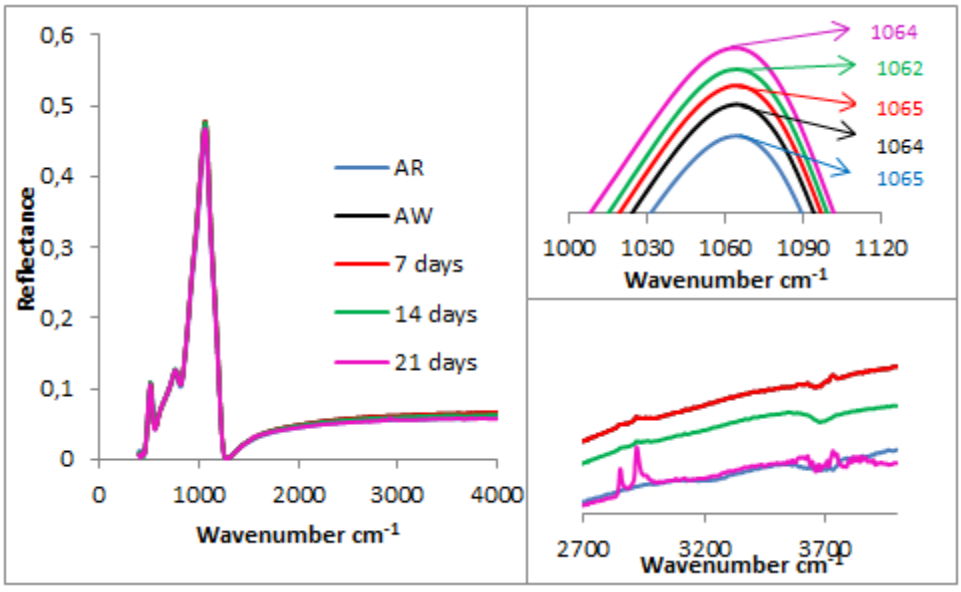

(d) G3_F4-L2

Figure B.1. (cont.)

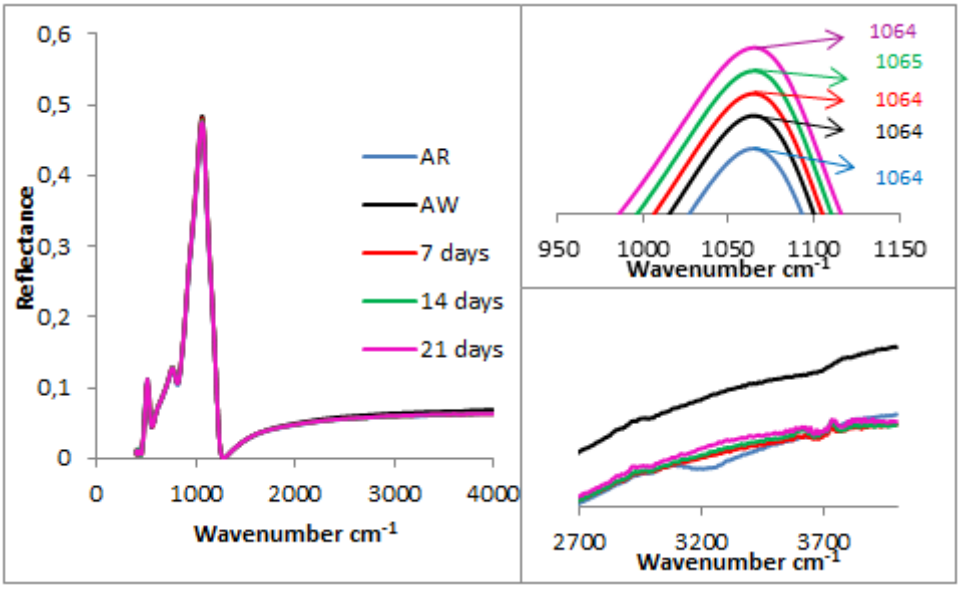

(a) G4_F1-L2

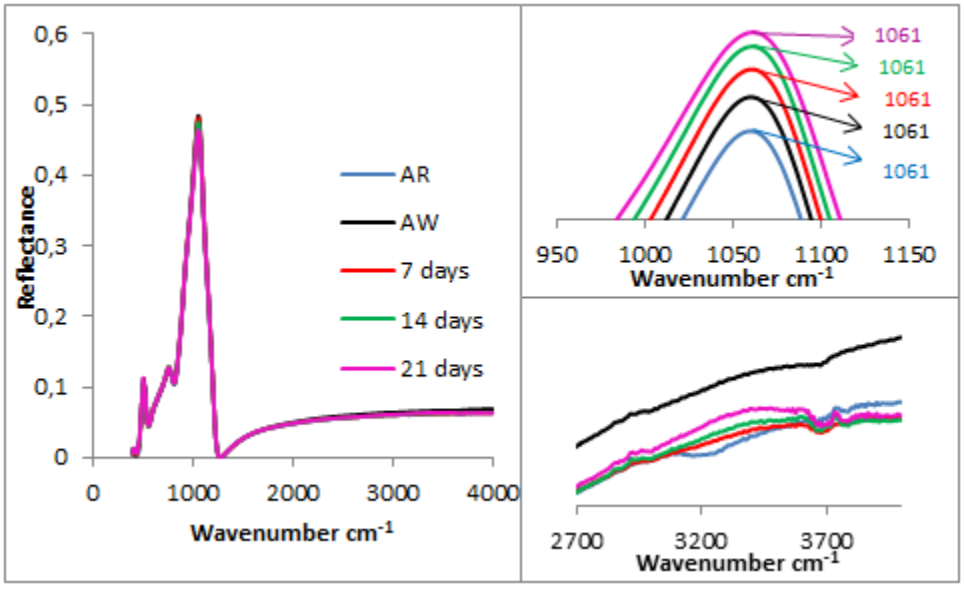

(b) G4_F2-L5

Figure B.2. SR-IR results of sample set G4 (a) F1-L2 (b) F2-L5 (c) F3-L7 (d) F4-L2

(cont. on next page)

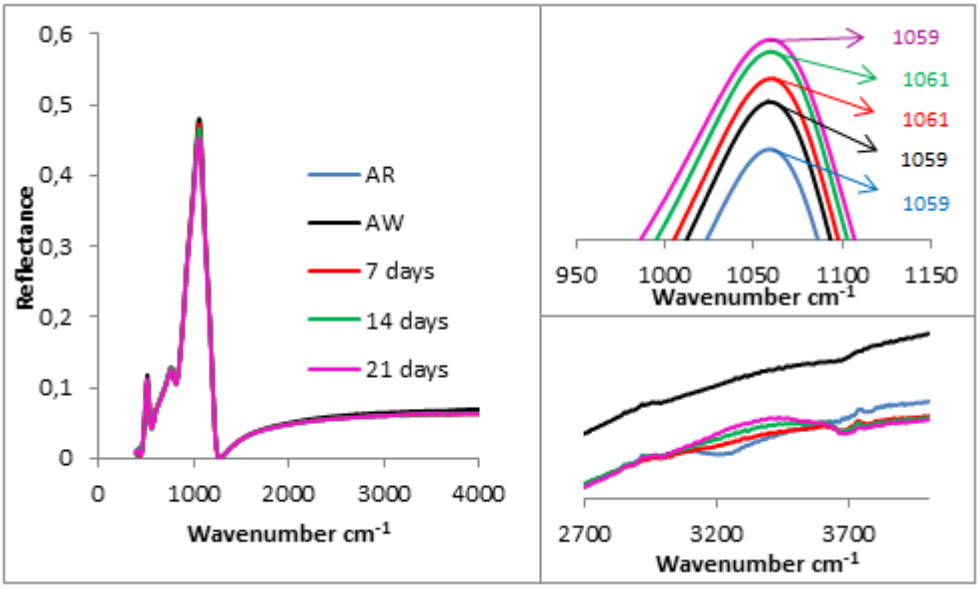

(c) G4_F3-L7

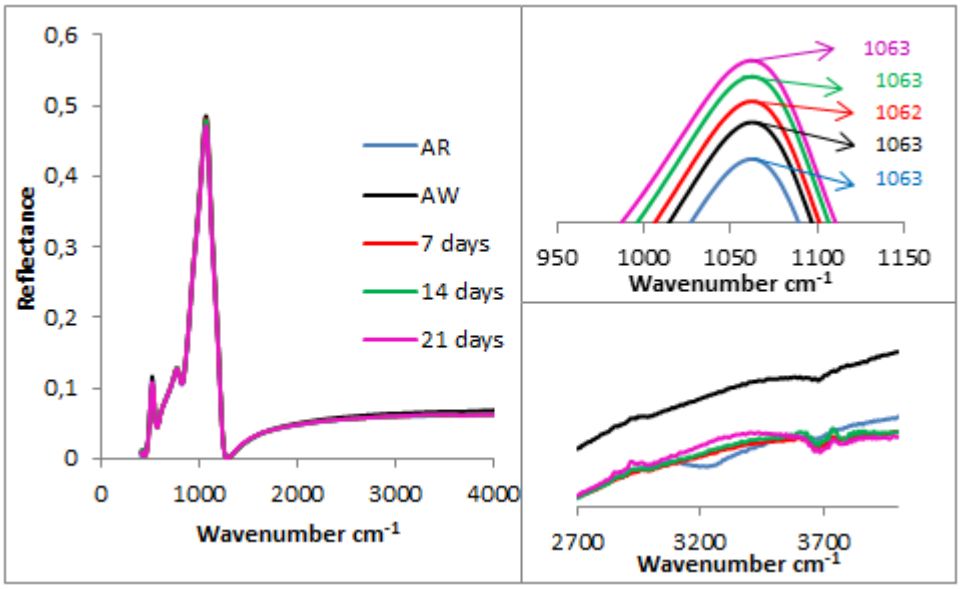

(d) G4_F4-L2

Figure B.2. (cont.)